JNRS

JOURNAL OF NEW RESULTS IN SCIENCE

http://dergipark.gov.tr/jnrs

ISSN: 1304 - 7981

VOLUME : 11
NUMBER : 2
YEAR : 2022

jnrs@gop.edu.tr

About

Journal of New Results in Science -an official journal of the Institute of Graduate Studies of Tokat Gaziosmanpasa University - started its publication in 2012.

J. New Results Sci. is an international, peer-reviewed, and fully open access journal which publishes original English research articles and reviews in **Mathematics and Statistics, Natural Science, Engineering Science, and Agricultural Science**.

JNRS has no processing charges.

Language: English only

Editor-in-Chief: Ali YAKAR

Email: togu.jnrs@gmail.com

Review Process: Blind Peer Review

The policy of Screening for Plagiarism: For a manuscript to be accepted from 2021 for pre-review, its reference-excluded similarity rate obtained via iThenticate, Turnitin, etc. should be a **maximum of 40%**.

Aim & Scope

Journal of New Results in Science (JNRS) is an Online, Peer-Reviewed, Open-Access journal that aims to contribute to the progress and application of scientific discoveries by publishing Original Research Papers, Review articles that are not published or not being considered for publication elsewhere.

Journal of New Results in Science (JNRS) is a multidisciplinary journal that accepts original research articles written in English in

- Mathematics and Statistics,
- Natural Science,
- Engineering Science,
- Agricultural Science.

Journal Boards

Editor-in-Chief

Associate Editor-in-Chief

Statistical Editors

Section Editors

Chemistry

Ömer Işıldak, Tokat Gaziosmanpaşa University, Turkiye
Cemil Alkan, Tokat Gaziosmanpaşa University, Turkiye
Fatma Aydın, Çanakkale Onsekiz Mart University, Turkiye
Fikret Büyükkaya, İstanbul University, Turkiye
Arianit A. Reka, University of Tetova, Republic of North Macedonia

Biology

Adem Keskin, Tokat Gaziosmanpaşa University, Turkiye
Dursun Kısa, Bartın University, Turkiye
Cengiz Yıldırım, Amasya University, Turkiye
Kiraz Erciyas Yavuz, Ondokuz Mayıs University, Turkiye

Molecular Biology

Ercan Çaçan, Tokat Gaziosmanpaşa University, Turkiye
Fatih Sezer, Çanakkale Onsekiz Mart University, Turkiye

Statistics

Burcu Mestav, Çanakkale Onsekiz Mart University, Turkiye
Verda Davaslıgil Atmaca, Çanakkale Onsekiz Mart University, Turkiye

Computer Science and Engineering

Serhat Kılıçarslan, Tokat Gaziosmanpaşa University, Turkiye
Uğur Erkan, Karamanoğlu Mehmetbey University, Turkiye
Kemal Adem, Aksaray University, Turkiye
Dang N H Thanh, Hue College of Industry, Vietnam

Mechatronics Engineering

Ahmet Fenercioğlu, Tokat Gaziosmanpaşa University, Turkiye
Levent Gökrem, Tokat Gaziosmanpaşa University, Turkiye
Cemil Közkurt, Bandırma Onyedi Eylül University, Turkiye

Food Engineering

Özlem Akpınar, Tokat Gaziosmanpaşa University, Turkiye
Mohammad Shafiur Rahman, Sultan Qaboos University, Turkiye
Rama Chandra Pradhan, National Institute of Technology (NIT), India

Bioengineering

Bilge Hilal Çadırcı Efeli, Tokat Gaziosmanpaşa University, Turkiye
Elif Apohan, İnönü University, Turkiye

Electrical and Electronics Engineering

Mahmut Hekim, Tokat Gaziosmanpaşa University, Turkiye
Abdurrahim Toktaş, Ankara University, Turkiye

Mechanical Engineering

Mithat ŞİMŞEK, Tokat Gaziosmanpaşa University, Turkiye
Uğur Köklü, Karamanoğlu Mehmetbey University, Turkiye

Geomatics Engineering

Ömer Yıldırım, Tokat Gaziosmanpaşa University, Turkiye
Levent Genç, Çanakkale Onsekiz Mart University, Turkiye

Civil Engineering

Ferit Yakar, Tokat Gaziosmanpaşa University, Turkiye
Serdar Çarbaş, Karamanoğlu Mehmetbey University, Turkiye

Materials Science and Engineering

M Fatih Kılıçarslan, Sivas University of Science and Technology, Turkiye
Necati Başman, Iskenderun Technical University, Turkiye
Raihan Rumman, Flinders University, South Australia

Industrial Engineering

Kadir Sarıkaya, Tokat Gaziosmanpaşa University, Turkiye

Agricultural Economics

Gülistan Erdal, Tokat Gaziosmanpasa University, Turkiye
Oğuz Parlakay, Hatay Mustafa Kemal University, Turkiye

Field Crops

Yasin Bedrettin Karan, Tokat Gaziosmanpasa University, Turkiye
Mahir Özkurt, Muş Alparslan University, Turkiye
Anna Wenda-Piesik, UTP University of Science and Technology, Poland

Horticulture

Çetin Çekiç, Tokat Gaziosmanpasa University, Turkiye
Burhan Öztürk, Ordu University, Turkiye
Kiril Bahcevandziev, Polytechnic Institute of Coimbra, Portugal

Soil Sciences and Plant Nutrition

İrfan Oğuz, Tokat Gaziosmanpaşa University, Turkiye
Mustafa Başaran, Çanakkale Onsekiz Mart University, Turkiye
Sudas D. Wanniarachchi, University of Ruhuna, Sri Lanka

Contents

Volume: 11 - Issue: 2

YEAR: 2022

Research Article

6. Not-ordered quasi-distance measures of generalised trapezoidal hesitant fuzzy numbers and their application to decision making problems

İrfan DELİ Elif Özge ÇELİK

Page: 162-181

Journal of New Results in Science 11(2) (2022) 100-110

Journal of New Results in Science
https://dergipark.org.tr/en/pub/jnrs
Research Article
Open Access

E-ISSN:1304-7981 https://doi.org/10.54187/jnrs.1103993

An investigation on quantitative detector characteristics of novel flexible skin dosimeter using Monte Carlo simulation method

Şenol Kaya[1]

Keywords:
Radiation sensors, Simulations, pyPENELOPE Code, Dosimeters

Abstract — Novel lead oxide-based flexible dosimeters with superior performance were experimentally tested for electron therapy. However, absorbed/transmitted primary particle fraction and secondary radiation distribution from the dosimeter surface have not been reported. These features should be specified to improve the dosimeter's reliability for medical applications. Hence, the absorbed primary particle fraction, transmitted particle and secondary radiations distributions of lead oxide-based flexible skin dosimeter under the incident 6 MeV electron radiation have been investigated by pyPenelope Monte Carlo Simulation. The results have demonstrated that the generated secondary irradiation probabilities are not significantly high to enhance the therapeutic dose abnormally. In addition, the angular distribution of the scattered secondary irradiations is low. No abnormal changes were observed in the fraction and energy distribution of the transmitted primary electrons. Hence, it can be concluded that the designed structure has promising potential to be used as dosimeters in electron beam therapy.

Subject Classification (2020):

1. Introduction

Ionising radiation is a useful tool for cancer treatment. Various photon and particle irradiations with different energies are used in radiation therapy [1-3]. The main aim is to prevent the death of cancer cells by protecting healthy tissue [4]. Controlling the photon radiation used in radiation therapy is difficult compared to the particle's irradiation, such as electron or proton. This is due to the high penetrating distance of photons which may also expose the deeper healthy tissues. Some malignant neoplasms or benign tumours can be localised on or close to the surface of the patient's skin, where electron beams can be effectively treated [5,6]. Electron beam therapy (EBT) can avoid exposing the deeper tissues by providing a high dose to the skin area [7]. Thus, possible side effects can be minimised.

The exposed dose of EBT value is also crucial for effectively treating the tumours. The treatment planning system estimates the therapeutic dose, which depends on the beam energy and penetration depth [8]. However, the treatment planning systems suffers from accuracy issues. The differences between the calculated and exposed skin dose may rise to $\pm 20\%$ [9]. Therefore, a skin dosimeter is used to verify exposed skin dose in clinical applications. Optically stimulated luminescent dosimeters (OSLs),

[1]senolkaya52@gmail.com (Corresponding Author)
[1]Mehmet Tanrıkulu Vocational School of Health Services, Abant İzzet Baysal University, Bolu, Turkiye
Article History: Received: 15 Apr 2022 — Accepted: 24 Jun 2022 — Published: 31 Aug 2022

diode and MOSFET dosimeters are most commonly used in clinical practice to control the skin dose. These dosimeters measure the point dose during the EBT. Thus, the dose distributions on the whole skin region cannot be controlled. In addition, the skin surface is naturally curved, and positional accuracy of the dosimeters can affect the verification of the therapeutic doses in clinical practice. For instance, the MOSFET dosimeter exhibits sensitivity variations from 5% to 22.8% depending on its angular location during radiation therapy [10,11]. To overcome this issue, studies have focused on developing flexible dosimeters with functional materials [12-14]. The flexible dosimeter can be localised on the human body contours, which can precisely measure the cumulative skin dose. Han et al. [8] have fabricated lead oxide-based flexible skin dosimeters exhibiting superior performance in this aspect. It has also been reported that the PbO dosimeters show promising potential as semiconductor dosimeters instead of diodes.

Together with superior experimental electron radiation sensing characteristics of the PbO-based flexible dosimeters, some quantitative detector characteristics should be investigated for clinical applications. Scattering particles and the generation of secondary radiation are critical phenomena in radiation therapy [15]. These generated radiations can be entirely absorbed by the dosimeters or may backscatter on their surfaces. Penetration of the secondary radiation tissue level or absorption of the primary radiation in the dosimeter body may cause dose enhancement/decrement in the patient body [16,17]. Hence, the assessment of these quantitative detector characteristics should be considered in evaluating the clinical potential of the novel dosimeter. Monte Carlo simulation is a crucial tool to specify the possible density of scattered particles, generation of the secondary radiation and transmission ratio of the primary particles from the dosimeter structure. Various simulation packages, including Geant4, MCNPX, and pyPENELOPE, were composed to simulate the interactions between particles and the designed structure. Most of these simulation programs depend on multiple-scattering theories for electron transport to decrease the computational time [18].

Nevertheless, step length must be cautiously determined to decrease possible inaccuracies in the simulation results acquired from the designed dosimeter structure. The PENELOPE (Penetration and Energy Loss of Positrons and Electrons in the matter) Monte Carlo package has been preferred for the simulation of PbO-based flexible skin dosimeters since it does not lead to difficulties concerning the determination of proper step length [18,19]. The pyPENELOPE simulates the relevant interactions of the particles through the consistent differential cross sections [20]. During the simulation, pyPENELOPE runs the main code called Penepma. This package codes cover combined outcomes from first-principles calculations, semi-empirical formulations and estimated databases. The pyPENELOPE processes the most accurate physics concepts present that align with the intended generality of the code [20], which can be seen in Refs [21-23]. In this aspect, the density of scattered particles, generation of the secondary radiation and transmission ratio of the primary particles under 6 MeV electron radiations from the PbO-based flexible skin dosimeters structure have been investigated via open-source pyPENELOPE Monte Carlo code. Possible dose enhancement/decrement results in particle scattering/secondary radiation generation from designed skin dosimeters during clinical applications has also been discussed.

2. Materials and Methods

This simulation study was carried out via open source pyPENELOPE Monte Carlo code. As reported in [8] and relevant works in [24,25], the first layer was a 1 micrometre (μm) thick gold electrode, the second layer was a 10 μm-thick passive layer of C-type perylene, the third layer was 50 μm-thick irradiation sensing layers of PbO, the fourth layer was 0.5 μm-thick indium tin oxide, and the last base layer was 100 μm-thick polyester substrates. These structures were designed by using the user-friendly interface of the pyPENELOPE software. The verification of the designed schematic structure was carried

out via gview2d.exe. The simulated lead oxide-based flexible dosimeter geometry is illustrated in Figure 1, and the simulated dosimeter structure reported in [8] is schematically depicted on the right bottom of Figure 1.

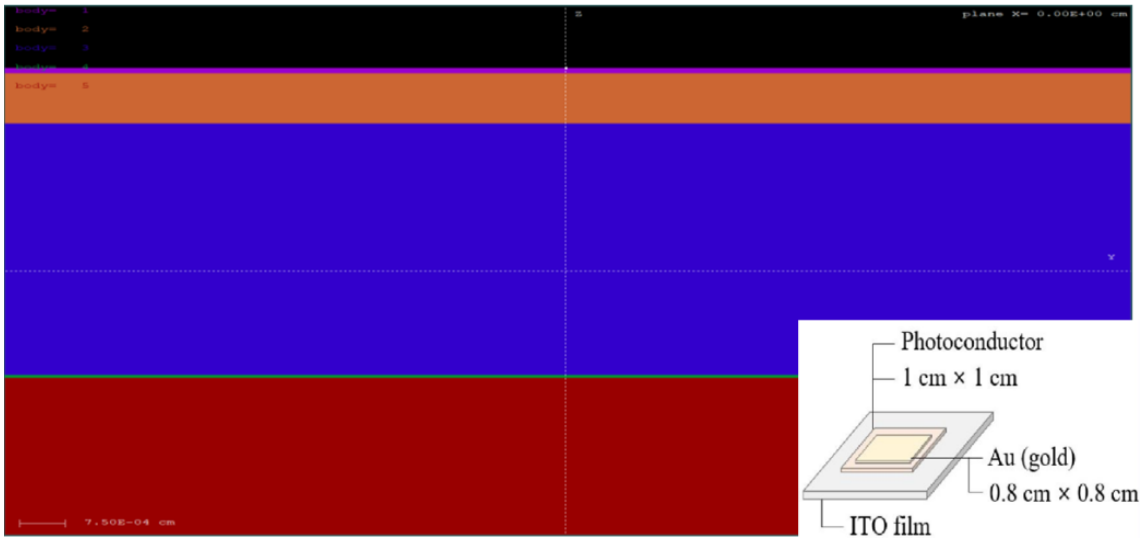

Figure 1. Simulated structure of the flexible skin dosimeter and the simulated dosimeter structure reported in [8]

Electron irradiations with various energies are used in electron beam therapy to treat tumour cells [3,6]. Among the different irradiation energies, the 6 MeV electrons are one of the most widely used electron beam therapy [6,26]. Hence, incident electron beam energy was set to 6 MeV during the evolution of the lead oxide-based flexible skin dosimeter. The numbers of 8.2×10^8 electrons were simulated to decrease possible errors or uncertainties. The absorbed primary particle fractions, transmitted particles and secondary radiation distributions of flexible skin dosimeters under 6 MeV electron exposure were estimated via pyPENELOPE simulation. The simulations of the particles were controlled by C1, C2, WCC, and WCR. The C1 specifies the mean-free path among the hard inelastic incidents, while C2 determines the maximum average energy loss in a single event. The WCC and WCR are cut-off energy losses for hard inelastic collision and Bremsstrahlung emission, respectively [27]. The C1 and C2 were set to 0.2 for the increased simulation speed. The WCC and WCR were set to 50 eV for the detailed simulation. The 50 eV is the lowest value for the pyPENELOPE that the user can select. A such low value of WCC and WCR may increase the simulation time. However, it promotes the reliability of the simulation by calculating the possible interaction contributions at low energies.

Similarly, the absorption energies were also set to 50 eV, and default interaction forcing was utilised during the simulation [28]. The default interaction forcing in the pyPENELOPE contains preternaturally enhancing the probability of inner-shell ionisation and bremsstrahlung emission and assigning proper statistical weights to the created secondary particles in such a way that the simulation outcomes stay unbiased [23]. It should be noted that although the pyPENELOPE can track particles down to 50 eV, the interaction cross sections for energies below 1 keV should be considered semi-quantitative [22]. Nevertheless, the reliability of pyPENELOPE has been tested by several research groups by comparing the simulated and experimental results for X-ray spectra from metal targets [28,29], annihilation photon detection [30,31], k-ratios of thin films [32] and different applications [22]. An office computer performed the simulation with i5 × 3.2 GHz CPU and 8 GB RAM under windows operating systems.

3. Results and Discussion

The absorbed, backscattered, and transmitted radiation fractions from the dosimeter structure were obtained after simulation of 8.2×10^8 electrons and their distributions were estimated via pyPENELOPE Monte Carlo code. The fractions of these parameters are listed in Table 1. The absorption fraction of the primary particles is 0.00014 with a low uncertainty factor. The dosimeter structure absorbs only 0.014% of the 6 MeV incident electrons. Similarly, the transmission percentage of the radiation was also estimated to be 102% $\pm$ 0.022%. This transmission value is the sum of the transmitted primary 6 MeV electrons and secondary irradiations emitted from the interaction of primary 6 MeV electrons with the dosimeter structure. Considering the simulation results, almost 99% of the primary 6 MeV electrons were transmitted from the dosimeter structure, and the remaining transmission values are contributions of the secondary radiations. The fraction of the transmitted secondary electrons is also tabulated in Table 1.

Table 1. Various results of the simulated primary and secondary irradiations

	Primary Irradiation		Secondary Electron		Secondary Photon	
	Fraction	Uncertainty x 10^{-5}	Fraction	Uncertainty x 10^{-5}	Fraction	Uncertainty x 10^{-5}
Absorbed	0.00014	1.246	-	-	-	-
Backscattered	0.0118	16.07	0.008	10.40	0.004	6.738
Transmitted	1.021	22.52	0.017	16.71	0.060	25.82

The transmission fraction of the generated secondary electrons is only 0.017. On the other hand, roughly 1.18% of the 6 MeV incident electrons is backscattered by the dosimeter structure. The low interaction and scattering fraction values can be attributed to the thin structure of the skin dosimeters. When the electron radiation propagates through the dosimeters, multiple Coulomb scattering interactions may deflect electrons [33]. Coulomb scattering probability of electron irradiation with the matter is also strictly connected to the thickness of the materials where radiation propagates [33,34]. The approximately 170 μm-thick structure of the designed dosimeters significantly decreases the interaction probability of electrons with the matter. Hence, such low fraction values were obtained after simulations. It seems that these calculated fractions would not anomalously increase or decrease the therapeutic dose during clinical applications. The backscattered and transmitted energy distributions of the 6 MeV electron irradiation from the dosimeter surface are illustrated in Figures 2a-b, respectively. These spectra show how incoming electrons energy varies along the path from the source through the detector structure [18]. As depicted in Figure 2a, some portions of the incident 6 MeV electrons are scattered backwards due to the elastic scattering interactions with atoms in the dosimeter structure [15]. Backscattered electrons increase in regions below 1 MeV and near 6 MeV energy. It can be expected that the large numbers of these backscattered electrons locate at low energies. This can be attributed to multiple elastic scattering of the incident electrons. Some of their incident energy is lost after each scattering during electron propagation. This explains why most backscattered electrons leave the sample after losing their energy.

On the other hand, it has been observed that the transmitted electrons' energies are close to the incident energy of 6 MeV, and no complex energy distribution has been observed. The spectra shown in Figure 2b include the secondary electrons transmitted from the dosimeter structure. In the transmitted electron spectra, no significant contribution has been observed from secondary electrons, which can be visible in the low energies and their transmission fraction is very low, as seen in Table 1. It is easy to complete the absorption of these secondary electrons by the dosimeter's surfaces [15]. Hence, they may not be visible in Figure 2b.

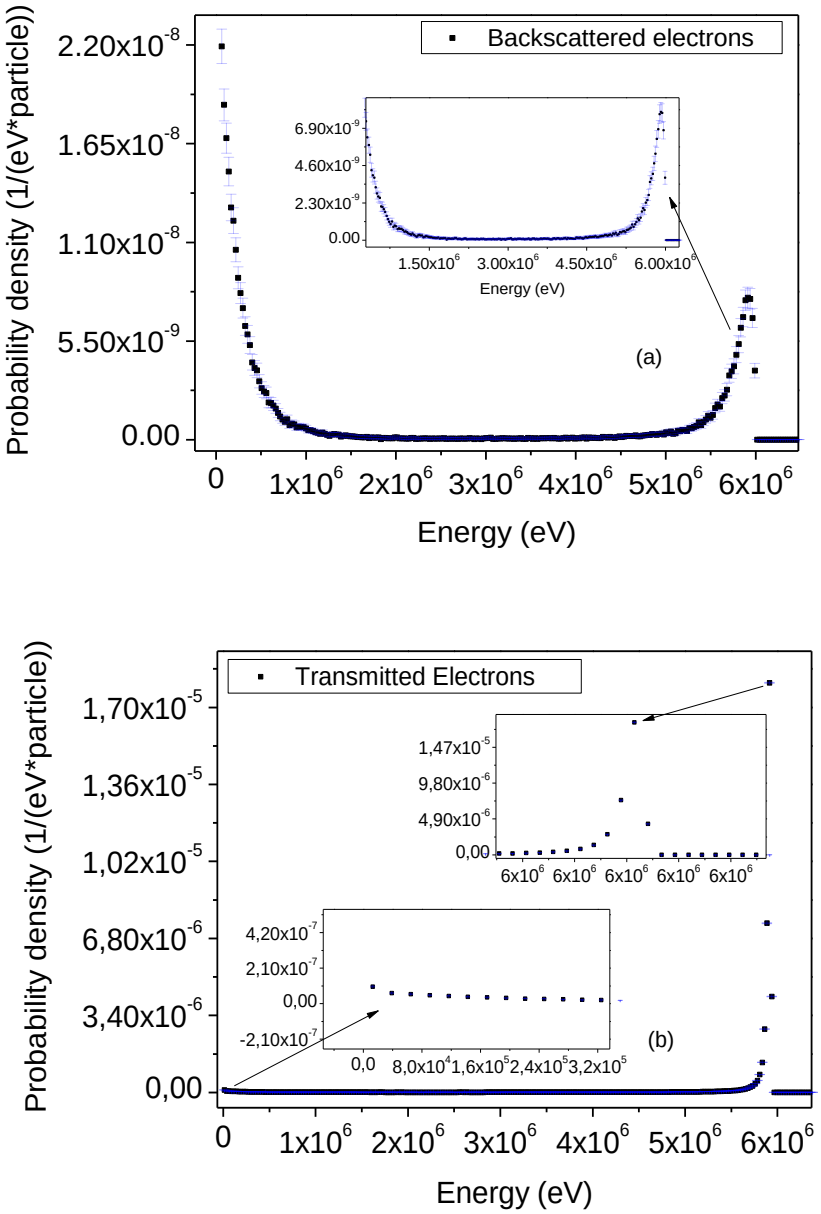

Figures 2. The energy distributions of the a-) backscattered electrons and b-) the transmitted electrons

Only a vaguely seen increment has been observed in the energy region of the few keV, which may be originated from secondary electrons or transmitted primary electrons after multiple interactions. On the other hand, this observed transmitted characteristic of electrons is an expected property for the dosimeters. The designed dosimeter does not cause multiple transmitted energy regions, which may deviate the therapeutic dose in clinical practices. Photons with various energies can be generated, resulting in the interaction between incident electrons and materials in the dosimeter. These generated photons can be classified as radiation contamination for dosimeter application [35]. In this aspect, potential radiation contamination consists of the generated x-rays, including the continuum (Bremsstrahlung), characteristics and fluorescence X-rays. Specifying these secondary photon irradiations was also crucial for the dosimeter application, which can lead to unfavourable side effects, e.g., a higher risk of secondary malignancy formation after the radiotherapy.

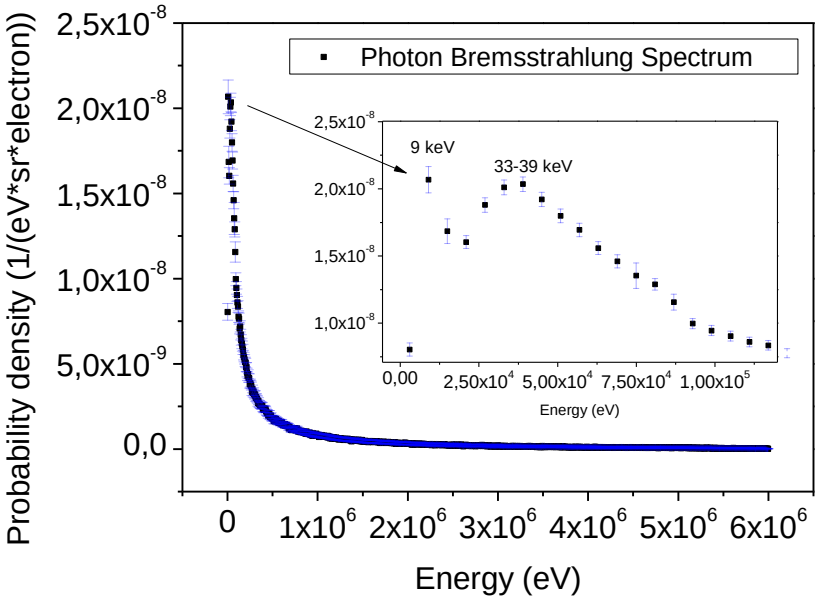

Figure 3. The energy distributions of the Bremsstrahlung X-ray spectra

The Bremsstrahlung X-ray radiation spectra are depicted in Figure 3. The Bremsstrahlung background radiation becomes more visible as X-ray energies below 100 keV. A peak at 9 keV was observed in the Bremsstrahlung background, which may correspond to the characteristic X-rays of the Au electrodes [36].

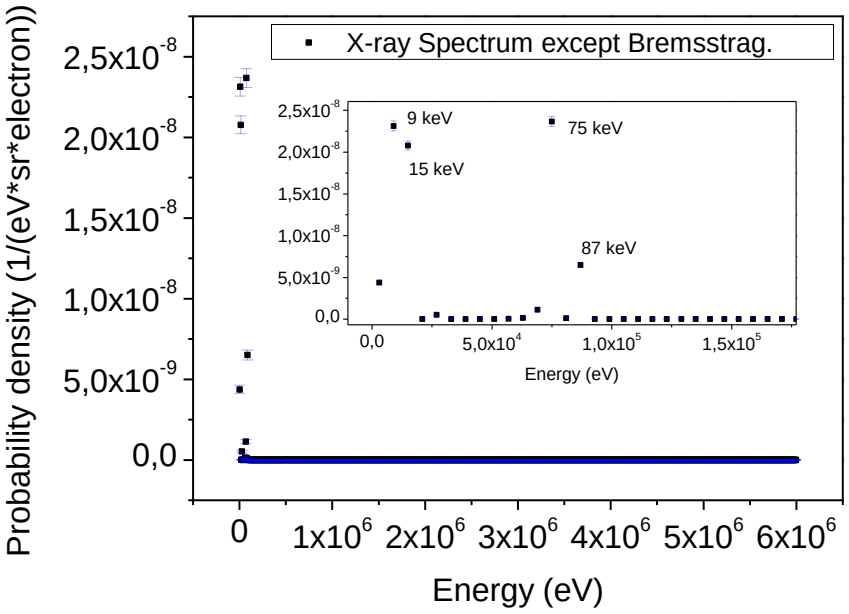

Figure 4. The energy distribution of generated photon contamination from the dosimeter surface

The generated X-ray spectra obtained after the simulation is depicted in Figure 4. These distributions in Figure 4 include the photons generated from electron interactions such as fluorescent X-rays but excluded Bremsstrahlung. The observed peaks on the spectra occur owing to the X-ray scattering characteristics of materials in dosimeter structure and the relatively low energy of X-ray fluorescence [37]. The backscattering and transmission ratios of the secondary photons are listed in Table 1. The transmission ratio is essential due to the high penetrating distance of the X-rays into the deeper tissue

levels. Only 6.0 % per cent of the generated secondary photons were transmitted to the tissue side of the dosimeters. It is also worth noting that the quantity of secondary photons generated per incident electron is at least two orders of degrees smaller than that of transmitted electrons (see probability density axes in Figure 2b and Figure 3.

Moreover, the interaction mean free paths for photons are characteristically much higher than electrons [34]. Therefore, these secondary photons' impact on the therapeutic dose is presumably negligible [34]. Nevertheless, it exhibits minimal risk for deep healthy tissues. The angular distributions of the emerging electrons and photons with any energy generated via interactions between incident electrons and dosimeter materials are illustrated in Figure 5. The schematic design of the simulation, including the polar angle distribution [23], has also been depicted in the left corner of Figure 5.

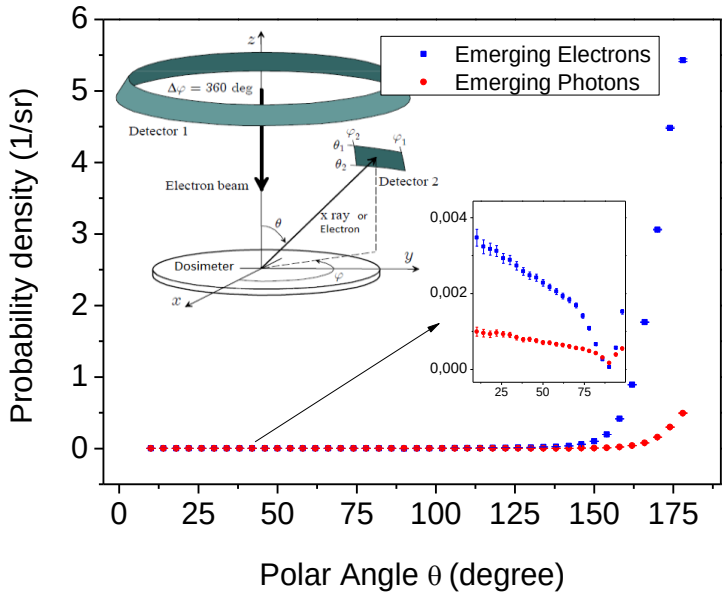

Figure 5. Polar angle dependency of emerging photons and electrons emitted from the dosimeter with any energy

The polar angles from zero to 90 degrees contain backscattered secondary photon and electron irradiations. It has been observed that at less than 90 degrees, the distribution varies very slowly with the angles. In addition, the backscattered probability/count of the second irradiation is very low. On the other hand, the polar angles from 90 to 180 degrees contain the transmitted secondary photon and electron irradiations which may cause the enhancement of the therapeutic doses on the patient body. The secondary photons were scattered in almost the same direction as the incident electron irradiations, as depicted in Figure 5.

On the other hand, the scattered region of the secondary electrons was a bit broad than the secondary photons. Due to the multiple elastic scattering, some portion of the secondary electrons deviated roughly 30 degrees from the target tissue. Nevertheless, the simulation results demonstrate that considering probability density, large numbers of emerging electrons are still oriented to the target tissue.

4. Conclusion

The fraction and energy distributions of the incident 6 MeV electrons and generated secondary electron and photon radiations scattered from novel lead oxide-based flexible skin dosimeters have been

investigated in detail. Considering simulation results, almost 99% of the primary 6 MeV electrons were transmitted from the dosimeter structure. The transmission fraction of the generated secondary electrons is only 0.017. On the other hand, roughly 1.18% of the 6 MeV incident electrons is backscattered by the dosimeter structure. The low scattering fraction values can be attributed to the thin structure of the skin dosimeters. No abnormal changes were observed in the fraction and energy distribution of the transmitted incident electrons.

Moreover, only 6.0 % per cent of the generated secondary photons were transmitted to the tissue side of the dosimeters. The observed peaks on the secondary photon spectra occur owing to the X-ray scattering properties of materials in the dosimeter structure. It is also worth noting that the quantity of secondary photons generated per incident electron is at least two orders of degrees smaller than the number of transmitted electrons, i.e., these secondary photons have limited effects on the therapeutic doses. Angular distributions of the scattered secondary radiation are not anomalous large to significantly enhance the radiation dose on the surrounding healthy tissue. The simulated results have demonstrated that the designed skin dosimeters may not significantly cause a large dose enhancement/decrement in the patient body. Hence, the lead oxide-based flexible skin dosimeter has great potential to be used as a measurement device during electron therapy.

Author Contributions

The author read and approved the last version of the paper. The author performed all simulations and discussions.

Conflicts of Interest

The author declares no conflict of interest.

Acknowledgement

The author would like to thank Mehmet Tanrıkulu Vocational School Bolu Abant Izzet Baysal University for providing an office-type computer to perform the simulation. The author also would like to thank pyPENELOPE development group (http://pypenelope.sourceforge.net) for the open source and free usage of the simulation package.

References

[1] P. E. Huber, J. Debus, D. Latz, D. Zierhut, M. Bischof, M. Wannenmacher, R. Engenhart-Cabillic, *Radiotherapy for advanced adenoid cystic carcinoma: neutrons, photons or mixed beam?*, Radiotherapy and Oncology, 59(2), (2001) 161–167.

[2] N. Adnani, B. G. Fallone, *Neutron therapy using medical linacs*, in: J. D. Enderle (Ed.), Proceedings of the 22nd Annual International Conference of the IEEE Engineering in Medicine and Biology Society 2020, Chicago, USA, 2000, pp. 133–136.

[3] W. Kawakami, S. Takamatsu, M. Taka, K. Ishii, T. Nakaichi, K. Funamoto, K. Yokoyama, *Factors associated with radiation pneumonitis in patients receiving electron boost radiation for breast-conserving therapy: a retrospective review*, Advances in Radiation Oncology, 5(6), (2020) 1141–1146.

[4] S. C. S. Cunha, L. A. V. Carvalho, P. C. Canary, M. Reisner, K. B. Corgozinho, H. J. M. Souza, A. M. R. Ferreira, *Radiation therapy for feline cutaneous squamous cell carcinoma using a hypofractionated protocol*, Journal of Feline Medicine and Surgery, 12(4), (2010) 306–313.

[5] S. Hyodynmaa, A. Gustafsson, A. Brahme, *Optimisation of conformal electron beam therapy using energy- and fluence-modulated beams*, Medical Physics, 23(5), (1996) 659–666.

[6] J. Narbutt, A. Chrusciel, A. Rychter, J. Fijuth, A. Sysa-Jedrzejowska, A. Lesiak, *Persistent improvement of previously recalcitrant Hailey-Hailey disease with electron beam radiotherapy*, Acta Dermato-Venereologica, 90(2), (2010) 179–182.

[7] A. M. Saadeldin, A. M. Elwan, *Characterisation of irregular electron beam for boost dose after whole breast irradiation*, Reports of Practical Oncology and Radiotherapy, 25(2), (2020) 168–173.

[8] M. J. Han, S. W. Yang, S. I. Bae, Y. M. Moon, W. Jeon, C. W. Choi, S. K. Park, J. Y. Kim, *Evaluation of monoxide film-based dosimeters for surface dose detection in electron therapy*, Plos One, 16(5), (2021) Article ID: e0251441, 1–10.

[9] L. E. Court, R. B. Tishler, A. M. Allen, H. Xiang, M. Makrigiorgos, L. Chin, *Experimental evaluation of the accuracy of skin dose calculation for a commercial treatment planning system*, Journal of Applied Clinical Medical Physics, 9(1), (2008) 29–35.

[10] D. Manigandan, G. Bharanidharan, P. Aruna, K. Devan, D. Elangovan, V. Patil, R. Tamilarasan, S. Vasanthan, S. Ganesan, *Dosimetric characteristics of a MOSFET dosimeter for clinical electron beams*, Physica Medica-European Journal of Medical Physics, 25(3), (2009) 141–147.

[11] A. G. Dias, D. F. S. Pinto, M. F. Borges, M. H. Pereira, J. A. M. Santos, L. T. Cunha, J. Lencart, *Optimisation of skin dose using in-vivo MOSFET dose measurements in bolus/non-bolus fraction ratio: A VMAT and a 3DCRT study*, Journal of Applied Clinical Medical Physics, 20(2), (2019) 63–70.

[12] K. Oh, M. Han, J. Kim, Y. Heo, K. Kim, G. Cho, Y. Song, S. Cho, S. Heo, J. Kim, S. Park, S. Nam, *Flexible X-ray detector for automatic exposure control in digital radiography*, Journal of Nanoscience and Nanotechnology, 16, (2016) 11473–11476.

[13] M. J. Han, S. W. Yang, S. I. Bae, Y. M. Moon, S. U. Heo, C. W. Choi, S. K. Park, J. Y. Kim, *Evaluation of attenuation rate error for optimisation of skin dosimeter in electron beam therapy*, Journal of Instrumentation, 15, (2020) Article ID: P07012.

[14] N. Chaudhary, A. Singh, D. K. Aswal, A. K. Debnath, S. Samanta, S. P. Koiry, S. Sharma, K. Shah, S. Acharya, K. P. Muthe, S. C. Gadkari, *Electron beam modified zinc phthalocyanine thin films for radiation dosimeter application*, Synthetic Metals, 231, (2017) 143–152.

[15] P. Dondero, A. Mantero, V. Ivanchencko, S. Lotti, T. Mineo, V. Fioretti, *Electron backscattering simulation in Geant4*, Nuclear Instruments & Methods in Physics Research Section B-Beam Interactions with Materials and Atoms, 425, (2018) 18–25.

[16] J. T. Rakowski, S. S. Laha, M. G. Snyder, M. G. Buczek, M. A. Tucker, F. C. Liu, G. Z. Mao, Y. Hillman, G. Lawes, *Measurement of gold nanofilm dose enhancement using unlaminated radiochromic film*, Medical Physics, 42(10), (2015) 5937–5944.

[17] T. Shimozato, K. Okudaira, H. Fuse, K. Tabushi, *Monte Carlo simulation and measurement of radiation leakage from applicators used in external electron radiotherapy*, Physica Medica-European Journal of Medical Physics, 29(4), (2013) 388–396.

[18] A. Kahraman, S. Kaya, A. Jaksic, E. Yilmaz, *A comprehensive study on the photon energy response of RadFET dosimeters using the PENELOPE Monte Carlo code*, Radiation Effects and Defects in Solids, 170(5), (2015) 367–376.

[19] J. Sempau, P. Andreo, *Configuration of the electron transport algorithm of PENELOPE to simulate ion chambers*, Physics in Medicine and Biology, 51(14), (2006) 3533–3548.

[20] M. Asai, M. A. Cortés-Giraldo, V. Giménez-Alventosa, V. Giménez Gómez, F. Salvat, *The PENELOPE physics models and transport mechanics. implementation into Geant4*, Frontiers in Physics, 9, (2021) Article ID: 738735, 1–20.

[21] F. Salvat, Penelope: A Code System for Monte Carlo Simulation of Electron and Photon Transport, OECD Nuclear Energy Agency, 2019.

[22] X. Llovet, F. Salvat, *PENEPMA: a Monte Carlo programme for the simulation of X-ray emission in EPMA*, IOP Conference Series: Materials Science and Engineering, 109, (2016) Article ID: 012009, 1–13.

[23] X. Llovet and F. Salvat, *PENEPMA: A Monte Carlo program for the simulation of X-Ray emission in electron probe microanalysis*, Microscopy and Microanalysis, 23(3), (2017) 634–646.

[24] J. S. Choi, D. W. Ko, J. Y. Seo, J. H. Nho, J. H. Chang, S. T. Lee, J. Y. Jung, M. J. Lee, *Electrical and chemical sensing properties of a printed indium-tin-oxide film for the detection of hazardous and noxious substances*, Journal of the Korean Physical Society, 76(11), (2020) 1005–1009.

[25] S. W. Yang, M. J. Han, S. K. Park, J. B. Chung, J. K. Kang, T. S. Yu, J. E. Rah, J. K. Kim, M. W. Lee, J. Y. Kim, *Development and evaluation of a monoxide-based flexible skin dosimeter for radiotherapy at photon energies*, Journal of Instrumentation, 16, (2021) Article ID: P07056.

[26] D. F. Craft, J. Lentz, M. Armstrong, M. Foster, J. Gagneur, D. Harrington, S.E. Schild, M. Fatyga, *Three-dimensionally printed on-skin radiation shields using high-density filament*, Practical Radiation Oncology, 10(6), (2020) e543–e550.

[27] C. Y. Yi, S. H. Hah, M. S. Yeom, *Monte Carlo calculation of the ionisation chamber response to Co-60 beam using PENELOPE*, Medical Physics, 33(5), (2006) 1213–1221.

[28] P. Adamson, C. Cannon, S. Williams, *Bremsstrahlung produced by 5 keV electrons incident on BeO and NaCl*, Nuclear Instruments & Methods in Physics Research Section B-Beam Interactions with Materials and Atoms, 490, (2021) 43–47.

[29] D. Gonzales, B. Cavness, S. Williams, *Angular distribution of thick-target Bremsstrahlung produced by electrons with initial energies ranging from 10 to 20 keV incident on Ag*, Physical Review A, 84, (2011) Article ID: 052726.

[30] L. Tao, J. H. Wang, M. Esmaeelpour, C. S. Levin, *Simulation studies to understand sensitivity of an optical property modulation-based radiation detection concept for PET*, IEEE Nuclear Science Symposium and Medical Imaging Conference Proceedings (Nss/Mic) 2018, Sydney, NSW, Australia, 2018 Article ID: 178.

[31] L. Tao, D. Jeong, J. H. Wang, Z. Adams, P. Bryan, C. S. Levin, *Simulation studies to understand sensitivity and timing characteristics of an optical property modulation-based radiation detection concept for PET*, Physics in Medicine and Biology, 65, (2020) Article ID: 215021, 1–17.

[32] P. Statham, X. Llovet, P. Duncumb, *Systematic discrepancies in Monte Carlo predictions of k-ratios emitted from thin films on substrates*, IOP Conference Series: Materials Science and Engineering, 32, (2012) Article ID: 012024, 1–7.

[33] O. Lundh, C. Rechatin, J. Faure, A. Ben-Ismail, J. Lim, C. De Wagter, W. De Neve, V. Malka, *Comparison of measured with calculated dose distribution from a 120-MeV electron beam from a laser-plasma accelerator*, Medical Physics, 39(6), (2012) 3501–3508.

[34] F. Salvat-Pujol, H. O. Jeschke, R. Valenti, *Simulation of electron transport during electron-beam-induced deposition of nanostructures*, Beilstein Journal of Nanotechnology, 4, (2013) 781–792.

[35] H. R. Baghani, B. Aminafshar, *In-field radiation contamination during intraoperative electron radiation therapy with a dedicated accelerator*, Applied Radiation and Isotopes, 155, (2020) Article ID: 108918.

[36] Y. H. Li, Z. An, J. J. Zhu, L. Li, *Characteristic X-ray yields and cross sections of thick targets of Al, Ti, Zr, W and Au induced by keV-electron impact*, Acta Physica Sinica, 69(13), (2020) Article ID: 133401, 1–13.

[37] W. Kim, J. Jang, D. H. Kim, *Monte Carlo simulation for the analysis of various solid samples using handheld X-ray fluorescence spectrometer and evaluation of the effect by environmental interferences*, Spectrochimica Acta Part B-Atomic Spectroscopy, 180, (2021) Article ID: 106203, 1–9.

Journal of New Results in Science
https://dergipark.org.tr/en/pub/jnrs
Research Article
Open Access

E-ISSN:1304-7981 https://doi.org/10.54187/jnrs.1109009

A hybrid algorithm for solving fractional Fokker-Planck equations arising in physics and engineering

Ozan Özkan[1], Ali Kurt[2]

Keywords:
Conformable fractional partial differential equations,
Fractional wave transform method,
Differential transform method,
Time fractional Fokker-Plank equation

Abstract — In this work, we proposed a hybrid algorithm to approximate the solution of Conformable Fractional Fokker-Planck Equation (CFFPE). This algorithm comprises of unification of two methods named Fractional Wave Transformation Method (FWTM) and Differential Transform Method (DTM). The method is based on two steps. The first step is to reduce the given CFPDEs to corresponding Partial Differential Equations (PDEs). Then, the second step is to solve obtained PDEs iteratively by using DTM. Moreover, the algorithm's efficiency is shown by employing the method successfully to conformable time-fractional Fokker-Planck equation arising in surface physics, plasma physics, polymer physics, laser physics, biophysics, engineering, neurosciences, nonlinear hydrodynamics, population dynamics, pattern formation and marketing. As a result, the obtained data demonstrate that the algorithm is reliable and applicable.

Subject Classification (2020): 35R11, 35A20.

Nomenclature

DTM differential transform method
FWTM fractional wave transformation method
CFFPE Conformable Fractional Fokker-Planck Equations
PDE Partial Differential Equations
u unknown function
A drift coefficient
B diffusion coefficient
x coordinate
t time
Γ gamma function
U differential transform of u
T wave transform of t
X wave transform of x
k, h order of differential transform
α, β fractional orders

[1]oozkan@selcuk.edu.tr; [2]akurt@pau.edu.tr (Corresponding Author)
[1]Department of Mathematics, Faculty of Science, Selçuk University, Konya, Turkiye
[2]Department of Mathematics, Faculty of Science, Pamukkale University, Denizli, Turkiye
Article History: Received: 25 Apr 2022 — Accepted: 07 Aug 2022 — Published: 31 Aug 2022

1. Introduction

In the last decade, arbitrary order calculus has seen rapid growth and is widely used in various applications of diverse fields in science and technology. Differential equations involving fractional-order derivatives are progressively implemented to model problems in fluid mechanics, chemistry, biology, electromagnetism, fluid mechanics, signal processing, material science and many other physical processes [1,2]. Solving fractional partial differential equations has attracted considerable attention from scientists in the last decades. As is known that the analytical results for most fractional differential equations cannot be acquired. However, it is possible to get an approximate solution for these problems using numerical methods such as linearization or perturbation. In the '90s, some mathematical tools, such as the Adomian decomposition method [3], variational iteration method [4], homotopy perturbation method [5], and homotopy analysis method [6] have been found to solve various fractional problems analytically. The differential transform method (DTM) was expressed by Zhou in 1986 [7]. With the aid of this method, the considered differential equation can be changed into a recurrence equation and then we can construct the approximate analytical results in a polynomial form.

Scientists have been applying various numerical and analytical methods to obtain solutions to mathematical models arising in nature. The transform methods are used more often due to their simplicity and efficiency. There are many transform methods to solve those problems, and the most popular ones are the Laplace transform [8], the Fourier transform [9], the integral transform (IT) [10], and the fractional IT [11].

This study regards the conformable fractional Fokker-Planck equation [12,13]. Some critical applications of the Fokker-Planck equation can be seen in various fields, such as surface physics, plasma physics, polymer physics, laser physics, biophysics, engineering, neurosciences, nonlinear hydrodynamics, population dynamics, pattern formation and marketing [12-14]. The Conformable Fractional Fokker-Planck Equations (CFFPEs) can be written in the following form. Assume that u(x, t) that depends on the space and time variables is the solution of the CFFP1

$$\frac{\partial^{\alpha} u}{\partial t^{\alpha}} = \left[-\frac{\partial^{\beta}}{\partial x^{\beta}} A(t,x,u) + \frac{\partial^{2\beta}}{\partial x^{2\beta}} B(t,x,u) \right] u(t,x), t > 0 \text{ and } 0 < \alpha, \beta \leq 1 \tag{1.1}$$

where the parameter α denotes the order of the conformable fractional time derivative, while β denotes the order of the conformable fractional space derivative and $\frac{\partial^{2\beta}}{\partial x^{2\beta}}$ denotes two times successive conformable fractional derivative also, $A(t,x,u)$ and $B(t,x,u)$ are conformable differentiable functions. One can obtain the classical Fokker-Planck equation [14] by letting $\alpha = 1$ and $\beta = 1$.

The key idea of the method expressed in this paper is to convert CFPDEs into integer order PDEs by using FWTM. After this transformation, we can find the solutions to the considered equation using DTM. The rest of the paper is organized as follows: Section 2 presents the basics of conformable fractional calculus. Section 3 expresses the basic idea of DTM. Section 4 states the Hybrid Wave Transform method. Section 5 presents two case studies and a discussion of the results. Finally, Section 6 provides a brief conclusion.

2. Conformable Fractional Derivative

The definition of conformable derivative and integral are firstly presented by Khalil et al. [15] as follows:

Definition 2.1. [15] Consider the function $f:(0,\infty)\to\mathbb{R}$. The $\alpha-th$ order *"conformable fractional derivative"* of f is stated as,

$$D_\alpha(f)(t)=\lim_{\varepsilon\to 0}\frac{f(t+\varepsilon t^{1-\alpha})-f(t)}{\varepsilon}$$

for all $t>0,\alpha\in(0,1)$.

Definition 2.2. Let f be α -differentiable in some $(0,a),a>0$ and $\lim_{t\to 0^+}f^{(\alpha)}(t)$ exists then define $f^{(\alpha)}(0)=\lim_{t\to 0^+}f^{(\alpha)}(t)$. The *"conformable fractional integral"* of a function f starting from $a\geq 0$ is defined as:

$$I_\alpha^a(f)(t)=\int_a^t f(x)d_\alpha x=\int_a^t\frac{f(x)}{x^{1-\alpha}}dx$$

where the integral is the Riemann improper integral, and $\alpha\in(0,1]$.

In fact, the conformable fractional derivative has great, decisive advantages over other well-known derivatives such as Grunwald-Letnikov, Caputo, and Riemann-Liouville-type fractional derivatives [2,16,17]. For instance

- The Riemann-Liouville derivative of a constant is not zero. For instance, $D_a^\alpha c\neq 0$ (Caputo derivative satisfies) if α is not a natural number.
- The derivative of the known formula of the derivative of the product of two functions is not satisfied by all fractional derivatives.

$$D_a^\alpha(fg)=gD_a^\alpha(f)+fD_a^\alpha(g)$$

- The derivative of the quotient of two functions is not satisfied by all fractional derivatives.

$$D_a^\alpha\left(\frac{f}{g}\right)=\frac{fD_a^\alpha(f)-gD_a^\alpha(g)}{g^2}$$

- The chain rule does not satisfy by all fractional derivatives.

$$D_a^\alpha(fog)(t)=f^\alpha(g(t))g^\alpha(t)$$

- All fractional derivatives do not satisfy $D^\alpha D^\beta=D^{\alpha+\beta}$ in general.
- In the Caputo definition, it is assumed that the function f is differentiable.

After these advantages came out, it attracted many researchers, and many studies have been done. For instance, Rezazadeh et al. [18] used two methods for solving the Conformable Fractional Diffusion-Reaction Equation (CFDRE), which is commonly applied in mathematical biology. Korkmaz et al. [19] investigated "investigated a method for the solution of the Conformable Fractional Zakharov-Kuznetsov Equation (CFZKE). Hashemi [20] obtained the exact solutions of integrable nonlinear Schrödinger type equation with conformable time-fractional derivative. Chen et al. [21] used the simplest equation method for acquiring the exact solutions of some FPDEs with conformable derivatives. Özkan et al. [22] introduced the conformable double Laplace transform and investigated the solutions of the fractional heat equation and fractional telegraph equation using this transform. See the references [15,23].

3. Differential Transform Method

A brief description of the two-dimensional DTM [13,14] is expressed as follows:

Definition 3.1. [14,24,25] Let $u(t,x)$ be a continuously differentiable function and an analytic function in the defined domain. Then we can express the two-dimensional DTM of the function $u(t,x)$ as

$$U(k,h)=\frac{1}{k!\,h!}\left[\frac{\partial^{k+h}}{\partial t^k \partial x^h}u(t,x)\right]_{\substack{t=0\\x=0}} \tag{3.1}$$

where $u(t,x)$ is the original function, and $U(k,h)$ is the transformed function.

Definition 3.2. [14,24,25] The inverse DTM of $U(k,h)$ can be stated as

$$u(t,x)=\sum_{k=0}^{\infty}\sum_{h=0}^{\infty}U(k,h)t^k x^h \tag{3.2}$$

Unifying Equations (3.1) and (3.2), we get

$$u(t,x)=\sum_{k=0}^{\infty}\sum_{h=0}^{\infty}\frac{1}{k!\,h!}\left[\frac{\partial^{k+h}}{\partial t^k \partial x^h}u(t,x)\right]_{\substack{t=0\\x=0}} t^k x^h \tag{3.3}$$

Equation (3.3) indicates that the concept of the two-dimensional DTM is obtained from to two-dimensional Taylor series expansion. In this work, the lower-case letters denote the original functions, and the upper-case letters show the transformed version of the considered functions (T-functions). With the help of the above definitions, the two-dimensional DTM of some basic mathematical operations and functions can be obtained as [14,24,25] and are listed in Table 1.

Table 1. Some operations of the two-dimensional differential transformation

Original Function	Transformed Function
$u(t,x)=w(x,y)\pm v(x,y)$	$U(k,h)=W(k,h)\pm V(k,h)$
$u(t,x)=\alpha w(t,x)$	$U(k,h)=\alpha W(k,h)$
$u(t,x)=e^{\lambda(t+x)}$	$U(k,h)=\frac{\lambda^{k+h}}{k!\,h!}$
$u(t,x)=w(t,x)v(t,x)$	$U(k,h)=\sum_{r=0}^{k}\sum_{s=0}^{h}W(r,h-s)V(k-r,s)$
$u(t,x)=\frac{\partial^{r+s}}{\partial x^r \partial y^s}w(t,x)$	$U(k,h)=\frac{(k+r)(h+s)}{r!\,s!}W(k+r,h+s)$
$u(t,x)=t^m x^n$	$U(k,h)=\delta(k-m,h-n)=\begin{cases}1, for\ k=m,h=n\\0, otherwise\end{cases}$

4. A Hybrid Method for CFPDEs: Wave Transform Method with DTM

To show the solution procedure of the method for obtaining the solution of CFPDEs by using the Hybrid Wave Transform Method (HWTM), which is a combination of the FWTM and DTM, we will consider the following nonlinear time CFFPE:

$$\frac{\partial^\alpha u}{\partial t^\alpha} = \left[-\frac{\partial}{\partial x}A(t,x,u) + \frac{\partial^2}{\partial x^2}B(t,x,u)\right]u(t,x),\ t \in \mathbb{R}_0^+, x \in \mathbb{R}, \text{and } 0 < \alpha \leq 1 \tag{4.1}$$

together with the initial condition

$$u(0,x) = f(x) = \sum_{n=0}^{\infty} a_n x^n \tag{4.2}$$

Where $D^\alpha = \frac{\partial^\alpha}{\partial t^\alpha}$ indicates the conformable derivative. The method is based on transforming conformable fractional partial differential Equation (4.1) into a partial differential equation via FWTM with the aid of $T = \frac{pt^\alpha}{\alpha}$ wave transform, setting $p = 1$ and applying the chain rule [23] result in a PDE as follows:

$$\frac{\partial u}{\partial T} = \left[-\frac{\partial}{\partial x}A(T,x,u) + \frac{\partial^2}{\partial x^2}B(T,x,u)\right]u(T,x) \tag{4.3}$$

$$u(0,x) = f(x) = \sum_{n=0}^{\infty} a_n x^n \tag{4.4}$$

which can be solved via DTM. Employing DTM to both sides of the Equation (4.3) yields the following recurrence formula

$$(k+1)U(k+1,h) = A(h)V(k,h) \tag{4.5}$$

where $A(h)$ is the coefficient of $V(k,h)$, which is the differential transform of the right-hand side of Equation (4.3). Similarly, we transform the initial condition (4.4) to $U(0,h) = a_h,\ h = 0,1,2,3,\cdots$ by using DTM. By using $U(0,h)$ and Equation (4.5), we can iteratively obtain $U(k,h), k = 1,2,3,\cdots, h = 0,1,2,3,\cdots$. Here, it should not be forgotten that $U(k,h)$ values are the components of the spectrum of $u(T,x)$. Finally, we acquire the solution of Equation (4.3) by

$$u(T,x) = \sum_{k=0}^{\infty}\sum_{h=0}^{\infty} U(k,h)T^k x^h \tag{4.6}$$

By turning back to the original variables, we get

$$u(T,x) = \sum_{k=0}^{\infty}\sum_{h=0}^{\infty} U(k,h)\left(\frac{t^\alpha}{\alpha}\right)^k x^h \tag{4.7}$$

which is the solution of problems (4.1)-(4.2).

5. Applications

In this part, the practicality of the algorithm shall be exemplified by two examples.

Example 5.1. Consider the nonlinear time-fractional Fokker-Planck equation:

$$D_t^{\alpha}u = \left[-\frac{\partial}{\partial x}\left(3u - \frac{x}{2}\right) + \frac{\partial^2}{\partial x^2}(xu)\right]u(t,x) \tag{5.1}$$

where $t > 0, x > 0$, and $0 < \alpha \leq 1$. D_t^{α} indicates the CFD of function $u(x,t)$ due to the initial condition:

$$u(0,x) = x \tag{5.2}$$

Applying the transformation $T = \frac{pt^{\alpha}}{\alpha}$ and for convenience, we set $p = 1$. Thus, we acquire the following PDE

$$\frac{\partial u}{\partial T} = \left[-\frac{\partial}{\partial x}\left(3u - \frac{x}{2}\right) + \frac{\partial^2}{\partial x^2}(xu)\right]u(T,x) \tag{5.3}$$

which can be solved with the aid of DTM. Implementing the DTM to the Equations (5.2) and (5.3), we have the following relations

$$\begin{aligned} U(k+1,h) = \frac{1}{(k+1)}\Bigg[-(h+1)\Bigg(3\sum_{r=0}^{k}\sum_{s=0}^{h+1}U(r,h+1-s)U(k-r,s) - \frac{1}{2}U(k,h) \\ +(h+1)(h+2)\sum_{r=0}^{k}\sum_{s=0}^{h+1}U(r,h+1-s)U(k-r,s)\Bigg)\Bigg] \end{aligned} \tag{5.4}$$

By using the initial condition, we get

$$U(0,h) = \delta(h-1) \tag{5.5}$$

Utilizing relation (5.4) and transformed condition (5.5), for $k = 1,2,\cdots$ we obtain

$$U(k,h) = \begin{cases} \frac{1}{k!} = \frac{1}{\Gamma(k+1)}, & h=1 \\ 0, & \text{otherwise} \end{cases} \tag{5.6}$$

By using the inverse transform of DTM given in Equation (4.6), we have

$$u(T,x) = \sum_{k=0}^{\infty}\sum_{h=0}^{\infty}U(k,h)\ T^k x^h = x + xT + \frac{x}{2!}T^2 + \frac{x}{3!}T^3 + \frac{x}{4!}T^4 + \cdots$$

The inverse transformation of FCTM will yield the solution, which is expressed by,

$$u(t,x) = x + x\frac{t^{\alpha}}{\alpha} + \frac{x}{2!}\frac{t^{2\alpha}}{\alpha^2} + \frac{x}{3!}\frac{t^{3\alpha}}{\alpha^3} + \frac{x}{4!}\frac{t^{4\alpha}}{\alpha^4} + \cdots$$

According to [23, Theorem 4.1.], the above series corresponds to the conformable fractional power series expansion of

$$u(x,t) = xe^{\frac{t^{\alpha}}{\alpha}}$$

which is the analytical solution of problems (5.1)-(5.2).

Example 5.2. Regarding the nonlinear time-fractional Fokker-Planck equation:

$$D_t^{\alpha} u = \left[-\frac{\partial}{\partial x}\left(\frac{4u}{x} - \frac{x}{3}\right) + \frac{\partial^2}{\partial x^2}(u) \right] u(t,x) \tag{5.7}$$

Where $t > 0$, $x > 0$, and $0 < \alpha \leq 1$ are subject to the initial condition:

$$u(0,x) = x^2$$

Utilizing the considered method, as we have employed in Example 5.1, we obtain the following solution:

$$u(t,x) = x^2 \left(\frac{t^{\alpha}}{\alpha} + \frac{1}{2!}\frac{t^{2\alpha}}{\alpha^2} + \frac{1}{3!}\frac{t^{3\alpha}}{\alpha^3} + \frac{1}{4!}\frac{t^{4\alpha}}{\alpha^4} + \cdots \right)$$

Now, for the fractional power series expansion [23], this series has the closed form of the solution

$$u(x,t) = x^2 e^{\frac{t^{\alpha}}{\alpha}}$$

which is also an exact solution of the given diffusion equation.

6. Conclusion

In this study, we have successfully expressed FWTM with the help of DTM to get the approximate solution of the conformable fractional Fokker-Planck equation. Conformable fractional PDE can easily be changed into integer order PDE by fractional wave transform; thus, one can easily use the differential transform algorithm to solve this equation. The fractional wave transform is straightforward and applicable. The method is accessible to all with basic knowledge of advanced calculus and little fraction calculus. It is understood that FWTM-DTM is a very powerful and efficient technique for finding analytical and numerical solutions for broad classes of conformable fractional differential equations.

Author Contributions

All the authors contributed equally to this work. They all read and approved the last version of the manuscript.

Conflicts of Interest

The authors declare no conflict of interest.

References

[1] S. G. Samko, A. A. Kilbas, O. I. Marichev, Fractional Integrals and Derivatives: Theory and Applications, Gordon and Breach, Yverdon, 1993.

[2] I. Podlubny, Fractional Differential Equations, Academic Press, San Diego, 1999.

[3] S. Saha Ray, R. K. Bera, *An approximate solution of a nonlinear fractional differential equation by Adomian decomposition method*, Applied Mathematics and Computation, 167(1), (2005) 561–571.

[4] Z. M. Odibat, S. Momani, *Application of variational iteration method to nonlinear differential equations of fractional order*, International Journal of Nonlinear Sciences and Numerical Simulation, 7(1), (2006) 27–34.

[5] S. Momani, Z. Odibat, *Homotopy perturbation method for nonlinear partial differential equations of fractional order*, Physics Letters A, 365(5–6), (2007) 345–350.

[6] L. Song, H. Zhang, *Application of homotopy analysis method to fractional KdV-Burgers-Kuramoto equation*, Physics Letters A, 367(1–2), (2007) 88–94.

[7] J. K. Zhou, Differential Transformation and its Applications for Electric Circuits, Huazhong University Press, Wuhan, China, 1986, (in Chinese).

[8] M. Casso, S. Wortmann, U. Rizza, *Analytic modeling of two-dimensional transient atmospheric pollutant dispersion by double GITT and Laplace transform techniques*, Environmental Modelling & Software, 24(1), (2009) 144–151.

[9] E. Sejdic, I. Djurovic, L. Stankovic, *Fractional Fourier transform as a signal processing tool: an overview of recent developments*, Signal Processing, 91(6), (2011) 1351–1369.

[10] R. M. Cotta, M. D. Mikhailov, *Integral transform method*, Applied Mathematical Modelling, 17(3), (1993) 156–161.

[11] X. Yang, *Local fractional integral transforms*, Progress in Nonlinear Science, 4, (2011) 1–225.

[12] Z. Odibat, S. Momani, *Numerical solution of Fokker-Planck equation with space and time fractional derivatives*, Physics Letters A, 369(5–6), (2007) 349–358.

[13] M. Garg, P. Manohar, *Analytical solution of space-time fractional Fokker-Planck equations by generalized differential transform method*, Le Matematiche, 66, (2011) 91–101.

[14] Ü. Cansu, O. Özkan, *Solving Fokker-Planck equation by two-dimensional differential transform*, Advances in Mathematical and Computational Methods, 73, (2011) 1368.

[15] R. Khalil, M. A. Horani, A. Yousef, M. Sababheh, *A new definition of fractional derivative*, Journal of Computational and Applied Mathematics, 264, (2014) 65–70.

[16] K. S. Miller, B. Ross, An Introduction to the Fractional Calculus and Fractional Differential Equations, John Wiley & Sons, New York, 1993.

[17] A. Kilbas, H. M. Srivastava, J. J. Trujillo, Theory and Applications of Fractional Differential Equations, Elsevier, San Diego, 2006.

[18] H. Rezazadeh, J. Manaan, F. S. Khodadad, F. Nazari, *Traveling wave solutions for density-dependent conformable fractional diffusion-reaction equation by the first integral method and the improved* $\tan\frac{1}{2}\varphi(\xi)$*-expansion method*, Optical and Quantum Electronics, 50(3), (2018) Article Number: 121, 1–15.

[19] A. Korkmaz, O. E. Hepson, *Hyperbolic tangent solution to the conformable time fractional Zakharov-Kuznetsov equation in 3D space*, In AIP Conference Proceedings, 1926(1), (2018) 020023.

[20] M. S. Hashemi, *Some new exact solutions of (2+1)-dimensional nonlinear Heisenberg ferromagnetic spin chain with the conformable time-fractional derivative*, Optical and Quantum Electronics, 50(2), (2018) Article Number: 79, 1–11.

[21] C. Chen, Y. L. Jiang, *Simplest equation method for some time-fractional partial differential equations with conformable derivative*, Computers & Mathematics with Applications, 75(8), (2018) 2978–2988.

[22] O. Özkan, A. Kurt, *On conformable double Laplace transform*, Optical and Quantum Electronics, 50(2), (2018) Article Number: 103, 1–9.

[23] T. Abdeljawad, *On conformable fractional calculus, Journal of Computational and Applied Mathematics*, 279, (2015) 57–66.

[24] M. J. Jang, C. L. Chen, Y. C. Liu, *Two-dimensional differential transform for partial differential equations*, Applied Mathematics and Computation 121(2–3), (2001) 261–270.

[25] C. L. Chen, S. H. Ho, *Solving partial differential equations by two-dimensional transform method*, Applied Mathematics and Computation, 106(2–3), (1999) 171–179.

Journal of New Results in Science
https://dergipark.org.tr/en/pub/jnrs
Research Article
Open Access

E-ISSN:1304-7981 https://doi.org/10.54187/jnrs.1129440

A novel data processing approach to detect fraudulent insurance claims for physical damage to cars

Ahmet Yücel[1]

Keywords:
Artificial neural network,
Tree-based decision systems,
Support vector machines,
Singular value decomposition,
Data processing,
Natural language processing

Abstract — Some automobile insurance companies use computerized auto-detection systems to expedite claims payment decisions for insured vehicles. Claims suspected of fraud are evaluated using empirical data from previously investigated claims. The main objective of this manuscript is to demonstrate a novel data processing system and its potential for use in data classification. The data processing approach was used to develop a machine learning-based sentiment classification model to describe property damage fraud in vehicle accidents and the indicators of fraudulent claims. To this end, Singular Value Decomposition-based components and correlation-based composite variables were created. Machine learning models were then developed, with predictors and composite variables selected based on standard feature selection procedures. Five machine learning models were used: Boosted Trees, Classification and Regression Trees, Random Forests, Artificial Neural Networks, and Support Vector Machines. For all models, the models with composite variables achieved higher accuracy rates, and among these models, the artificial neural network was the model with the highest accuracy performance at 76.56%.

Subject Classification (2020): 62C25, 62P25.

1. Introduction

The insurance industry is constantly evolving. New technologies, such as artificial intelligence (AI) and machine learning (ML), provide new opportunities for insurers to detect fraudulent claims. These technologies can analyse data from various sources, such as social media and credit card transactions, etc., to determine the risk ratio of clients. Fraudulent insurance claims are a significant problem for the insurance industry. In 2004, the Insurance Information Institute calculated that fraudulent property and casualty claims were more than $30 billion annually [1]. Insurance claims for physical damage to cars are usually filed by taking pictures of the car and uploading them as evidence. This has become a significant problem because it can lead to increased premiums for all drivers [2], not just those who have made fraudulent claims. There are also costs associated with people who are falsely accused of fraud, which can lead to serious consequences, including job loss and even imprisonment [3]. Baader

[1]ayucel@ybu.edu.tr (Corresponding Author)
[1]Department of Finance and Banking, Şereflikoçhisar Faculty of Applied Sciences, Ankara Yıldırım Beyazıt University, Ankara, Turkiye
Article History: Received: 11 Jun 2022 — Accepted: 22 Aug 2022 — Published: 31 Aug 2022

and Krcmar aim to decrease the number of false positives in internal fraud detection using a novel approach based on process mining [4].

Machine learning is a type of AI that uses algorithms to learn from data and make predictions or decisions [5]. Fraudulent insurance claims are one example of how machine learning can be used to make decisions by identifying patterns and trends in fraudulent claims, which will help insurers save money and reduce the number of fraudulent claims they pay out. Ma et al. use ML algorithms to detect radio frequency identification (RFID) reading problems. One of the technical problems hindering the effective and reliable use of RFID is false positive detection. In other words, it is a misclassified labelling problem. Based on the features obtained from the data, logistic regression (LR), SVM, and tree-based models were built to distinguish the false-positive reads. The outcomes indicate that SVM provides the best accuracy [6]. Chand and Zhang provide a fraud prediction model for property insurance claims using different ML models based on real data from a large Brazilian insurance company. The accuracy of the models was evaluated by counting the number of false positives and negatives. The main techniques used were Random Forest (RF), Gradient Boosted Trees (BT), and Artificial Neural Networks (ANN) [7].

This kind of AI system aims to detect fraudulent transactions with high accuracy and low false positives. This AI system can detect fraudulent transactions in different sectors, such as banking, insurance, healthcare, and retail. Mishra and Dash propose an AI-based approach to determine fraudulent transactions. This type of online transaction can be easily performed with a person's stolen bank card details. Decision tree and ANN models were used for detection [8]. Van Capelleveen et al. explain how unsupervised outlier techniques can be applied post-payment to determine fraudulent patterns in health insurance claims [9]. Sabetti and Heijmans apply a specific ANN model to detect abnormal payment activity in the Canadian retail payment system. The study examines the model's ability to detect irregular changes in transaction flows [10].

An Artificial Neural Network (ANN) is a computer system modelled on the human brain, composed of a large number of interconnected artificial neurons [11]. ANNs are well suited to solving problems that are either too complex for humans to solve or too vast in size. Therefore, ANNs can be used to detect fraudulent cases and make decisions or predictions. Ansari and Riasi propose an ANN-based approach to assess customer loyalty in newly established insurance companies [12].

A tree-based decision system is a type of decision system that uses a tree structure to represent the possible decisions and their outcomes. The tree is generated by considering all the possible combinations of input variables, and the decision node is used to evaluate each combination.

Frempong et al. present an estimation model that calculates the probability of insurance coverage based on some potential risk factors of vehicle insurance. The age of the vehicle, the age of the insured, etc., are the main risk factors that predict the occurrence of vehicle damage [13].

Support Vector Machines (SVM) are an algorithm that predicts a data set's binary classification. SVMs are one of the most popular algorithms for binary classification, which is the prediction of two possible outcomes for an input value. This can be seen in fraud detection, which predicts whether an individual transaction is fraudulent or not. Gyamfi and Abdulai examine various forms of fraud in the database of monetary transactions in banking systems to determine potentially fraudulent transactions. They also introduce an SVM model that represents regular and irregular transaction behaviour and then use it to assess transaction validity [14]. It can also be seen in cancer detection. Badr et al. propose an SVM model for breast cancer diagnosis with effective scaling methods [15]. Support vector machines are often confused with other machine learning algorithms because they use similar terminology and techniques; however, they have different purposes and training procedures [16].

Natural Language Processing (NLP) has been on the rise in recent years. NLP is a subfield of Text Mining (TM) that focuses on understanding text and speech and the language used to represent unstructured information [17]. TM is an umbrella term for technologies that can be used to extract meaning from unstructured data, such as sentiment analysis [18], semantic analysis [19], discourse analysis [20], and summarization [21]. NLP has been applied to many fields to extract information from complex unstructured data sets in different industries. Zhang et al. propose a model to detect potentially fraudulent financial activities through textual analysis of financial reports of some Chinese companies [22]. Fu et al. use an NLP algorithm to analyse a dataset based on periprosthetic joint disease [23].

Data processing is an essential part of data analytics. It converts raw data into a format that a computer can use. Data is often processed to make it more useful, for example, by converting it to the machine-readable binary format or compressing the data's size. Nourani et al. used three methods to pre-process the data. These are wavelet-based de-noising (WD), jitted data-training (JD), and the hybrid method resulting from integrating these two methods. The objective of this study was to observe the effect of different data pre-processing approaches on the estimated values of the ANN-based prediction interval analysis. It has been concluded that pre-processing methods significantly contribute to reducing the impact of uncertainty [24]. Zhang et al. present a novel approach to data pre-processing based on nonparametric kernel-based modelling. The performance of the proposed approach was observed on SVM. Experimental results show that the proposed data pre-processing approach provides more reliable and stable results than the regular data processing methods [25]. Chilipirea et al. propose a novel data processing model for the datasets operated by smart cities. The model consists of the entire data flow from the source to the user of the extracted information. In general, the model includes the phases of data collection, normalization, categorization, storage, analysis, visualization, and decision support [26]. Using real-world data, Hanafy and Ming evaluate 13 ML methods. Due to the imbalanced datasets in the field, insurance fraud prediction has become a major challenge. They propose an approach to improve the results of ML algorithms by using novel resampling methods such as random over sampler, random under sampler, and combination of these two methods to solve the problem of imbalanced data. And Hanafy and Ming compare them with each other. The results show that the resampling techniques significantly improve the efficiency of all ML classifiers [27]. Severino and Pend investigated the prediction of property insurance claim fraud using several ML models based on real data. The models were tested iteratively, and the average prediction results were compared. Results showed that RF, BT, and ANN produced the best results compared to logistic regression (LR) [28]. Roy and George propose a study on detecting automobile insurance claims fraud using ML methods [29].

Feature selection (FS) is one of the most important stages of a data analysis process. FS techniques reduce the number of input variables by eliminating redundant or irrelevant features. The goal of FS in ML is to identify the most useful features that can be used to build the best model for the case study. Especially in the field of TM, it simplifies the multidimensional structure and complexity of the data while eliminating the overfitting problem. Secondly, the advantage of such an approach is that it leads to a drastic reduction of the computational cost, which can become very important in the analysis of unstructured real-time data. Reducing the number of features to as few as possible increases the model's accuracy and speed of analysis and makes it seem less cumbersome. The new approach presented in this study has shown that speed and accuracy have increased for all models in the literature with different algorithmic structures.

The novel approach in this study is about how we can use data processing and machine learning algorithms to generate correlation-based variables to improve the performance of AI-based decision-making models. The importance of the data processing approach in this study is that it is a kind of dimension reduction method that helps to make sense of the raw data, and it also helps to reduce the time needed for analysis. The ML models introduced in this study analyse the data of all the customers

who have submitted a claim for physical damage to their cars to detect any suspicious activity. They are mainly used to find out if there are any fraudulent claims for physical damage to cars.

The rest of the article is organized as follows. Section 2 presents the material and methodology of the study. Section 3 introduces the results of the proposed approach and models. Section 4 provides the conclusions.

2. Methodology

The data used in this study were collected from kaggle.com. The dataset, consisting of a total of 25 variables and 5589 cases, was collected to identify physical damage fraud related to vehicle accidents and to explain the indicators of fraud claims. In addition to the accuracy of fraud detection, this study also aims to identify the main factors that cause fraud. The definitions of the variables in the data are presented in Table 1.

Table 1. Variable definitions

Variable	Type	Role	Description
accident_site	Categorical	Input	Accident site
address_change_ind	Categorical	Input	Whether the driver has changed home address in the last 1 year
age_of_driver	Continuous	Input	Driver age
age_of_vehicle	Continuous	Input	Age of first-party vehicle
annual_income	Continuous	Input	Driver's annual income
channel	Categorical	Input	Policy buying channel
claim_day_of_week	Categorical	Input	Day of the week of first claim notification
claim_est_payout	Continuous	Input	Estimated claim payment
fraud	Categorical	Target	Fraud indicator (0=no, 1=yes)
gender	Categorical	Input	Driver's gender
high_education_ind	Categorical	Input	Driver's higher education index
liab_prct	Continuous	Input	Responsibility percentage of the request
living_status	Categorical	Input	Driver's living situation, owner or rental
marital_status	Categorical	Input	Driver's marital status
past_num_of_claims	Continuous	Input	Number of claims filed by the driver in the last 5-years
policy_report_filed_ind	Categorical	Input	Policy statement filed indicator
safty_rating	Continuous	Input	Driver's safety rating index
vehicle_category	Categorical	Input	First-party vehicle category
vehicle_color	Categorical	Input	First-party vehicle colour
vehicle_price	Continuous	Input	First-party vehicle price
vehicle_weight	Continuous	Input	First-party vehicle weight
witness_present_ind	Categorical	Input	Evidence of the allegation

The data contains information about the vehicle, such as age_of_vehicle, vehicle_color, and personal information about the driver who reported an accident, such as age_of_driver and gender. The fraud variable is a binary variable consisting of 0 and 1 and is used as the dependent variable. 0 means that the accident report is genuine, and 1 means that it is fake. The frequencies of the categorical variables are presented in table 2, and the descriptive statistics of the continuous variables are presented in Table 3.

Table 2. Frequency table of categorical variables

		Count	Per cent			Count	Per cent
vehicle_color	white	391	7	vehicle_category	Compact	1910	34.17
	grey	392	7.01		Large	1813	32.44
	red	400	7.16		Medium	1866	33.39
	other	383	6.85	accident_site	Local	2869	51.33
	black	2140	38.29		Highway	1308	23.40
	blue	1465	26.21		Parking Lot	1412	25.26
	silver	418	7.48	policy_report_filed_ind	not reported	2171	38.84
living_status	Rent	2510	44.91		reported	3418	61.16
	Own	3079	55.09	marital_status	not married	1791	32.05
claim_day_of_week	Friday	753	13.47		married	3798	67.95
	Thursday	746	13.35	high_education_ind	highschool	1930	34.53
	Tuesday	830	14.85		undergrad	3659	65.47
	Saturday	818	14.64	address_change_ind	changed	3399	60.82
	Wednesday	817	14.62		not changed	2190	39.18
	Sunday	835	14.94	witness_present	not present	4446	79.55
	Monday	790	14.13		present	1143	20.45
channel	Broker	2929	52.41	gender	female	2755	49.29
	Online	821	14.69		male	2834	50.71
	Phone	1839	32.90				

Table 3. Descriptive statistics of continuous variables

	Valid N	Mean	Median	Minimum	Maximum	Std.Dev.
age_of_driver	5589	42.82	42	18	229.0	11.53
safty_rating	5589	0.73	0.76	0.01	1.0	0.16
annual_income	5589	37220.51	37382	28910	54333.0	2671.84
past_num_of_claims	5589	0.61	0	0	6.0	1.07
liab_prct	5589	49.27	50	0	100.0	33.23
claim_est_payout	5589	4951.37	4615.43	282.64	17218.4	2303.72
age_of_vehicle	5589	5.11	5	0	15.0	2.26
vehicle_price	5589	22960.15	20871.74	2722.86	100224.7	11988.58
vehicle_weight	5589	23180.90	20904	2713.47	95464.4	12096.46

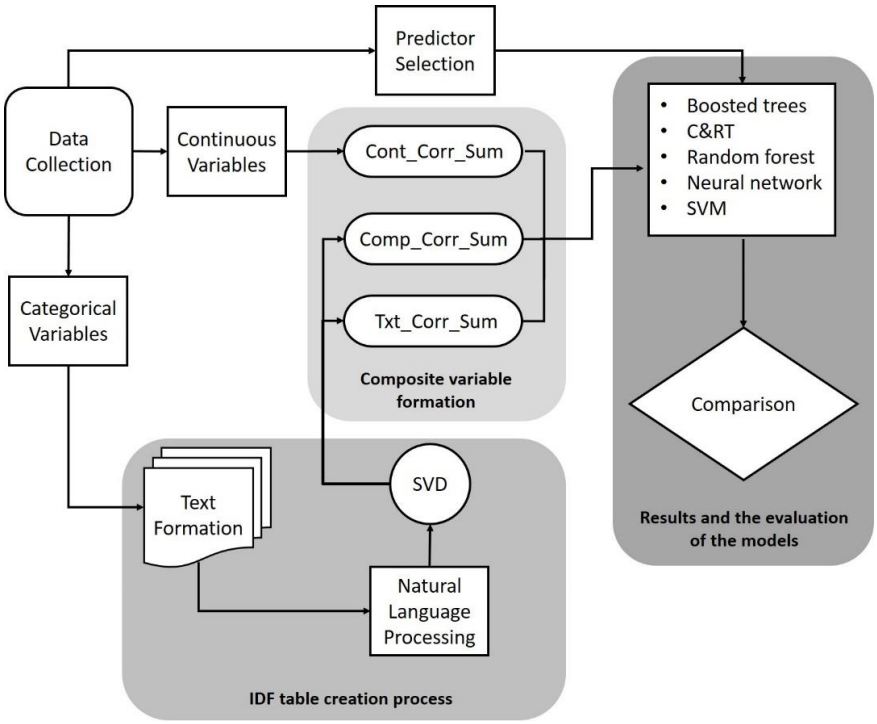

Figure 1. Overview of the proposed methodology

The proposed novel data processing approach (as depicted in Figure 1) consists of 3 basic steps. In the first step, the variables in the data are divided into a categorical and a continuous part, and the categories of the categorical variables are labelled with the words to which they correspond. Thus, for each case, a text is formed consisting of the categories of the categorical variables. In the second step, the texts were processed with Natural Language Processing (NLP), and then a table of frequency of terms and documents was created, where each category was a variable. The inverse document frequency (IDF) method was used to create the frequency table. Natural Language Processing (NLP) is the field of computer science and artificial intelligence that deals with the relations between computers and human (natural) language, specifically how to program computers to process and investigate large amounts of natural textual data. NLP has a wide range of applications, from search engines (e.g., Google) that can automatically find online information relevant to a query to speech recognition systems that can translate spoken words into text. Inverse document frequency (IDF) is a statistical measure of how important a word or phrase is in a document. It is calculated as the logarithm of the number of documents containing the term divided by the total number of documents in which it occurs [30].

Then, the new variables created based on the categories were reduced to composite variables (SVD components) using the singular value decomposition (SVD) method. SVD is a linear algebra technique used to generate the best approximation to a matrix [31].

The covariance value between x and y is calculated with the formula

$$cov(x,y) = \sum_{i=1}^{n} (x_i - \bar{x})(y_i - \bar{y})/n \tag{2.1}$$

The values $\bar{x}$ and $\bar{y}$ are the arithmetic mean of the variables x and y. The correlation value between x and y is calculated with the formula

$$r_{xy} = cov(x,y)/S_x S_y \tag{2.2}$$

where the standard deviations S_x and S_y are any two non-zero variables, and r_{xy} takes a value in the range [0,1].

Let $r_i,\ i = 1,2,\dots,n$ be correlations between the continuous variables $C_1,\ C_2,\ C_3,\ \dots\ C_n$ and dependent variable 'fraud' and let R_{Cont} be a vector of the correlations such that

$$R_{Cont} = \begin{bmatrix} r_1 \\ r_2 \\ r_3 \\ \vdots \\ r_n \end{bmatrix} \tag{2.3}$$

Therefore,

$$\text{Cont\_Corr\_Sum} = [C_1 \quad C_2 \quad C_3 \quad \dots \quad C_n] \cdot R_{Cont} \tag{2.4}$$

Let $t_i,\ i = 1,2,\dots,m$ be correlations between the NLP-generated IDF-based variables $T_1,\ T_2,\ T_3,\ \dots\ T_m$ and dependent variable 'fraud' and let R_{Text} be a vector of the correlations such that

$$R_{Text} = \begin{bmatrix} t_1 \\ t_2 \\ t_3 \\ \vdots \\ t_m \end{bmatrix} \tag{2.5}$$

$$\text{Txt\_Corr\_Sum} = [T_1,\ T_2,\ T_3,\ \dots\ T_m] \cdot R_{Text} \tag{2.6}$$

Similarly, let $s_i,\ i = 1,2,\dots,k$ be correlations between the SVD-generated IDF-based components $K_1, K_2, K_3, \dots, K_k$ and dependent variable 'fraud' and let R_{Comp} be a vector of the correlations such that

$$R_{Comp} = \begin{bmatrix} s_1 \\ s_2 \\ s_3 \\ \vdots \\ s_k \end{bmatrix} \tag{2.7}$$

$$\text{Comp\_Corr\_Sum} = [K_1,\ K_2,\ K_3,\ \dots\ K_k] \cdot R_{Comp} \tag{2.8}$$

In the third step, weight was assigned according to the correlation values of the continuous variables with the dependent variable. The correlation matrices R_Cont, R_Text, and R_Comp, were used to assign the weights, resulting in the composite variables *Cont_Corr_Sum*, *Txt_Corr_Sum*, and *Comp_Corr_Sum*. The rank order of importance of the predictors of the composite variables is shown in Table 4. In Statistica, the importance of the estimator is calculated by subtracting or adding the change (delta) in impurity (in other words, the measure of homogeneity) of all nodes in the decision tree. The order of the values obtained corresponds to the order of importance of the estimators [32].

Table 4. Composite predictors' importance

Variable	Rank	Importance
Txt_Corr_Sum	100.00	1.00
Comp_Corr_Sum	94.00	0.94
Cont_Corr_Sum	12.00	0.12

All available variables were used to construct each composite variable, a size reduction method. This approach minimizes the loss of information in the raw data. To observe the difference in performance between the two approaches, standard and composite, all independent variables were used in the predictor selection step when constructing standard models. The variables labelled as important at a confidence level of alpha 0.05 are listed in order of importance in Table 5.

Table 5. Raw data predictor importance

Variable	Rank	Importance
vehicle_color	100	1.00
annual_income	43	0.43
age_of_driver	39	0.39
past_num_of_claims	33	0.33
claim_est_payout	29	0.29
gender	27	0.27
policy_report_filed_ind	21	0.21
high_education_ind	21	0.21
safty_rating	20	0.20
liab_prct	20	0.20
vehicle_weight	19	0.19
claim_day_of_week	19	0.19
accident_site	19	0.19
marital_status	19	0.19
age_of_vehicle	18	0.18
witness_present_ind	17	0.17
vehicle_price	15	0.15
address_change_ind	12	0.12
channel	10	0.10
living_status	5	0.05
vehicle_category	4	0.04

In the fourth step, machine learning models (ML) were designed with variables selected from the raw data using the standard predictor selection method, and composite variables were produced based on the original data processing approach. 5 different ML models were used, namely BT, C&RT, RF, ANN, and SVM. The models were trained and developed on a 70% training set and applied on a 30% test set.

3. Results and Discussion

C&RT is a type of decision tree used to predict values. The classification tree divides the data into two or more groups, while the regression tree predicts an output value for an input value. The number of non-terminal nodes is 17, and the number of terminal nodes is 18 in C&RT, which was designed using the standard method.

Support Vector Machines (SVM) is an ML algorithm for classification and regression. An SVM consists of two collections of data points: The first collection is called support vectors, and the other collection is called margins. The margin is created by selecting a point on either side of the dividing line and then finding all points on either side of that line. In the models created according to standard and composite variables, the Radial Basis Function (RBF) was used as the kernel function, the fixed value was set to 1, and the gamma value was set to 3. In addition, in the standard method, a total of 1000 separating lines (SVs) in 500 categories 0s and 500 categories 1s were used to estimate the categories (0/1) of the dependent variable. In the composite variable-based method, a total of 890 SVs (452 (0s) + 438 (1s)) were used.

ANN is a computer model inspired by the brain's biological neural networks. They are used for various applications, from medical diagnosis to image mining [33,34]. ANN is also increasingly used for prediction tasks. A typical ANN consists of many neurons arranged in layers, with connections between the layers. These connections form a pattern known as the synaptic weight for that neuron and its neighbours. The process of training an artificial neural network is called backpropagation. In this process, the synaptic weights are iteratively adjusted to improve the predictive ability of the system for future data points [35].

The multi-layer perceptron (MLP) ANN model was used for both approaches. There are 46 predictors and 2 outputs (prediction) in the model ANN, which was built using the standard approach, and there are 3 predictors and 2 outputs in the composite-based ANN model. In addition, both models have 9 hidden layers. When training the models based on the training data, the Broyden-Fletcher-Goldfarb-Shanno (BFGS) 6 training algorithms were used in the standard approach, and BFGS 18 training algorithms were used in the composite approach. In the standard and composite approaches, SOS and entropy were used as error functions, identity as the hidden layer activation function for both, and Tanh and softmax as the output activation functions, respectively.

RF is an ML method used for classification and regression. It is an ensemble model that combines multiple decision trees to make more accurate predictions. The RF can be used for many tasks, from predicting the stock market to classifying documents. In this study, the maximum number of trees is 100 in RF, which are created using standard and composite methods.

Boosted trees (BT) are a type of classification algorithm. The algorithm is based on the idea that classification accuracy can be improved by training a set of decision trees on different subsets of the data and combining their decisions into a final prediction. The optimal number of trees is 88, and the maximum tree size is 13 in the model BT, which was built using the standard method. In the BT model, which was created with composite variables, the optimal number of trees is 49, and the maximum tree size is 13.

Table 6. Cross-tabulation and accuracy rates

Method \ Model		Boosted Trees Prediction		CandRT Prediction		Random Forest Prediction		ANN Prediction		SVM Prediction	
		0	1	0	1	0	1	0	1	0	1
Standard	0	478	358	382	454	364	472	314	522	476	360
	1	162	674	160	676	169	667	151	685	378	458
Accuracy Rates		68.9		63.28		61.66		59.75		55.86	
Composite	0	599	237	467	369	608	228	634	202	543	293
	1	182	654	168	668	172	664	190	646	170	666
Accuracy Rates		74.94		67.88		76.08		76.56		72.31	
Improvement rate (%)		8.77		7.27		23.39		28.13		29.45	

The aggregate results of the cross-tabulation prediction in a confusion matrix are shown in Table 6. As can be seen from the results, among the models based on the standard procedure, Boosted Trees outperformed the other models with an accuracy of 68.9%, while CandRT, RF, ANN, and SVM achieved accuracy rates of 63.28%, 61.66%, 59.75%, and 55.86%, respectively. In addition, as is represented in the results, among the models built based on the SVD components and composite variable procedure, ANN outperformed the other models by achieving an accuracy rate of 76.56%, while BT, C&RT, RF, and SVM achieved accuracy rates of 74.94%, 67.88%, 76.08%, and 72.31%, respectively.

4. Conclusion

The main objective of this manuscript is to demonstrate a novel data processing framework and its potential for use in data classification. The framework was used to develop an ML-based sentiment classification model to describe the physical damage fraud in vehicle accidents and the indicators of fraud claims. This study is not only concerned with the accuracy of fraud detection but also with determining the main factors that cause fraud.

For this purpose, SVD-based components and correlation-based composite variables were created. Machine learning models (ML) were then developed, with predictors and composite variables selected based on standard feature selection methods. 5 different ML models were used, namely BT, C&RT, RF, ANN, and SVM. For all models, the models with composite variables achieved higher accuracy rates, and among these models, ANN was the model with the highest accuracy performance at 76.56%.

As shown in Table 6, the novel data processing approach proposed in this study resulted in an increase in the accuracy of the models ranging from 7.27% to 29.45%. This represents a successful and significant improvement of 22.06% on average.

Author Contributions

The author read and approved the last version of the manuscript.

Conflicts of Interest

The author declares no conflict of interest.

Appendix 1. Data

The raw data used in this article can be found online at

https://www.kaggle.com/datasets/surekharamireddy/fraudulent-claim-on-cars-physical-damage

Appendix 2. Coding

The coding of the statistical procedures used in this article can be found online at

CODES - A novel data processing approach to detect fraudulent insurance

References

[1] S. Viaene, M. Ayuso, M. Guillen, D. V. Gheel, G. Dedene, *Strategies for detecting fraudulent claims in the automobile insurance industry*, European Journal of Operational Research, 176(1), (2007) 565–583.

[2] T. Baldock, Insurance fraud. Australian Institute of Criminology: Trends and issues in crime and criminal justice, 66, (1997).

[3] I. Akomea-Frimpong, C. Andoh, E. Ofosu-Hene, *Causes, effects and deterrence of insurance fraud: evidence from Ghana*, Journal of Financial Crime, 23(4), (2016) 678–699.

[4] G. Baader, H. Krcmar, *Reducing false positives in fraud detection: Combining the red flag approach with process mining*, International Journal of Accounting Information Systems, 31, (2018) 1–16.

[5] J. Nahr, H. Nozari, M. E. Sadeghi, *Artificial intelligence and machine learning for real-world problems (A survey)*, International journal of innovation in Engineering, 1(3), (2021) 38–47.

[6] H. Ma, Y. Wang, K. Wang, *Automatic detection of false positive RFID readings using machine learning algorithms*, Expert Systems with Applications, 91, (2018) 442–451.

[7] S. Chand, Y. Zhang, *Learning from machines to close the gap between funding and expenditure in the Australian National Disability Insurance Scheme*, International Journal of Information Management Data Insights, 2(1), (2022) 1–15.

[8] M. K. Mishra, R. Dash, *A comparative study of Chebyshev functional link artificial neural network, multi-layer perceptron and decision tree for credit card fraud detection*, in: S. P. Mohanty, R. K. Patnaik, M. Gomathisankaran, B. S. Panda (Eds.) International Conference on Information Technology 2014, Bhubaneswar, India, 2014, pp. 228–233.

[9] G. van Capelleveen, M. Poel, R. M. Mueller, D. Thornton, J. van Hillegersberg, *Outlier detection in healthcare fraud: A case study in the Medicaid dental domain*, International Journal of Accounting Information Systems, 21, (2016) 18–31.

[10] L. Sabetti, R. Heijmans, *Shallow or deep? Training an autoencoder to detect anomalous flows in a retail payment system*, Latin American Journal of Central Banking, 2(2), (2021) 1–14.

[11] J. Jiang, P. Trundle, J. Ren, *Medical image analysis with artificial neural networks*, Computerized Medical Imaging and Graphics, 34(8), (2010) 617–631.

[12] A. Ansari, A. Riasi, *Modelling and evaluating customer loyalty using neural networks: Evidence from startup insurance companies*, Future Business Journal, 2(1), (2016) 15–30.

[13] N. K. Frempong, N. Nicholas, M. A. Boateng, *Decision tree as a predictive modeling tool for auto insurance claims*, International Journal of Statistics and Applications, 7(2), (2017) 117–120.

[14] N. K. Gyamfi, J. D. Abdulai, *Bank fraud detection using support vector machine*, in: V. Leung, S. Vuong, S. Chakrabarti (Eds.), IEEE 9th Annual Information Technology, Electronics and Mobile Communication Conference (IEMCON) 2018, Vancouver, BC, Canada, 2018, pp. 37–41.

[15] E. Badr, S. Almotairi, M. A. Salam, H. Ahmed, *New sequential and parallel support vector machine with grey wolf optimizer for breast cancer diagnosis*. Alexandria Engineering Journal, 61(3), (2022) 2520–2534.

[16] G. Tolan, T. Abou-El-Enien, M. Khorshid, *A comparison among support vector machine and other machine learning classification algorithms*, IPASJ International Journal of Computer Science (IIJCS), 3(5), (2015) 25–35.

[17] A. Kao, S. R. Poteet, Natural language processing and text mining, Springer Publishing Company, 2006.

[18] N. Chintalapudi, G. Battineni, M. D. Canio, G. G. Sagaro, F. Amenta, *Text mining with sentiment analysis on seafarers' medical documents*, International Journal of Information Management Data Insights, 1(1), (2021) 1–9.

[19] R. Alfrjani, T. Osman, G. Cosma, *A hybrid semantic knowledgebase-machine learning approach for opinion mining*, Data and Knowledge Engineering, 121, (2019) 88–108.

[20] E. Teso, M. Olmedilla, M. Martínez-Torres, S. Toral, *Application of text mining techniques to the analysis of discourse in eWOM communications from a gender perspective*, Technological Forecasting and Social Change, 129, (2018) 131–142.

[21] O. Rouane, H. Belhadef, M. Bouakkaz, *Combine clustering and frequent itemsets mining to enhance biomedical text summarisation*, Expert Systems with Applications, 135, (2019) 362–373.

[22] Y. Zhang, A. Hu, J. Wang, Y. Zhang, *Detection of fraud statement based on word vector: Evidence from financial companies in China*, Finance Research Letters, 46, (2022) 1–7.

[23] S. Fu, C. C. Wyles, D. R. Osmon, M. L. Carvour, E. Sagheb, T. Ramazanian, H. M. Kremers, *Automated detection of periprosthetic joint infections and data elements using natural language processing*, The Journal of Arthroplasty, 36(2), (2021) 688–692.

[24] V. Nourani, M. Sayyah-Fard, M. T. Alami, E. Sharghi, *Data pre-processing effect on ANN-based prediction intervals construction of the evaporation process at different climate regions in Iran*, Journal of Hydrology, 588, (2020) 1–15.

[25] W. Zhang, T. Liu, L. Ye, M. Ueland, S. L. Forbes, S. W. Su, *A novel data pre-processing method for odour detection and identification system*, Sensors and Actuators A: Physical, 287, (2019) 113–120.

[26] C. Chilipirea, A. C. Petre, L. M. Groza, C. Dobre, F. Pop, *An integrated architecture for future studies in data processing for smart cities*, Microprocessors and Microsystems, 52, (2017) 335–342.

[27] M. Hanafy, R. Ming*, Using machine learning models to compare various resampling methods in predicting insurance fraud*, Journal of Theoretical and Applied Information Technology, 99(12), (2021), 2819–2833.

[28] M. K. Severino, Y. Peng, *Machine learning algorithms for fraud prediction in property insurance: Empirical evidence using real-world microdata*, Machine Learning with Applications, 5, (2021) 1–14.

[29] R. Roy, K. T. George, *Detecting insurance claims fraud using machine learning techniques*, in: K. P. Isaac, A. Rahiman, G. P. Padmakumar (Eds.), International Conference on Circuit, Power and Computing Technologies (ICCPCT) 2017, Kollam, India, 2017, pp. 1–6.

[30] G. Miner, D. Delen, J. Elder, A. Fast, T. Hill, R. A. Nisbet, *Conceptual foundations of text mining and pre-processing steps, practical text mining and statistical analysis for non-structured text data applications*, Academic Press. (2012) 43–51.

[31] A. K. Menon, C. Elkan, *Fast algorithms for approximating the singular value decomposition*, ACM Transactions on Knowledge Discovery from Data, 5(2), (2011) 1–36.

[32] TIBCO product documentation, Data Science Textbook, https://docs.tibco.com/data-science/GUID-4C6F72C1-F4F8-48A9-83C7-D4C72A66A3AC.html (Accessed on 14.08.2022)

[33] C. Peña-Bautista, T. Durand, C. Oger, M. Baquero, M. Vento, C. Cháfer-Pericás, *Assessment of lipid peroxidation and artificial neural network models in early Alzheimer disease diagnosis*, Clinical Biochemistry, 72, (2019) 64–70.

[34] R. Azadnia, K. Kheiralipour, *Recognition of leaves of different medicinal plant species using a robust image processing algorithm and artificial neural networks classifier*, Journal of Applied Research on Medicinal and Aromatic Plants, 25, (2021) 1–10.

[35] C. Li, R. Chen, C. Moutafis, S. Furber, *Robustness to noisy synaptic weights in spiking neural networks*, in: A. Roy (Ed.), International Joint Conference on Neural Networks (IJCNN) 2020, Glasgow, UK, 2020, pp. 1–8.

Journal of New Results in Science 11(2) (2022) 132-142

Journal of New Results in Science

https://dergipark.org.tr/en/pub/jnrs

Research Article

Open Access

E-ISSN: 1304-7981 https://doi.org/10.54187/jnrs.1143905

Some generalised extended incomplete beta functions and applications

Oğuz Yağcı[1], **Recep Şahin**[2], **İsmail Onur Kıymaz**[3], **Ayşegül Çetinkaya**[4]

Keywords

Gamma function,
Beta function,
Incomplete beta function,
Beta distribution

Abstract — This paper introduces generalised incomplete beta functions defined by the generalised beta function. Firstly, we provide some of the generalised beta function's basic properties, such as integral representations, summation formulas, Mellin transform, and beta distribution. We then present several fundamental properties, such as integral representations, summation formulas, and recurrence relations with the help of the generalised incomplete beta functions.

Subject Classification (2020): 33B20, 60B99.

1. Introduction

The classical beta function $B(a,b)$ is defined by [1–4]

$$B(a,b)=\int_0^1 t^{a-1}(1-t)^{b-1}dt,\quad \Re(a),\Re(b)>0 \tag{1.1}$$

Moreover, the incomplete beta function $B_\tau(a,b)$ is defined by [1, 2]

$$B_\tau(a,b)=\int_0^\tau t^{a-1}(1-t)^{b-1}dt,\quad \Re(a),\Re(b)>0,\ \text{and } 0<\tau<1 \tag{1.2}$$

In 1997, Chaudhry and Zubair [5] defined and investigated extension of beta function

$$B_p(a,b)=\int_0^1 t^{a-1}(1-t)^{b-1}\exp\left(\frac{-p}{t(t-1)}\right)dt,\quad \Re(p)>0\,\Re(a),\Re(b)>0 \tag{1.3}$$

Here, if $p=0$, this equation reduces to the classical beta function provided in Equation (1.1). Furthermore, the extension of incomplete beta function $B_\tau(a,b)$ is given by [5]

$$B_p(a,b;\tau)=\int_0^\tau t^{a-1}(1-t)^{b-1}\exp\left(\frac{-p}{t(t-1)}\right)dt,\quad \Re(p)>0,\Re(a),\Re(b)>0 \text{ and } 0<\tau<1 \tag{1.4}$$

[1]oguzyagci26@gmail.com (Corresponding Author); [2]recepsahin@kku.edu.tr; [3]iokiymaz@ahievran.edu.tr; [4]acetinkaya@ahievran.edu.tr

[1,2]Department of Mathematics, Faculty of Arts and Sciences, Kırıkkale University, Kırıkkale, Turkiye

[3,4]Department of Mathematics, Faculty of Arts and Sciences, Ahi Evran University, Kırşehir, Turkiye

Article History: Received: 14 Jul 2022 - Accepted: 22 Aug 2022 - Published: 31 Aug 2022

It is easily yielded that setting $\tau = 1$ in Equation (1.4), which provides us the special case of extension of beta function (1.3), and taking $p = 0$ and $\tau = 1$ in Equation (1.4) reduces to Equation (1.1). It will be observed that this expansion is fruitful because it expresses most of the properties of the beta function naturally and simply. They also expressed various integral representations, Mellin transform, a large number of properties and cases from the point of special functions.

Afterwards, Özergin et al. [6] introduced and considered the generalisation of beta function as given:

$$B_p^{\{\alpha,\beta\}}(a,b) = \int_0^1 t^{a-1}(1-t)^{b-1}\,{}_1F_1\left(\alpha;\beta;\frac{-p}{t(t-1)}\right)dt, \quad \Re(p)>0, \Re(\alpha),\Re(\beta)>0, \Re(a),\Re(b)>0 \tag{1.5}$$

In 2011, Parmar and Chopra [7] obtainded the generalisation of incomplete beta function given as follows:

$$B_{p;\tau}^{\{\alpha,\beta\}}(a,b) = \int_0^\tau t^{a-1}(1-t)^{b-1}\,{}_1F_1\left(\alpha;\beta;\frac{-p}{t(t-1)}\right)dt, \quad \Re(p)>0, \Re(\alpha),\Re(\beta)>0, \Re(a),\Re(b)>0 \text{ and } 0<\tau<1 \tag{1.6}$$

It is observed that putting $\alpha = \beta$ and $p = 0$ in Equation (1.5), which gives us Equation (1.1). Besides, setting $\tau = 1$ in Equation (1.6) reduces to Equation (1.5).

Proceeding from the generalisations of the beta function expressed above, various generalisations of Equation (1.1) have been introduced and investigated by many authors (see [8–23]).

Throughout this paper, let $\mathbb{C}$, $\mathbb{Z}_0^-$, and $\mathbb{N}$ be the sets of complex numbers, non-positive integers, and positive integers, respectively, and assume that $\Re(p),\Re(q),\Re(\kappa),\Re(\mu)>0,\Re(\nu)>0,\Re(x)>0$. Recently, Şahin et al. [24] proposed a generalisation of the extended beta function as follows:

$$B_{p,q}^{(\kappa,\mu)}(a,b) = \int_0^1 t^{a-1}(1-t)^{b-1}\exp\left(-\frac{p}{t^\kappa}-\frac{q}{(1-t)^\mu}\right)dt \tag{1.7}$$

First, by selecting a known generalisation of Equation (1.7), systematically, we goal to determine further properties and representations for this beta function such as integral representations, Mellin transform. Next, we introduce a new generalisation of the extended incomplete beta function using Equation (1.7). Moreover, we obtain its integral representations and examine its various properties. Finally, we provide the beta distribution for a new generalisation of the extended beta function provided in Equation (1.7).

2. Integral Representaions of Equation (1.7)

This section presents various integral representations of Equation (1.7), professed in the following theorem.

Theorem 2.1. The following integral representation for the function $B_{p,q}^{(\kappa,\mu)}(a,b)$ given by Equation (1.7) holds true:

$$\int_0^\infty\int_0^\infty p^{\zeta-1}q^{\eta-1}B_{p,q}^{(\kappa,\mu)}(a,b)\,dp\,dq = \Gamma(\zeta)\Gamma(\eta)B(a+\kappa\zeta,b+\mu\eta), \quad \Re(a+\kappa\zeta),\Re(b+\mu\eta)>0 \tag{2.1}$$

Proof.
Multiplying each side of Equation (1.7) by $p^{\zeta-1}q^{\eta-1}$ and integrating with respect to $0 \le p, q < \infty$, we get

$$\int_0^\infty\int_0^\infty p^{\zeta-1}q^{\eta-1}B_{p,q}^{(\kappa,\mu)}(a,b)\,dp\,dq = \int_0^\infty\int_0^\infty p^{\zeta-1}q^{\eta-1}\left\{\int_0^1 t^{a-1}(1-t)^{b-1}\exp\left(-\frac{p}{t^\kappa}-\frac{q}{(1-t)^\mu}\right)dt\right\}dp\,dq \tag{2.2}$$

Because of the uniform convergence, we can be changed the order of integration in Equation (2.2). Thus,

we obtain

$$\int_0^\infty \int_0^\infty p^{\zeta-1} q^{\eta-1} B_{p,q}^{(\kappa,\mu)}(a,b)\,dp\,dq = \int_0^1 t^{a-1}(1-t)^{b-1}\Big\{\int_0^\infty p^{\zeta-1}\exp\Big(-\frac{p}{t^\kappa}\Big)dp \int_0^\infty q^{\eta-1}\exp\Big(-\frac{q}{(1-t)^\mu}\Big)dq\Big\}dt \quad (2.3)$$

Further, the above integrals can be reduced in terms of the gamma function to give Theorem 2.1.

$$\begin{aligned}\int_0^\infty \int_0^\infty p^{\zeta-1} q^{\eta-1} B_{p,q}^{(\kappa,\mu)}(a,b)\,dp\,dq &= \Gamma(\zeta)\Gamma(\eta)\int_0^1 t^{a+\kappa\zeta-1}(1-t)^{b+\mu\eta-1}dt \\ &= \Gamma(\zeta)\Gamma(\eta)B(a+\kappa\zeta, b+\mu\eta)\end{aligned} \quad (2.4)$$

Remark 2.2. Taking $\zeta = 1$ and $\eta = 1$ in (2.1), we have

$$\int_0^\infty \int_0^\infty B_{p,q}^{(\kappa,\mu)}(a,b)\,dp\,dq = B(a+\kappa, b+\mu) \quad (2.5)$$

Moreover, taking $\kappa = 1$ and $\mu = 1$ in Equation (2.5), which gives us the special case of integral representation for extended beta function [9].

Theorem 2.3. The following integral representations for the function $B_{p,q}^{(\kappa,\mu)}(a,b)$ given by Equation (1.7) hold true, for $\Re(a), \Re(b) > 0$,

$$B_{p,q}^{(\kappa,\mu)}(a,b) = \int_0^\infty \frac{u^{a-1}}{(1+u)^{a+b}}\exp\Big(-\frac{p(1+u)^\kappa}{u^\kappa} - q(1+u)^\mu\Big)du \quad (2.6)$$

$$B_{p,q}^{(\kappa,\mu)}(a,b) = 2^{1-a-b}\int_{-1}^1 (1+u)^{a-1}(1-u)^{b-1}\exp\Big(-\frac{p2^\kappa}{(1+u)^\kappa} - \frac{q2^\mu}{(1-u)^\mu}\Big)du \quad (2.7)$$

$$B_{p,q}^{(\kappa,\mu)}(a,b) = 2\int_0^{\frac{\pi}{2}} \cos^{2a-1}\theta \sin^{2b-1}\theta \exp\big(-p\sec^{2\kappa}\theta - q\csc^{2\mu}\theta\big)d\theta \quad (2.8)$$

$$B_{p,q}^{(\kappa,\mu)}(a,b) = (y-x)^{1-a-b}\int_x^y (u-x)^{a-1}(y-u)^{b-1}\exp\Big(-\frac{p(y-x)^\kappa}{(u-x)^\kappa} - \frac{q(y-x)^\mu}{(y-u)^\mu}\Big)du \quad (2.9)$$

$$B_{p,q}^{(\kappa,\mu)}(a,b) = 2\int_0^\infty \tanh^{2a-1}\theta\, sech^{2b}\theta \exp\big(-p\coth^{2\kappa}\theta - q\cosh^{2\mu}\theta\big)\,d\theta \quad (2.10)$$

Proof.

Putting to use the transformations $t = \frac{u}{u+1}$, $t = \frac{1+u}{2}$, $t = \cos^2\theta$, and $t = \frac{u-x}{y-u}$ in Equation (1.7) and $\sinh^2\theta$ in Equation (2.1). Therefore, we can be obtained Equations (2.6), (2.7), (2.8), (2.9), and (2.10), respectively.

Corollary 2.4. If setting $\kappa = \mu$ in Equations (2.6), (2.7), and (2.9), the following integral representations are obtained, respectively.

$$B_{p,q}^{(\kappa,\kappa)}(a,b) = \int_0^\infty \frac{u^{a-1}}{(1+u)^{a+b}}\exp\Big((1+u)^\kappa\Big[-q - \frac{p}{u^\kappa}\Big]\Big)du \quad (2.11)$$

$$B_{p,q}^{(\kappa,\kappa)}(a,b) = 2^{1-a-b}\int_{-1}^1 (1+u)^{a-1}(1-u)^{b-1}\exp\Big(\Big[\frac{2}{1-u^2}\Big]^\kappa\big[-p(1-u)^\kappa - q(1+u)^\kappa\big]\Big)du \quad (2.12)$$

$$B_{p,q}^{(\kappa,\kappa)}(a,b) = (y-x)^{1-a-b}\int_x^y (u-x)^{a-1}(y-u)^{b-1}\exp\Big(\Big[\frac{(y-x)}{u^2+(x+y)u-xy}\Big]^\kappa\big[-p(y-u)^\kappa - q(u-x)^\kappa\big]\Big)du \quad (2.13)$$

Remark 2.5. Applying $\kappa = 1$ in Equations (2.11), (2.12), and (2.13), we obtain a special case of integral representation for extended beta function [9].

3. Certain Formulas for Equation (1.7)

This part obtains a functional relation and some summation formulas for Equation (1.7).

Theorem 3.1. The following functional relation for the function $B_{p,q}^{\kappa,\mu}(a,b)$ given by Equation (1.7) holds true:

$$B_{p,q}^{(\kappa,\mu)}(a,b) = B_{p,q}^{(\kappa,\mu)}(a+1,b) + B_{p,q}^{(\kappa,\mu)}(a,b+1) \tag{3.1}$$

Proof.

The right hand side of (3.1) occurs

$$B_{p,q}^{(\kappa,\mu)}(a+1,b) + B_{p,q}^{(\kappa,\mu)}(a,b+1) = \int_0^1 \left[t^a (1-t)^{b-1} + t^{a-1}(1-t)^b \right] \exp\left(-\frac{p}{t^\kappa} - \frac{q}{(1-t)^\mu} \right) dt \tag{3.2}$$

which after a simple arrangement, becomes to the left hand side of (3.1).

Theorem 3.2. The following summation formula for the function $B_{p,q}^{\kappa,\mu}(a,b)$ given by Equation (1.7) holds true:

$$B_{p,q}^{(\kappa,\mu)}(a,1-b) = \sum_{m=0}^{\infty} \frac{(b)_m}{m!} B_{p,q}^{(\kappa,\mu)}(a+m,1) \tag{3.3}$$

Proof.

Using the following binomial series

$$(1-t)^{-b} = \sum_{m=0}^{\infty} \frac{(b)_m t^m}{m!} \tag{3.4}$$

in Equation (1.7), we have

$$B_{p,q}^{(\kappa,\mu)}(a,1-b) = \int_0^1 \sum_{m=0}^{\infty} \frac{(b)_m t^{a+m-1}}{m!} \exp\left(-\frac{p}{t^\kappa} - \frac{q}{(1-t)^\mu} \right) dt \tag{3.5}$$

Then, shifting integration and summation in Equation (3.5) and taking advantage of Equation (1.7) gives the required result.

Theorem 3.3. The following summation formula for the function $B_{p,q}^{\kappa,\mu}(a,b)$ given by Equation (1.7) holds true:

$$B_{p,q}^{(\kappa,\mu)}(a,b) = \sum_{m=0}^{\infty} B_{p,q}^{(\kappa,\mu)}(a+m,b+1) \tag{3.6}$$

Proof.

Setting the following binomial series

$$(1-t)^{b-1} = (1-t)^b \sum_{m=0}^{\infty} t^m \tag{3.7}$$

in Equation (1.7), we have

$$B_{p,q}^{(\kappa,\mu)}(a,b) = \int_0^1 (1-t)^b \sum_{m=0}^{\infty} t^{a+m-1} \exp\left(-\frac{p}{t^\kappa} - \frac{q}{(1-t)^\mu} \right) dt \tag{3.8}$$

Then, changing integration and summation in Equation (3.8) and taking into consideration of Equation (1.7) obtains the required result.

Definition 3.4. The extended Gamma function is defined by

$$\Gamma_p^{(\nu)}(x) = \int_0^\infty t^{x-1} \exp\big(-t - \frac{p}{t^\nu}\big) dt \tag{3.9}$$

Theorem 3.5. The following product formula for the function $B_{p,q}^{\kappa,\mu}(a,b)$ given by Equation (1.7) holds true:

$$\Gamma_p^{(\kappa)}(a)\Gamma_q^{(\mu)}(b) = 2\int_0^\infty r^{2(a+b)-1} \exp(-r^2) B^{(\kappa,\mu)}_{\frac{p}{r^{2\kappa}},\frac{q}{r^{2\mu}}}(a,b) dr \tag{3.10}$$

Proof.
Putting $t = \zeta^2$ and $t = \eta^2$ in Equation (3.9), we obtain

$$\Gamma_p^{(\kappa)}(x) = 2\int_0^\infty \zeta^{2a-1} \exp\left(-\zeta^2 - \frac{p}{\zeta^{2\kappa}}\right) d\zeta \tag{3.11}$$

and

$$\Gamma_q^{(\mu)}(b) = 2\int_0^\infty \eta^{2b-1} \exp\left(-\eta^2 - \frac{q}{\eta^{2\mu}}\right) d\eta \tag{3.12}$$

Therefore,

$$\Gamma_p^{(\kappa)}(a)\Gamma_q^{(\mu)}(b) = 4\int_0^\infty \int_0^\infty \zeta^{2a-1}\eta^{2b-1} \exp(-\zeta^2-\eta^2) \exp\left(-\frac{p}{\zeta^{2\kappa}} - \frac{q}{\eta^{2\mu}}\right) d\zeta\, d\eta \tag{3.13}$$

Replacing $\zeta = r\cos\theta$ and $\eta = r\sin\theta$ in Equation (3.13), we get

$$\Gamma_p^{(\kappa)}(a)\Gamma_q^{(\mu)}(b) = 2\int_0^\infty r^{2(a+b)-1} \exp(-r^2) \left[2\int_0^\infty \cos^{2a-1}\theta \sin^{2b-1}\theta \exp\left(-\frac{p}{r^{2\kappa}\cos^{2\kappa}\theta} - \frac{q}{r^{2\mu}\sin^{2\mu}\theta}\right) d\theta\right] dr \tag{3.14}$$

Taking advantage of Equation (2.8) in Equation (3.14) obtains the required result.

Theorem 3.6. The following summation formula for the function $B_{p,q}^{\kappa,\mu}(a,b)$ given by Equation (1.7) holds true:

$$B_{p,q}^{(\kappa,\mu)}(-\zeta,-\zeta-n) = \sum_{m=0}^{n} \binom{n}{m} B_{p,q}^{(\kappa,\mu)}(\zeta+m,-\zeta-m) \tag{3.15}$$

Proof.
Applying $a = \zeta$ and $b = -\zeta - n$ in Equation (3.1), we have

$$B_{p,q}^{(\kappa,\mu)}(\zeta,-\zeta-n) = B_{p,q}^{(\kappa,\mu)}(\zeta+1,-\zeta-n) + B_{p,q}^{(\kappa,\mu)}(\zeta,-\zeta-n+1) \tag{3.16}$$

Begin with $n = 1$, we can write this formula recursively to have

$$\begin{aligned}
B_{p,q}^{(\kappa,\mu)}(\zeta,-\zeta-1) &= B_{p,q}^{(\kappa,\mu)}(\zeta+1,-\zeta-1) + B_{p,q}^{(\kappa,\mu)}(\zeta,-\zeta)\\
B_{p,q}^{(\kappa,\mu)}(\zeta,-\zeta-2) &= B_{p,q}^{(\kappa,\mu)}(\zeta+2,-\zeta-2) + 2B_{p,q}^{(\kappa,\mu)}(\zeta+1,-\zeta-1) + B_{p,q}^{(\kappa,\mu)}(\zeta,-\zeta)\\
B_{p,q}^{(\kappa,\mu)}(\zeta,-\zeta-3) &= B_{p,q}^{(\kappa,\mu)}(\zeta+3,-\zeta-3) + 3B_{p,q}^{(\kappa,\mu)}(\zeta+2,-\zeta-2) + 3B_{p,q}^{(\kappa,\mu)}(\zeta+1,-\zeta-1) + B_{p,q}^{(\kappa,\mu)}(\zeta,-\zeta)
\end{aligned}$$

and so on. Then, it can be seen from the above equation that the coefficients of the expression come from the finite binomial expansion. Thus, we can get the required result.

4. Mellin Transform of Equation (1.7)

This section provides the Mellin transform and recurrence relation for Equation (1.7).

Theorem 4.1. The following Mellin transform for the function $B_{p,q}^{\kappa,\mu}(a,b)$ given by Equation (1.7) holds true:

$$B_{p,q}^{(\kappa,\mu)}(a,b)=\frac{1}{(2\pi i)^2}\int_{\nu_1-i\infty}^{\nu_1+i\infty}\int_{\nu_2-i\infty}^{\nu_2+i\infty}\frac{\Gamma(\zeta)\Gamma(\eta)\Gamma(a+\kappa\zeta)\Gamma(b+\mu\eta)}{\Gamma(a+b+\kappa\zeta+\mu\eta)}p^{-\zeta}q^{-\eta}d\zeta\,d\eta \tag{4.1}$$

Proof.

Using the Mellin transform in [1–3] for Equation (1.7), we have

$$M\{B_{p,q}^{(\kappa,\mu)}(a,b);p\to\zeta,q\to\eta\}=\frac{\Gamma(\zeta)\Gamma(\eta)\Gamma(a+\kappa\zeta)\Gamma(b+\mu\eta)}{\Gamma(a+b+\kappa\zeta+\mu\eta)} \tag{4.2}$$

Then, taking the inverse Mellin transform in [1–3] for Equation (4.2), we can obtain the required result.

Theorem 4.2. The following recurrence relation for the function $B_{p,q}^{\kappa,\mu}(a,b)$ given by Equation (1.7) holds true:

$$aB_{p,q}^{(\kappa,\mu)}(a,b+1)-bB_{p,q}^{(\kappa,\mu)}(a+1,b)=\mu qB_{p,q}^{(\kappa,\mu)}(a+1,b-1)-\kappa pB_{p,q}^{(\kappa,\mu)}(a-1,b+1) \tag{4.3}$$

Proof.

The Mellin transform of Equation (1.7) is

$$B_{p,q}^{(\kappa,\mu)}(a,b)=M\{f_{p,q}^{(\kappa,\mu)}(t,b);a\}$$

and

$$H(1-t)\quad=\begin{cases}0, & t>1\\ 1, & t<1\end{cases}$$

Differentiating with respect to t, we have

$$\frac{d}{dt}\left\{f_{p,q}^{(\kappa,\mu)}(t,b)\right\}=\left[-\delta(1-t)(1-t)^{b-1}-(b-1)H(1-t)(1-t)^{b-2}+H(1-t)(1-t)^{b-1}\left(-\frac{\kappa p}{t^{\kappa+1}}-\frac{\mu q}{(1-t)^{\mu+1}}\right)\right]\exp\left(-\frac{p}{t^{\kappa}}-\frac{q}{(1-t)^{\mu}}\right)$$

where $\frac{d}{dt}H(1-t)=-\delta(1-t)$ and δ symbolizes the Dirac delta function such that $\delta(1-t)=\delta(t-1)$, for $t\neq 0$ [1–3]. Taking advantage of the relationship between the Mellin transform of a function and its derivative:

$$M\{f(t);a\}=F(a)\implies M[f^{'}(t)]=-(a-1)F(a-1)$$

Then, making a simple arrangment, we have that

$$(a-1)B_{p,q}^{(\kappa,\mu)}(a-1,b)-(b-1)B_{p,q}^{(\kappa,\mu)}(a,b-1)=\mu qB_{p,q}^{(\kappa,\mu)}(a,b-2)-\kappa pB_{p,q}^{(\kappa,\mu)}(a-2,b) \tag{4.4}$$

Setting a and b by $a+1$ and $b+1$ in Equation (4.4), respectively, yields the required result.

5. Generalisation of Extended Incomplete Beta Function

This section defines the generalisation of the extended incomplete beta function using Equation (1.7) as follows:

$$B_{p,q}^{(\kappa,\mu)}(x,y;\tau)=\int_0^{\tau}t^{x-1}(1-t)^{y-1}\exp\left(-\frac{p}{t^{\kappa}}-\frac{q}{(1-t)^{\mu}}\right)dt,\quad -\infty<x,y<\infty,\text{ and }0<\tau<1 \tag{5.1}$$

Here, the special cases of Equation (5.1) are $B_{0,0}^{(\kappa,\mu)}(x,y;\tau)=B_{\tau}(x,y)$, $B_{p,p}^{(1,1)}(x,y;\tau)=B_{\tau}(x,y;p)$, $B_{p,p}^{(m,m)}(x,y;\tau)=B_{\tau}(x,y;\ p:m)$, and $B_{p,q}^{(1,1)}(x,y;\tau)=B_{\tau}(x,y;p,q)$ where $B_{\tau}(x,y)$ is the incomplete beta function provided in Equation (1.2). $B_{\tau}(x,y;p)$ is extended incomplete beta function given in Equation (1.4), $B_{\tau}(x,y;p:m)$ and $B_{\tau}(x,y;p,q)$ are generalised incomplete beta functions defined in [8, 9], respectively.

6. Integral Representations of Equation (5.1)

This section presents various integral representations for the generalisation of the extended incomplete beta function provided in Equation (5.1), professed in the following theorem.

Theorem 6.1. The following integral representation for the function $B_{p,q}^{(\kappa,\mu)}(a,b;\tau)$ given by Equation (5.1) holds true:

$$\int_0^{\infty}\int_0^{\infty}p^{\zeta-1}q^{\eta-1}B_{p,q}^{(\kappa,\mu)}(a,b;\tau)\,dp\,dq=\Gamma(\zeta)\Gamma(\eta)B_{\tau}(a+\kappa\zeta,b+\mu\eta),\quad \Re(a+\kappa\zeta),\Re(b+\mu\eta)>0 \tag{6.1}$$

where $B_{\tau}(a,b)$ is the incomplete beta function provided in Equation (1.2).

Proof.

The proof of Equation (6.1) is similar to that of Equation (2.1).

Theorem 6.2. The following integral representations for the function $B_{p,q}^{\kappa,\mu}(a,b;\tau)$ given by Equation (5.1) hold true:

$$B_{p,q}^{(\kappa,\mu)}(a,b;\tau)=\int_0^{\sigma}\frac{u^{a-1}}{(1+u)^{a+b}}\exp\left(-\frac{p(1+u)^{\kappa}}{u^{\kappa}}-q(1+u)^{\mu}\right)du,\quad 0<\sigma=\frac{\tau}{1-\tau}<\infty \tag{6.2}$$

$$B_{p,q}^{(\kappa,\mu)}(a,b;\tau)=2\int_0^{\sigma}\cos^{2a-1}\theta\sin^{2b-1}\theta\exp\left(-p\sec^{2\kappa}\theta-q\csc^{2\mu}\theta\right)d\theta,\quad 0<\sigma=\arcsin(\sqrt{\tau})\leq\frac{\pi}{2} \tag{6.3}$$

$$B_{p,q}^{(\kappa,\mu)}(a,b;\tau)=2\int_0^{\sigma}\tanh^{2a-1}\theta\,sech^{2b}\theta\exp\left(-p\coth^{2\kappa}\theta-q\cosh^{2\mu}\theta\right)d\theta,\quad 0<\sigma=\sinh^{-1}\left(\sqrt{\frac{\tau}{1-\tau}}\right)<\infty \tag{6.4}$$

Proof.

Putting to use the transformations $t=\frac{u}{u+1}$ and $t=\cos^2\theta$ in Equation (5.1) and $t=\sinh^2\theta$ in Equation (6.2), we can be obtained Equations (6.2), (6.3), and (6.4), respectively.

7. Certain Formulas for Equation (5.1)

This part obtains functional relation and summation formulas for the generalisation of the extended incomplete function (5.1). Besides, we present the relationship between Equation (1.7) and Equation (5.1).

Theorem 7.1. The following functional relation for the function $B_{p,q}^{\kappa,\mu}(a,b;\tau)$ given by Equation (5.1) holds true:

$$B_{p,q}^{(\kappa,\mu)}(a,b;\tau)=B_{p,q}^{(\kappa,\mu)}(a+1,b;\tau)+B_{p,q}^{(\kappa,\mu)}(a,b+1;\tau) \tag{7.1}$$

Proof.

The proof of Equation (7.1) is similar to that of Equation (3.1).

Theorem 7.2. The following summation formula for the function $B_{p,q}^{\kappa,\mu}(a,b;\tau)$ given by Equation (5.1) holds true:

$$B_{p,q}^{(\kappa,\mu)}(a,1-b;\tau)=\sum_{m=0}^{\infty}\frac{(b)_m}{m!}B_{p,q}^{(\kappa,\mu)}(a+m,1;\tau) \tag{7.2}$$

Proof.

The proof of Equation (7.2) is similar to that of Equation (3.3).

Theorem 7.3. The following summation formula for the function $B_{p,q}^{\kappa,\mu}(a,b;\tau)$ given by Equation (5.1) holds true:

$$B_{p,q}^{(\kappa,\mu)}(a,b;\tau)=\sum_{m=0}^{\infty}B_{p,q}^{(\kappa,\mu)}(a+m,b+1;\tau) \tag{7.3}$$

Proof.

The proof of Equation (7.3) is similar to that of Equation (3.6).

Theorem 7.4. The following identity for the function $B_{p,q}^{\kappa,\mu}(a,b;\tau)$ given by Equation (5.1) holds true:

$$B_{q,p}^{(\kappa,\mu)}(b,a;\tau)=B_{p,q}^{(\kappa,\mu)}(a,b)-B_{p,q}^{(\kappa,\mu)}(a,b;1-\tau) \tag{7.4}$$

Proof.

The right hand side of Equation (7.4) gives

$$B_{p,q}^{(\kappa,\mu)}(a,b)-B_{p,q}^{(\kappa,\mu)}(a,b;1-\tau)=\int_{1-\tau}^{1}x^{b-1}(1-x)^{a-1}\exp\left(-\frac{p}{x^{\kappa}}-\frac{q}{(1-x)^{\mu}}\right)dx \tag{7.5}$$

Setting $x=1-t$ in Equation (7.4), we obtain

$$\int_{0}^{\tau}t^{b-1}(1-t)^{a-1}\exp\left(-\frac{q}{t^{\kappa}}-\frac{p}{(1-t)^{\mu}}\right)dt \tag{7.6}$$

which gives the left hand side of (7.4).

Theorem 7.5. The following summation formula for the function $B_{p,q}^{\kappa,\mu}(a,b;\tau)$ given by Equation (5.1) holds true:

$$B_{p,q}^{(\kappa,\mu)}(-\zeta,-\zeta-n;\tau)=\sum_{m=0}^{n}\binom{n}{m}B_{p,q}^{(\kappa,\mu)}(\zeta+m,-\zeta-m;\tau) \tag{7.7}$$

Proof.

The proof of Equation (7.7) is similar to that of Equation (3.15).

8. Beta Distribution of Equation (1.7)

This section anticipated that $B_{p,q}^{(\kappa,\mu)}(\mathfrak{x},\mathfrak{y})$ would have several applications in generalising Equation (1.7). One of these that comes to mind is applications in statistics. For example, the conventional beta distribution can be expanded, by considering $B_{p,q}^{(\kappa,\mu)}(\mathfrak{x},\mathfrak{y})$, to variables $\mathfrak{x}$ and $\mathfrak{y}$ with an infinite range. Such an extension seems desirable for the project consideration and review technique used in certain special cases.

We define the beta distribution of Equation (1.7) by

$$f(t)=\begin{cases}\frac{1}{B_{p,q}^{(\kappa,\mu)}(\mathfrak{x},\mathfrak{y})}t^{\mathfrak{x}-1}(1-t)^{\mathfrak{y}-1}\exp\left(-\frac{p}{t^{\kappa}}-\frac{q}{(1-t)^{\mu}}\right), & 0<t<1\\ 0, & \text{otherwise}\end{cases} \tag{8.1}$$

A random variable $\mathfrak{X}$ with probability density function (pdf) given by Equation (8.1) will be said to have the generalisation of the extended beta distribution with parameters $\mathfrak{x}$ and $\mathfrak{y}$ such that $-\infty<\mathfrak{x},\mathfrak{y}<\infty$. If δ is any real number

$$E(\mathfrak{X}^{\delta})=\frac{B_{p,q}^{(\kappa,\mu)}(\mathfrak{x}+\delta,\mathfrak{y})}{B_{p,q}^{(\kappa,\mu)}(\mathfrak{x},\mathfrak{y})} \tag{8.2}$$

In particular, $\delta=1$

$$\nu=E(\mathfrak{X})=\frac{B_{p,q}^{(\kappa,\mu)}(\mathfrak{x}+1,\mathfrak{y})}{B_{p,q}^{(\kappa,\mu)}(\mathfrak{x},\mathfrak{y})} \tag{8.3}$$

shows the mean of the distribution, and

$$\sigma^2=E(\mathfrak{X}^2)-(E(\mathfrak{X}))^2=\frac{B_{p,q}^{(\kappa,\mu)}(\mathfrak{x}+2,\mathfrak{y})B_{p,q}^{(\kappa,\mu)}(\mathfrak{x},\mathfrak{y})-[B_{p,q}^{(\kappa,\mu)}(\mathfrak{x}+1,\mathfrak{y})]^2}{[B_{p,q}^{(\kappa,\mu)}(\mathfrak{x},\mathfrak{y})]^2} \tag{8.4}$$

is the variance of the distribution. The moment generating function of the distribution is

$$M(t)=\sum_{m=0}^{\infty}\frac{t^m}{m!}E(\mathfrak{X}^m)=\frac{1}{B_{p,q}^{(\kappa,\mu)}(\mathfrak{x},\mathfrak{y})}\sum_{m=0}^{\infty}B_{p,q}^{(\kappa,\mu)}(\mathfrak{x}+m,\mathfrak{y})\frac{t^m}{m!} \tag{8.5}$$

The cumulative distribution of Equation (8.1) can be written as

$$F(\tau)=\frac{B_{p,q}^{(\kappa,\mu)}(\mathfrak{x},\mathfrak{y};\tau)}{B_{p,q}^{(\kappa,\mu)}(\mathfrak{x},\mathfrak{y})} \tag{8.6}$$

where $B_{p,q}^{(\kappa,\mu)}(\mathfrak{x},\mathfrak{y};\tau)$ is the generalisation of the extended incomplete beta function provided in Equation (5.1). Probably, this distribution should be useful in expanding the statical results for quite simply positive variables to deal with variables that can take arbitrarily large negative values as well.

9. Conclusion

Recently, Şahin et al. [24] have defined and investigated certain properties of Equation (1.7). This paper obtains several new formulas for generalising the beta function provided in Equation (1.7), for example, several integral representations, functional relations, summation formulas, Mellin transform and recurrence relation. Furthermore, we defined and studied a generalisation of the extended incomplete beta function provided in Equation (5.1) with the help of Equation (1.7). Then, we present some essential properties, for instance, integral representations, functional relations, summation formulas and recurrence relations. Finally, the conventional beta distribution can be extended using Equation (1.7).

This paper produces results with a general character and encourages further interesting studies involving integral representations. Moreover, opening up creative horizons in applied mathematics, this paper inspires the researchers to define and study various new fractional derivatives and integral operators.

Author Contributions

All the authors contributed equally to this work. They all read and approved the last version of the manuscript.

Conflicts of Interest

The authors declare no conflict of interest.

References

[1] G. E. Andrews, R. Askey, R. Roy, Special Functions. Cambridge University Press, Cambridge, 1999.

[2] M. A. Chaudhry, S. M. Zubair, On a Class of Incomplete Gamma with Applications. CRC Press (Chapman and Hall), Boca Raton, FL, 2002.

[3] E. D. Rainville, Special Functions. Macmillan Company, New York, 1960, Reprinted by Chelsea Publishing Company, Bronx, NewYork, 1971.

[4] R. Şahin, O. Yağcı, *Note on the certain special functions representable as* Φ, Journal of Fractional Calculus and Applications, 11(2), (2020) 1–11.

[5] M. A. Chaudhry, A. Qadir, M. Raque, S. M. Zubair, *Extension of Euler's beta function*, Journal of Computational and Applied Mathematics, 78(1), (1997) 19–32.

[6] E. Özergin, M. A. Özarslan, A. Altın, *Extension of gamma, beta and hypergeometric functions*, Journal of Computational and Applied Mathematics, 235(16), (2011) 4601–4610.

[7] R. K. Parmar, P. Chopra, *Generalization of the incomplete extended beta function and beta distribution*, International Journal of Engineering Research and Development, 2(4), (2012) 58–62.

[8] D. Lee, A. K. Rathie, R. K. Parmar, Y. S. Kim, *Generalization of extended beta function, hypergeometric and confluent hypergeometric Functions*, Honam Mathematical Journal, 33(2), (2011) 187–206.

[9] J. Choi, A. K. Rathie, R. K. Parmar, *Extension of extended beta, hypergeometric and confluent hypergeometric functions*, Honam Mathematical Journal, 33, (2014) 357–385.

[10] E. Ata, İ. O. Kıymaz, *A study on certain properties of generalized special functions defined by Fox-Wright function*, Applied Mathematics and Nonlinear Sciences, 5(1), (2020) 147–162.

[11] A. Fernandez, C. Ustaoğlu, M. A. Özarslan,*On the analytical development of incomplete Riemann-Liouville fractional calculus*, Turkish Journal of Mathematics, 45(3), (2021) 1418–1443.

[12] M. J. Luo, G. V. Milovanovic, P. Agarwal, *Some results on the extended beta and extended hypergeometric functions*, Applied Mathematics and Computation, 248, (2014) 631–651.

[13] M. A. Özarslan, C. Ustaoğlu, *Incomplete Caputo fractional derivative operators*, Advances in Difference Equations, 2018, (2018) Article Number: 209, 1–18.

[14] M. A. Özarslan, C. Ustaoğlu, *Extension of incomplete gamma, beta and hypergeometric functions*, Progress in Fractional Differentiation and Applications, 5(1), (2019) 21–35.

[15] M. A. Özarslan, C. Ustaoğlu, *Some incomplete hypergeometric functions and incomplete Riemann-Liouville fractional integral operators*, Mathematics, 7(5), (2019) 1–17.

[16] M. A. Özarslan, C. Ustaoğlu, *Extended incomplete version of hypergeometric functions*, Filomat, 34(2), (2020) 653–662.

[17] M. A. Özarslan, C. Ustaoğlu, *Extended incomplete Riemann-Liouville fractional integral operators and related special functions*, Electronic Research Archive, 30(5), (2022), 1723–1747.

[18] R. K. Parmar, *A new generalization of gamma, beta, hypergeometric and confluent hypergeometric functions*, Le Mathematiche, 68, (2013) 33–52.

[19] R. Şahin, O. Yağcı, *A new generalization of Pochhammer symbol and its applications*, Applied Mathematics and Nonlinear Sciences, 5(1), (2020) 255–266.

[20] R. Şahin, O. Yağcı, *Fractional calculus of the extended hypergeometric function*, Applied Mathematics and Nonlinear Sciences, 5(1), (2020) 269–284.

[21] U. M. Abubakar, *New generalized beta function associated with the Fox-Wright function*, Journal of Fractional Calculus and Application, 12(2), (2021) 204–227.

[22] U. M. Abubakar, *A comparative analysis of modified extended fractional derivative and integral operators via modified extended beta function with applications to generating functions*, Çankaya University Journal of Science and Engineering, 19(1), (2022) 40–50.

[23] U. M. Abubakar, H. M. Tahir, I. S. Abdulmumini, *Extended gamma, beta and hypergeometric functions: Properties and applications: Extended gamma, beta and hypergeometric functions*, Journal of Kerala Statistical Association, 32(1), (2021) 18–40.

[24] R. Şahin, O. Yağcı, M. B. Yağbasan, A. Çetinkaya, İ. O. Kıymaz, *Further generalizations of gamma, beta and related functions*, Journal of Inequalities and Special Functions, 9(4), (2018) 1–7.

Journal of New Results in Science
https://dergipark.org.tr/en/pub/jnrs
Research Article
Open Access

E-ISSN:1304-7981 https://doi.org/10.54187/jnrs.1159263

A suitable wind turbine selection for achieving maximum efficiency from wind energy by an adaptive hybrid multi-criteria decision-making approach

Cem Emeksiz[1], Abdullah Yüksel[2]

Keywords:
Wind energy,
Wind turbine,
Multi-criteria decision-making,
Wind energy efficiency,
Entropy

Abstract — Wind energy is rapidly developing and gaining great importance among renewable energy sources. Moreover, wind energy is an important renewable energy option that is clean and environmentally friendly but has comparatively high costs. Wind turbines especially play an essential role in increasing wind energy conversion systems costs. For this reason, choosing the most suitable turbine in planning wind energy systems is very valuable for investors. The approaches used in literature studies have a limited perspective. Therefore, this study presented an adaptive hybrid multi-criteria decision-making approach for the first time in the appropriate wind turbine selection. Expert interviews and literature reviews were considered in the application phase of the model. Four mains (technical, economic, environmental, and customer service criteria) and seventeen sub-criteria were applied for the thirty-five wind turbine brands selected in the suggested adaptive hybrid assessment model. Additionally, the consistency analysis performed to test the consistency of comparisons shows that the analyses and choices have high consistency. The adaptive hybrid model suggested in this study can also be easily used to select a suitable wind turbine for onshore and offshore wind farm planning.

Subject Classification (2020): 28D20, 62C99.

1. Introduction

Energy has critical importance for the economic growth and development of world states. However, there is no energy component among the millennium development goals of the United Nations. Recently, Ban-Ki-Moon [1], Secretary General of the United Nations, has highlighted that development is not possible without energy, and sustainable development is not possible without sustainable energy. In the last decade, energy has become one of the sustainable development goals because of its impact on sustainable development. Nonetheless, many countries still provide their energy needs from fossil fuels [2]. Fossil fuels, such as coal, oil, natural gas and nuclear, are environmentally unfriendly to harvest, become exhausted, diminish faster, draw on limited resources and are non-renewable. The utility of fossil fuels in meeting energy demand is considered the most important cause of climate change and global warming. This situation threatens the sustainability and security of the global.

[1]cem.emeksiz@gop.edu.tr (Corresponding Author); [2]ayuksel79@gmail.com
[1,2]Department of Electric-Electronic Engineering, Faculty of Engineering and Architecture, Tokat Gaziosmanpaşa University, Tokat, Turkiye
Article History: Received: 08 Aug 2022 — Accepted: 23 Aug 2022 — Published: 31 Aug 2022

Renewable energy sources are the only viable energy option for environmentally friendly, clean energy. Thus, the greenhouse gas effect and climate change can be reduced by using renewable energy sources. Among renewable resources, such as wind, solar, water (hydro) and mini-hydro, geothermal heat, biomass and tides, wind energy has significant importance due to its economic attributes, the potential for energy generation and wide application range [3]. Wind energy showed the biggest annual capacity increase in 2020 after the peak in 2015. In 2020, the new capacity (93 GW) was added to the world's electric grids, and the global wind power market grew by 14%. Thus, the global installed wind power capacity increased to around 743 GW overall (Fig. 1) [4].

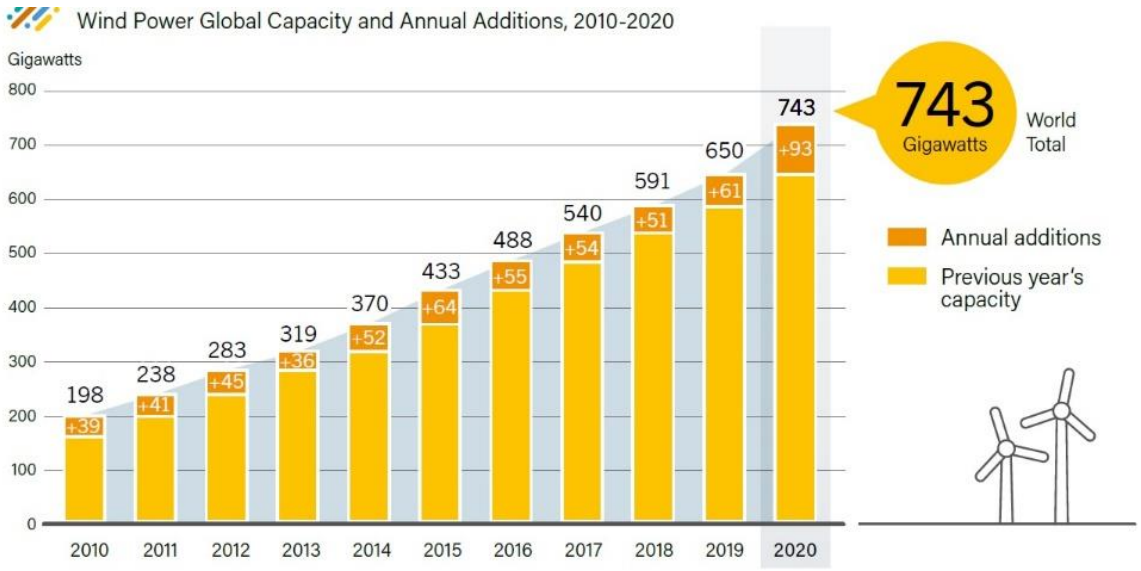

Figure 1. Wind power global capacity and annual additions

At the end of 2020, China maintained its leadership with additional capacities. The United States, Brazil, Netherlands, Germany and Spain followed. Other countries in the top 10 for total capacity additions were Norway, France, Turkiye and India (Fig 2) [4].

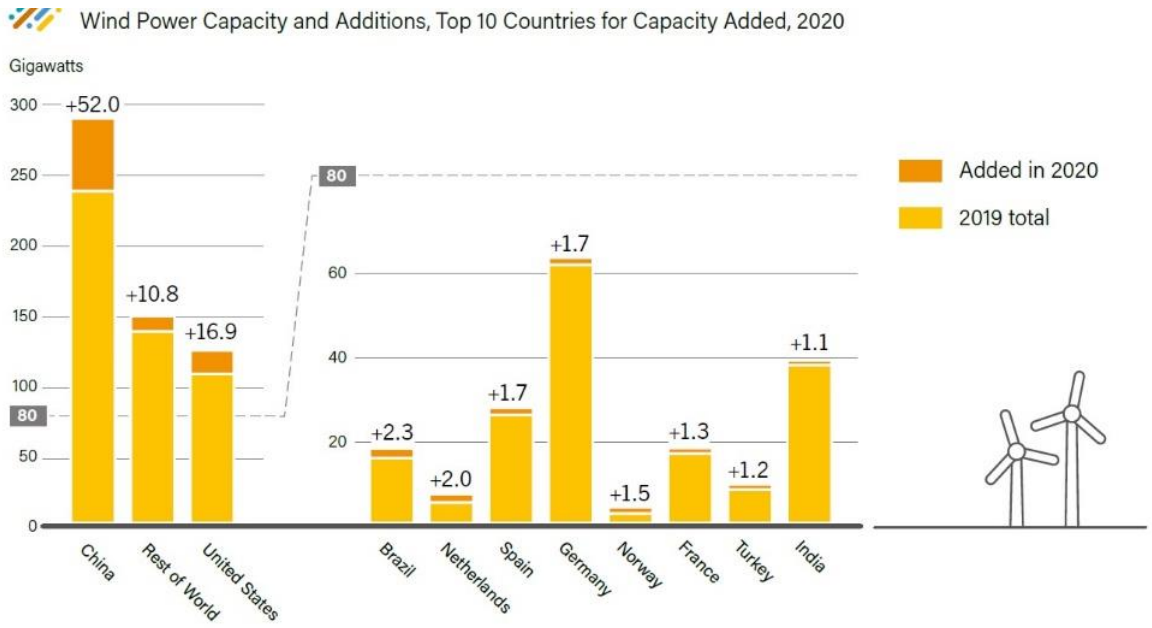

Figure 2. Wind power capacity and additions, top 10 countries

To utilise wind power generation, a better understanding of the wind characteristics of a wind field and the performance of the wind turbines will be installed crucial because the wind turbines used in the wind energy conversion system are essential to evaluate the wind source correctly. For every wind turbine model, the turbine power curve created by the manufacturer is used in power calculation [5,6]. This way, different wind turbines can be evaluated for regions with varying wind regimes. According to the market share in 2019, the leading wind turbine suppliers on a global scale are shown in Figure 3 [7].

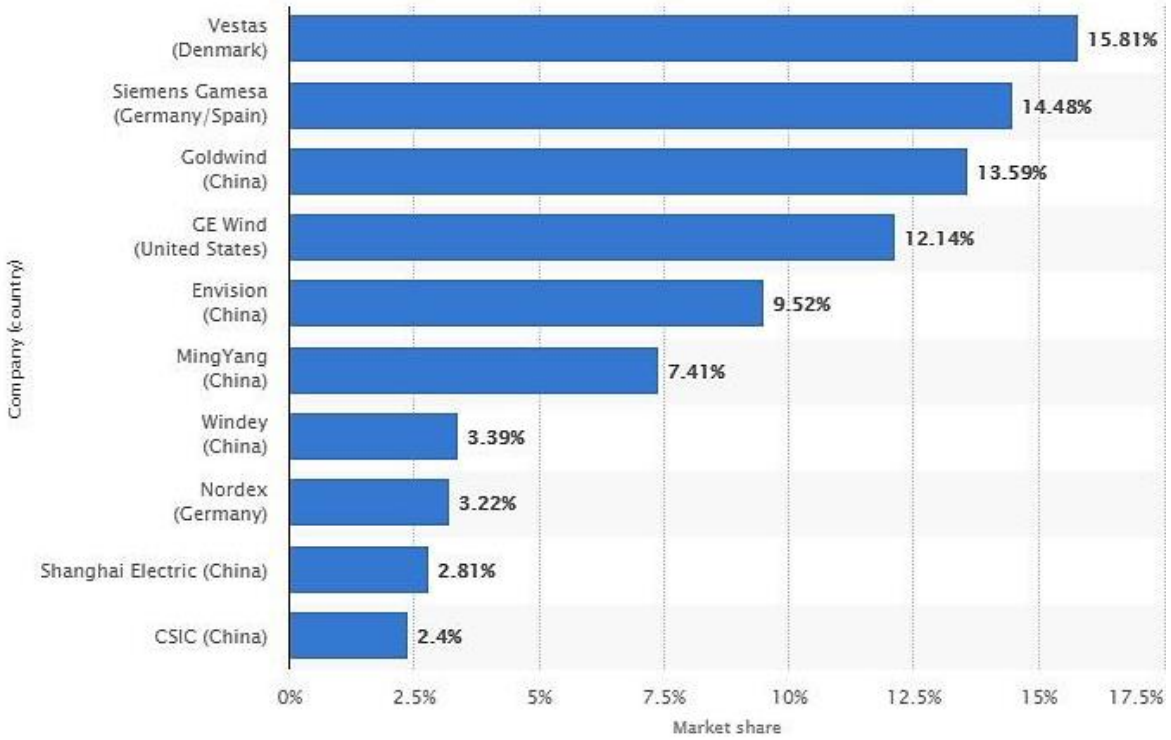

Figure 3. Leading wind turbine suppliers globally based on market share in 2019

Nowadays, the best wind turbine selection problem for specific wind regimes has been the subject of many studies in the literature. Five wind turbines at 60 m height (Nordex N80, Gamesa G80, Nordex 70, Nordex N60 and Gamesa G58) were compared using a classical method by Jowder. It was determined that Gamesa G58 is the most suitable turbine [8]. Alimi et al. [9] examined the wind energy production on the central coast of Tunis by using eight different commercial wind turbines at different hub-heights (Repower (2000 kW) MM 70-65, Dewind 1250 kW, GE 1500 kW, V39-35, V82-0.9, Anbonus MK III-30, Vestas V80, Nordex (2300 kW) N90-100). De Araujo Lima and Filho [10] examined wind energy of São João do Cariri (SJC) in Paraiba (PB) state using 3 different types of wind turbine (Vestas V27, Bonus Mk III and Bonus Mk III). A multi-criteria decision-making method was used to choose a suitable wind turbine for the wind energy station project by Lee et al. [11]. The concepts of the costs, benefits, opportunities and risks came to the fore in the Analytical Hierarchy Process (AHP) method. The wind power generation of Ghana's coastal region was assessed using four different wind turbines (Garbi150/ 28, Polaris 15–50, CF-100 and WES30) [12].

Four wind turbine models (ZEUS 500, WES-30, P19-100 and G-3120) were examined by Adaramola et.al. [13]. The performance of turbines was compared for the Niger Delta region, and it was determined that the highest energy output was obtained from G-3120 wind turbine. A systematical methodology was presented using the Technique for Order Preference by Similarity to Ideal Solution (TOPSIS) by Kolios et al. [14]. They proposed this methodology for classifying and evaluating wind turbine support structures. Montoya et al. [15] used a multi-objective optimisation algorithm for the best wind turbine selection. This algorithm was applied to the energy outputs of twenty-six different wind turbines.

Nahi and Nabavi [16] characterised the new network using the Monte Carlo method to select the best wind turbine used in the Manjil region. Wind speed data were simulated using MATLAB and EXCEL software. The performances of parametric and nonparametric methods were analysed by Shokrzadeh [17]. Four wind turbines were selected for the study, and simulated data sets were used in the analysis. The results of studies realised by Somma et al. [18] and Yan et al. [19] demonstrated that exergy efficiency could be developed while the energy cost is reduced. Different ecological and economic criteria were applied in the study of Haaren and Vasilis [20]. One of these criteria is preventing economic costs in wind energy production.

This study presents an adaptive assessment model with a wide range of criteria. Although many literature studies using various decision-making techniques were summarised above, the approaches used in these studies have a limited perspective. The proposed adaptive approach was used for the first time for turbine selection, especially in wind energy planning. This situation also constitutes the original and innovative side of the study. Therefore, the idea of overcoming this gap in the literature with the adaptive model we presented in the study excited us. The proposed adaptive assessment model evaluated 35 wind turbine brands using four main and 17 sub-criteria. In addition, experts and stakeholders in the field of wind energy management were interviewed and included in the process. The power of the wind turbines used in the case study was selected as 3 MW. No market research has been conducted on the selected turbines; conversely, it was focused on the model that will make the most appropriate choice among the wind turbines that have the same power to be used in wind farms. The consistency of the proposed model was achieved by consistency analysis, and the consistency ratio was calculated as 0.0956. This value shows that the analysis and selections are quite consistent. In addition, the results obtained are commercially viable and applicable.

2. Methodology

The proposed adaptive assessment model, classification of main and sub-criteria and consistency analysis are presented in detail in the following sections.

2.1. The Adaptive Assessment Model That Is Entropy-Based Multi-Attribute Utility Theory (MAUT)

MAUT [21] is a systematic method that analyses and identifies multiple variables to provide a common decision. MAUT is a much more precise methodology [22,23], an extension of Multi-Attribute Value Theory (MAVT), in which both uncertainties and risk preferences are included in decision support methods. MAUT aims to maximise the utility function ($U(a_i)$), defined in the set of alternatives in decision problems. The MAUT method is based on several key ideas. These are listed as follows [24]:

- ✓ As much as possible, evaluations should be comparative.
- ✓ Usually, the program has multiple regions of service.
- ✓ The program should focus on many goals.
- ✓ Trials must be part of the evaluation.
- ✓ It should be necessary to criticise numerically great values.
- ✓ Evaluations should typically be about decisions or at least covered.

This method's most useful alternative is based on qualitative and quantitative criteria. During the decision-making phase, quantitative criteria determined are countable and easily evaluated. 5, 10 or 100-point scoring system can be used for comprehensibility by everyone in evaluating qualitative

criteria. This helps to facilitate the evaluation. (For example: Very bad: 1, bad: 2, medium: 3, good: 4, very good: 5, Very bad: 0 bad: 25, medium: 50, good: 75, very good: 100) [25]. While making these evaluations, paired comparisons are used by utilising expert opinions. In other words, how good or bad one alternative is compared to another is considered. Therefore, an expert group of 7 people was formed to determine the criteria and in determining the relationships between the criteria. This group consists of 2 electrical-electronic engineers, two energy systems engineers, one economist and two statistics experts. In particular, open-ended questions were asked to 7 experts to determine the criteria, and in line with the answers given to these questions, four main and 17 sub-criteria criteria, which are thought to be important in the selection of wind turbines, were determined. In evaluating the qualitative criteria used in our study, a 5-point scoring system was preferred. The application steps of the MAUT method are shown as follows [26]:

Step 1. The criteria (a_n) and qualities/alternatives (x_m) that are the subject of the decision problem should be determined.

Step 2. To evaluate the qualities correctly, the weight values (w_j) where the priorities are determined must be provided. The sum of the weight values must be equal to 1, as shown in Equation (2.1).

$$\sum_{j}^{n} w_j = 1 \tag{2.1}$$

Step 3. The value measurements of the criteria are assigned. This assignation is made by considering the paired comparisons for qualitative criteria while having quantitative values for quantitative criteria. Thus, the decision matrix is created.

Step 4. The assigned values are placed in the decision matrix, and the normalisation process is started. In the normalisation process, the best and the worst values are determined for each feature. For best and worst values, 1 and 0 are assigned, respectively. Equation (2.2) is used to calculate other values.

$$f_j(a_i) = \frac{f_i(a_i) - \min(f_i)}{\max(f_i) - \min(f_i)} \tag{2.2}$$

Step 5. After the normalisation process, utility values are determined. The utility function is calculated by Equation (2.3).

$$U(a_i) = \sum_{j=1}^{n} f_j(a_i) w_j \tag{2.3}$$

$U(a_i)$: Utility value of the alternative

$f_j(a_i)$: Normalised utility values for each criterion and alternative

w_j : Weight values

Step 6. The utility value calculated with Equation (2.3) is obtained by preference ranking by descending sort. The alternative, which takes the first place at the end of the ranking, represents the alternative that provides the most benefit.

The weight values (w_j) were calculated using the entropy method. The entropy method can be applied if the decision matrix data is known to calculate the objective weights. Entropy is defined as a measure of uncertainty and disorder in a system [27]. It is the most essential decisive of the accuracy and reliability of the decision to be made in a decision-making problem. Entropy is used to measure the amount of helpful information from which the available data are provided [28]. The application steps of the entropy method are shown as follows [29]:

Step 1. A decision matrix is created to evaluate the original data in a multiple decision-making problem with 'm' alternatives and 'n' criteria.

$$P = \begin{bmatrix} a_{11} & a_{12} & \dots & a_{1j} & \dots & a_{1n} \\ a_{21} & a_{22} & \dots & a_{2j} & \dots & a_{2n} \\ \vdots & \vdots & \vdots & \vdots & \vdots & \vdots \\ a_{i1} & a_{i2} & \dots & a_{ij} & \dots & a_{in} \\ \vdots & \vdots & \vdots & \vdots & \vdots & \vdots \\ a_{m1} & a_{m2} & \dots & a_{mj} & \dots & a_{mn} \end{bmatrix}$$

According to the j^{th} criteria, the a_{ij} ; i^{th} *the* alternative is the utility value. $i = 1, 2, ..., m$ and $j = 1, 2, ..., n$.

Step 2. The entropy-based normalised decision matrix: To eliminate the discrepancies in different units of measurement, P_{ij} is calculated using Equation (2.4) by normalisation.

$$P_{ij} = \frac{a_{ij}}{\sum_i^m a_{ij}}, \qquad i = 1, 2, \dots m \text{ and } j = 1, 2, \dots, n \tag{2.4}$$

Step 3. Entropy values are calculated as below:

$$E_j = \frac{-1}{\ln(m)} \sum_{i=1}^{m} \left[P_{ij} \ln(P_{ij}) \right], \qquad j = 1, 2, \dots, n \tag{2.5}$$

Here, P_{ij} denotes entropy-based normalised decision matrix and E_j denotes entropy value.

Step 4. Calculation of uncertainty as a degree of diversity

$$d_j = 1 - E_j, \qquad j = 1, 2, \dots, n \tag{2.6}$$

Step 5. Weights of each criterion are calculated.

$$w_j = \frac{d_j}{\sum_{j=1}^{n} d_j}, \qquad j = 1, 2, \dots, n \tag{2.7}$$

Many methods are used to determine whether the comparisons performed are consistent. One of them is the calculation of the coefficient called the "Consistency Index (CI)". Hence, the consistency index (CI) put forth is defined by Equation (2.8) put forth by [30]:

$$CI = \frac{\lambda_{max} - n}{n - 1} \tag{2.8}$$

n and λ_{max} represents the number of criteria and the maximum eigenvalue of the comparison matrix, respectively [31]. Moreover, λ_{max} acts as a reference index during the consistency. λ_{max} is calculated by using Equation (2.9):

$$\lambda_{max} = \frac{1}{n} \sum_{i=1}^{n} \left(\frac{\sum_{j=1}^{n} a_{ij} w_j}{w_i} \right) \tag{2.9}$$

To evaluate the consistency, the value of the "Random Index (RI)" should be known. RI values defined for n-dimensional comparison matrices are given in Table 1 [32,33].

Table 1. Random index (RI) values

n	1	2	3	4	5	6	7	8	9	10
RI	0.01	0.00	0.58	0.90	1.12	1.24	1.32	1.41	1.45	1.49
n	**11**	**12**	**13**	**14**	**15**	**16**	**17**	**18**	**19**	**20**
RI	1.51	1.48	1.56	1.57	1.58	1.59	1.60	1.61	1.62	1.63

After determining the CI and RI values, the "Consistency Ratio (CR)" is calculated as follows:

$$CR = \frac{CI}{RI} \tag{2.10}$$

If the CR defined by Equation (2.10) is less than 0.10, it is decided that the comparison is consistent [34].

2.2. Determination of Criteria in Turbine Selection

Many factors influence the choice of turbines to be used in a wind turbine power plant. Among these factors, technical, economic, environmental and customer service criteria are presented in the literature as the main criteria [35]. In addition, these criteria are generally divided into several sub-criteria. Therefore, the basic criteria in this study were examined in four main groups technical, economic, environmental and customer service. Technical criteria were created from sub-criteria: cut-in wind speed (WS), rated wind speed, cut-out wind speed, rotor diameter, swept area, power density, hub height, and capacity factor (CF). The economic criteria are subdivided into government support and total cost. The environmental criteria include noise, shadow vibration and glare, impact on living things and electromagnetic effect. Finally, service support, spare parts and reliability created the sub-criteria of the customer service criteria. The hierarchy created from these criteria is shown in Figure 4.

Figure 4. The hierarchical structure of the criteria

35 pieces of 3 MW wind turbines selected in the study are coded as T1, T2, T3, ..., and T35. Selected turbines and turbine codes (TC) are shown in Table 2.

Table 2. Selected turbines and turbine codes

Wind Turbines	TC	Wind Turbines	TC
Alstom ECO 122/3000	T1	MBB Messerschmitt Aeolus II	T19
Amperax A3000	T2	Nordex N131/3000 Delta	T20
AMSC wt3000fc TC IIIB	T3	PROKON P3000/116	T21
CATUM CA-3.0 MW-WD R120	T4	Repower 3.0M122	T22
CCWE CCWE-3000D/D103	T5	Senvion 3.0M122	T23
CSIC H146-3.0	T6	GFF GF121-3.0	T24
Doosan WinDS3000/134	T7	Swiss Electric YZ121/3.0	T25
Enercon E-115 3.000	T8	Siemens SWT-3.0-133	T26
Fuhrlander LLC WTU3.0-132	T9	Sinovel SL3000/121	T27
FWT 120/3000	T10	TYHI - Taiyuan TZ3000/140	T28
MingYang MySE3.0-135	T11	Vensys 136/3000	T29
United Power UP3000-120	T12	Vestas V126-3.0	T30
Jacobs PowerTec JPT 3-120	T13	W2E Wind to Energy W2E-145/3.0fc	T31
Karlskronavarvet WTS-3 Maglarp	T14	WEG Wind EnergyGroup LS1	T32
Kvaerner Turbin AB Nasudden II	T15	WinWinD WWD-3 D120	T33
Lagerwey L100 3.0 MW	T16	Goldwind GW 150/3000	T34
Leitwind LTW101 3000	T17	Windey WD156-3000	T35
MAN GROWIAN	T18		

The technical, economic, environmental and customer service criteria of the selected 3 MW wind turbines are summarised in Tables 3-6 [36].

2.3. The Sub-Criteria of Technical Criterion

The minimum wind speed at which the turbine blades start rotating is called “cut-in wind speed”. To increase the turbine’s operating time, choosing turbines with a low cut-in wind speed is reasonable. The wind speed that the rotation of the turbine blades will create danger and therefore automatically turn off itself is called the ‘cut-out wind speed’. The wind speed at which energy is produced from the wind turbine with maximum capacity is called “rated wind speed”. That is, it is the lowest speed at which maximum power can be obtained. Having the nominal speed as low as possible will increase the efficiency of the wind turbines. The rotor diameter is related to the area where the blades of the wind turbine sweep. The rotor diameter changes according to the height of the wind turbine from the ground. Turbines with a rotor diameter of 10 to 90 meters are widely used. Energy production is high in turbines with large rotor diameters. The swept area refers to the area of the circle created by the blades as they sweep through the air.

Power density is a measure of power output per unit volume. If a system has a high-power density, then it can output large amounts of energy based on its volume. As altitude increases, turbulence decreases and wind speed increases. Therefore, tower height is essential. Rotor rotation speed also increases with tower height. The capacity factor is the ratio that the turbine can provide its rated power in a percentage of the time. The values of these sub-criteria of technical criteria are shown in Table 3.

Table 3. The values of the sub-criteria of technical criterion

Turbine Code	Cut-In WS (m/s)	Rated WS (m/s)	Cut-Out WS (m/s)	Rotor Diameter (m)	Swept Area (m^2)	Power Density (W/m^2)	Hub Height (m)	CF
T1	3	10.5	25	122	11683	256.7	139	36.197
T2	3	11.3	23	116	105623	283.9	142	32.121
T3	3	11	20	120	11304	265.3	110	32.538
T4	5	11	25	118.2	10967	273.4	140	33.536
T5	3	11.5	25	103	8328	360.2	85	38.671
T6	3	9.1	22	146	16733	179.2	120	38.824
T7	3	10	20	134	14095	212.8	90	34.737
T8	2	11.5	25	115.7	10508	285.3	149	30.626
T9	3	12	25	132	13677	219.2	160	20.712
T10	3	12	25	120.6	11417	262.6	140	24.814
T11	3	9.3	20	135	14306	209.6	140	42.541
T12	3.5	10.2	25	120	11304	265.3	90	40.809
T13	3	10.1	25	120	11304	265.3	126	42.033
T14	6	14	21	78	4775	627.9	80	37.358
T15	6	14.5	25	80.5	5087	589	78	31.543
T16	2.1	16	28	100	7850	382	135	15.225
T17	3	15	25	101	8008	374.4	143	18.113
T18	5.4	12	24	100.4	7913	382	100	36.089
T19	3.5	14	20	80.5	5087	589	92	35.045
T20	3	11.9	20	131	13471	222.6	134	21.565
T21	3	11.3	23	116	10563	283.9	142	32.121
T22	3	11.5	22	122	11684	256.6	139	27.549
T23	3	11.5	22	122	11684	256.6	139	27.549
T24	3	10.4	22	121.4	11569	260.9	90	37.863
T25	1.8	9.7	20	121	11493	261	140	46.695
T26	4	12.5	25	113	10023	300	142	25.078
T27	3	10.5	10.5	121	11493	261	110	36.814
T28	3	9.1	22	140	15386	194.9	100	42.222
T29	3	11	22	136	14519	206.5	136	25.332
T30	3	12	22.5	126	12462	240.6	119	22.732
T31	3	10.5	22	145	16504	181.7	100	25.622
T32	7	17	27	60	2826	1061.2	45	35.265
T33	3	11	25	120	11304	263.9	120	32.376
T34	2.5	9	18	150	17662	169.8	140	38.019
T35	2.5	8.8	25	156	19103	157	160	37.604

2.4. The Sub-Criteria of Economic Criterion

Costs per unit turbine were calculated according to the determined turbine cost, maintenance and repair costs and installation costs. Total costs were determined with these data. The dollar ($) was used as the currency in total cost calculations. In addition, the government support rates to be given are determined according to the turbine capacities and presented in Table 4.

Table 4. The values of the sub-criteria of economic criterion

Turbine Code	Total Cost (million $)	Government support	Turbine Code	Total Cost (million $)	Government support
T1	1.75	36.19	T19	1.8	35.04
T2	1.75	32.12	T20	1.85	21.56
T3	1.75	32.53	T21	1.8	32.12
T4	1.8	33.53	T22	1.95	27.54
T5	1.8	38.67	T23	1.8	27.54
T6	1.75	38.82	T24	1.75	37.86
T7	1.8	34.73	T25	1.85	46.69
T8	1.8	30.62	T26	1.95	25.07
T9	1.85	20.71	T27	1.8	36.81
T10	1.75	24.81	T28	1.75	42.22
T11	1.7	42.54	T29	1.75	25.33
T12	2	40.80	T30	2	22.73
T13	2	42.03	T31	1.8	25.62
T14	1.95	37.35	T32	1.75	35.26
T15	1.9	31.54	T33	1.8	32.37
T16	1.85	15.22	T34	1.85	38.01
T17	1.75	18.11	T35	1.8	37.60
T18	1.95	36.08			

2.5. The Sub-Criteria of Environmental Criterion

The turbines were evaluated according to noise, shadow vibration and glare, impact on living things and electromagnetic effect. The impact level of the turbines on living things was taken equally. Shadow vibration and glare effects were evaluated according to the shadow size that occurred depending on the rotor diameters and heights of the turbines. Point scoring was given to the wind turbine brands from 1 to 5. In the electromagnetic effect, the blade rotation speeds of the turbines were utilised. The values of the sub-criteria of environmental criteria are shown in Table 5.

Table 5. The values of the sub-criteria of environmental criterion

Turbine Code	Noise	Shadow vibration and glare	Impact on living things	Electroma g. effect	Turbine Code	Noise	Shadow vibration and glare	Impact on living things	Electroma g. effect
T1	3	2	1	3	T19	3	2	1	3
T2	3	2	1	3	T20	5	5	1	5
T3	3	2	1	3	T21	3	2	1	3
T4	3	2	1	3	T22	3	2	1	3
T5	3	2	1	3	T23	4	3	1	4
T6	3	2	1	3	T24	3	2	1	3
T7	3	2	1	3	T25	3	3	1	3
T8	5	5	1	5	T26	4	4	1	4
T9	4	4	1	4	T27	4	3	1	4
T10	3	3	1	3	T28	3	2	1	3
T11	4	3	1	4	T29	4	3	1	4
T12	3	4	1	3	T30	5	5	1	5
T13	4	4	1	4	T31	3	2	1	3
T14	3	3	1	3	T32	3	2	1	3
T15	3	4	1	3	T33	3	3	1	3
T16	3	2	1	3	T34	3	2	1	3
T17	4	3	1	4	T35	3	3	1	3
T18	3	2	1	3					

2.6. The Sub-Criteria of Custom Service Criterion

Under the heading of customer service, turbine brands were compared according to the service support, spare parts and brand reliability they provide to their customers. While making these comparisons, the necessary information provided by using web addresses of turbine brands, the guarantees, and the number of wind power plants and turbines they have built were used. The values of the sub-criteria of customer service criteria are shown in Table 6.

Table 6. The values of the sub-criteria of the customer service criterion

Turbine Code	Service support	Spare parts	Reliability	Turbine Code	Service support	Spare parts	Reliability
T1	3	2	3	T19	3	2	3
T2	3	2	3	T20	5	5	5
T3	3	2	3	T21	3	2	3
T4	3	2	3	T22	3	2	3
T5	3	2	3	T23	4	3	4
T6	3	2	3	T24	3	2	3
T7	3	2	3	T25	3	3	3
T8	5	5	5	T26	4	4	4
T9	4	4	4	T27	4	3	4
T10	3	3	3	T28	3	2	3
T11	4	3	4	T29	4	3	4
T12	3	4	3	T30	5	5	5
T13	4	4	4	T31	3	2	3
T14	3	3	3	T32	3	2	3
T15	3	4	3	T33	3	3	3
T16	3	2	3	T34	3	2	3
T17	4	3	4	T35	3	3	3
T18	3	2	3				

3. Results

The novelty assessment model was applied to 3 MW wind turbines selected for the case study. The Entropy-based Novelty Multi-Attribute Utility Theory used in the novelty assessment model is explained in detail in Section 2.1. In addition, the criteria are coded as shown in Table 7 so that the tables containing the results can be evaluated easily.

Table 7. Criteria codes

Criteria	Criteria Code
Cut-In WS (m/s)	C1
Rated WS (m/s)	C2
Cut-Out WS (m/s)	C3
Rotor Diameter (m)	C4
Swept Area (m^2)	C5
Power Density (W/m^2)	C6
Hub height (m)	C7
CF	C8
Total cost (million $)	C9
Government support	C10
Noise	C11
Shadow vibration and glare	C12
Impact on living things	C13
Electromagnetic effect	C14
Service support	C15
Spare parts	C16
Reliability	C17

35 × 17 decision matrix, which includes wind turbines and selection criteria, was created. The decision matrix is shown in Table 8. The decision matrix is also the matrix in which all criteria are combined with their values. Each criterion is evaluated in the decision matrix, and the best and worst values are determined.

Table 8. The decision matrix

Turbines & Criteria	C1	C2	C3	C4	C5	C6	C7	C8	C9	C10	C11	C12	C13	C14	C15	C16	C17
T1	3	10.5	25	122	11683	256.7	139	36.19	1.75	36.197	3	2	1	3	3	2	3
T2	3	11.3	23	116	105623	283.9	142	32.12	1.75	32.121	3	2	1	3	3	2	3
T3	3	11	20	120	11304	265.3	110	32.53	1.75	32.538	3	2	1	3	3	2	3
T4	5	11	25	118.2	10967	273.4	140	33.53	1.80	33.536	3	2	1	3	3	2	3
T5	3	11.5	25	103	8328	360.2	85	38.67	1.80	38.671	3	2	1	3	3	2	3
T6	3	9.1	22	146	16733	179.2	120	38.82	1.75	38.824	3	2	1	3	3	2	3
T7	3	10	20	134	14095	212.8	90	34.73	1.80	34.737	3	2	1	3	3	2	3
T8	2	11.5	25	115.7	10508	285.3	149	30.62	1.80	30.626	5	5	1	5	5	5	5
T9	3	12	25	132	13677	219.2	160	20.71	1.85	20.712	4	4	1	4	4	4	4
T10	3	12	25	120.6	11417	262.6	140	24.81	1.75	24.814	3	3	1	3	3	3	3
T11	3	9.3	20	135	14306	209.6	140	42.54	1.70	42.541	4	3	1	4	4	3	4
T12	3.5	10.2	25	120	11304	265.3	90	40.80	2.00	40.809	3	4	1	3	3	4	3
T13	3	10.1	25	120	11304	265.3	126	42.03	2.00	42.033	4	4	1	4	4	4	4
T14	6	14	21	78	4775	627.9	80	37.35	1.95	37.358	3	3	1	3	3	3	3
T15	6	14.5	25	80.5	5087	589	78	31.54	1.90	31.543	3	4	1	3	3	4	3
T16	2.1	16	28	100	7850	382	135	15.22	1.85	15.225	3	2	1	3	3	2	3
T17	3	15	25	101	8008	374.4	143	18.11	1.75	18.113	4	3	1	4	4	3	4
T18	5.4	12	24	100.4	7913	382	100	36.08	1.95	36.089	3	2	1	3	3	2	3
T19	3.5	14	20	80.5	5087	589	92	35.04	1.80	35.045	3	2	1	3	3	2	3
T20	3	11.9	20	131	13471	222.6	134	21.56	1.85	21.565	5	5	1	5	5	5	5
T21	3	11.3	23	116	10563	283.9	142	32.12	1.80	32.121	3	2	1	3	3	2	3
T22	3	11.5	22	122	11684	256.6	139	27.54	1.95	27.549	3	2	1	3	3	2	3
T23	3	11.5	22	122	11684	256.6	139	27.54	1.80	27.549	4	3	1	4	4	3	4
T24	3	10.4	22	121.4	11569	260.9	90	37.86	1.75	37.863	3	2	1	3	3	2	3
T25	1.8	9.7	20	121	11493	261	140	46.69	1.85	46.695	3	3	1	3	3	3	3
T26	4	12.5	25	113	10023	300	142	25.07	1.95	25.078	4	4	1	4	4	4	4
T27	3	10.5	10.5	121	11493	261	110	36.81	1.80	36.814	4	3	1	4	4	3	4
T28	3	9.1	22	140	15386	194.9	100	42.22	1.75	42.222	3	2	1	3	3	2	3
T29	3	11	22	136	14519	206.5	136	25.33	1.75	25.332	4	3	1	4	4	3	4
T30	3	12	22.5	126	12462	240.6	119	22.73	2.00	22.732	5	5	1	5	5	5	5
T31	3	10.5	22	145	16504	181.7	100	25.62	1.80	25.622	3	2	1	3	3	2	3
T32	7	17	27	60	2826	1061.2	45	35.26	1.75	35.265	3	2	1	3	3	2	3
T33	3	11	25	120	11304	263.9	120	32.376	1.80	32.376	3	3	1	3	3	3	3
T34	2.5	9	18	150	17662	169.8	140	38.019	1.85	38.019	3	2	1	3	3	2	3
T35	2.5	8.8	25	156	19103	157	160	37.604	1.80	37.604	3	3	1	3	3	3	3

The best and worst values determined based on the decision matrix are shown in Table 9.

Table 9. Best and worst values of decision matrix according to the criteria

Values	C1	C2	C3	C4	C5	C6	C7	C8	C9	C10	C11	C12	C13	C14	C15	C16	C17
Best Value	1.8	8.8	28	156	19103	1061.2	160	46.69	1.7	46.695	5	5	1	5	5	5	5
Worst Value	7	17	10.5	60	2826	157	45	15.22	2.0	15.225	3	2	1	3	3	2	3

After determining the best and worst values, the calculated normalised decision matrix is presented in Table 10.

Table 10. Normalised decision matrix

Turbines & Criteria	C1	C2	C3	C4	C5	C6	C7	C8	C9	C10	C11	C12	C13	C14	C15	C16	C17
T1	0.769	0.793	0.829	0.646	0.544	0.110	0.817	0.666	0.833	0.666	0.000	0.000	0.000	0.000	0.000	0.000	0.000
T2	0.769	0.695	0.714	0.583	0.475	0.140	0.843	0.537	0.833	0.537	0.000	0.000	0.000	0.000	0.000	0.000	0.000
T3	0.769	0.732	0.543	0.625	0.521	0.120	0.565	0.550	0.833	0.550	0.000	0.000	0.000	0.000	0.000	0.000	0.000
T4	0.385	0.732	0.829	0.606	0.500	0.129	0.826	0.582	0.667	0.582	0.000	0.000	0.000	0.000	0.000	0.000	0.000
T5	0.769	0.671	0.829	0.448	0.338	0.225	0.348	0.745	0.667	0.745	0.000	0.000	0.000	0.000	0.000	0.000	0.000
T6	0.769	0.963	0.657	0.896	0.854	0.025	0.652	0.750	0.833	0.750	0.000	0.000	0.000	0.000	0.000	0.000	0.000
T7	0.769	0.854	0.543	0.771	0.692	0.062	0.391	0.620	0.667	0.620	0.000	0.000	0.000	0.000	0.000	0.000	0.000
T8	0.962	0.671	0.829	0.580	0.472	0.142	0.904	0.489	0.667	0.489	1.000	1.000	0.000	1.000	1.000	1.000	1.000
T9	0.769	0.610	0.829	0.750	0.667	0.069	1.000	0.174	0.500	0.174	0.500	0.667	0.000	0.500	0.500	0.667	0.500
T10	0.769	0.610	0.829	0.631	0.528	0.117	0.826	0.305	0.833	0.305	0.000	0.333	0.000	0.000	0.000	0.333	0.000
T11	0.769	0.939	0.543	0.781	0.705	0.058	0.826	0.868	1.000	0.868	0.500	0.333	0.000	0.500	0.500	0.333	0.500
T12	0.673	0.829	0.829	0.625	0.521	0.120	0.391	0.813	0.000	0.813	0.000	0.667	0.000	0.000	0.000	0.667	0.000
T13	0.769	0.841	0.829	0.625	0.521	0.120	0.704	0.852	0.000	0.852	0.500	0.667	0.000	0.500	0.500	0.667	0.500
T14	0.192	0.366	0.600	0.188	0.120	0.521	0.304	0.703	0.167	0.703	0.000	0.333	0.000	0.000	0.000	0.333	0.000
T15	0.192	0.305	0.829	0.214	0.139	0.478	0.287	0.519	0.333	0.519	0.000	0.667	0.000	0.000	0.000	0.667	0.000
T16	0.942	0.122	1.000	0.417	0.309	0.249	0.783	0.000	0.500	0.000	0.000	0.000	0.000	0.000	0.000	0.000	0.000
T17	0.769	0.244	0.829	0.427	0.318	0.240	0.852	0.092	0.833	0.092	0.500	0.333	0.000	0.500	0.500	0.333	0.500
T18	0.308	0.610	0.771	0.421	0.309	0.249	0.478	0.663	0.167	0.663	0.000	0.000	0.000	0.000	0.000	0.000	0.000
T19	0.673	0.366	0.543	0.214	0.139	0.478	0.409	0.630	0.667	0.630	0.000	0.000	0.000	0.000	0.000	0.000	0.000
T20	0.769	0.622	0.543	0.740	0.654	0.073	0.774	0.201	0.500	0.201	1.000	1.000	0.000	1.000	1.000	1.000	1.000
T21	0.769	0.695	0.714	0.583	0.475	0.140	0.843	0.537	0.667	0.537	0.000	0.000	0.000	0.000	0.000	0.000	0.000
T22	0.769	0.671	0.657	0.646	0.544	0.110	0.817	0.392	0.167	0.392	0.000	0.000	0.000	0.000	0.000	0.000	0.000
T23	0.769	0.671	0.657	0.646	0.544	0.110	0.817	0.392	0.667	0.392	0.500	0.333	0.000	0.500	0.500	0.333	0.500
T24	0.769	0.805	0.657	0.640	0.533	0.115	0.391	0.719	0.833	0.719	0.000	0.000	0.000	0.000	0.000	0.000	0.000
T25	1.000	0.890	0.543	0.635	0.532	0.115	0.826	1.000	0.500	1.000	0.000	0.333	0.000	0.000	0.000	0.333	0.000
T26	0.577	0.549	0.829	0.552	0.440	0.158	0.843	0.313	0.167	0.313	0.500	0.667	0.000	0.500	0.500	0.667	0.500
T27	0.769	0.793	0.000	0.635	0.532	0.115	0.565	0.686	0.667	0.686	0.500	0.333	0.000	0.500	0.500	0.333	0.500
T28	0.769	0.963	0.657	0.833	0.772	0.042	0.478	0.858	0.833	0.858	0.000	0.000	0.000	0.000	0.000	0.000	0.000
T29	0.769	0.732	0.657	0.792	0.718	0.055	0.791	0.321	0.833	0.321	0.500	0.333	0.000	0.500	0.500	0.333	0.500
T30	0.769	0.610	0.686	0.688	0.592	0.092	0.643	0.239	0.000	0.239	1.000	1.000	0.000	1.000	1.000	1.000	1.000
T31	0.769	0.793	0.657	0.885	0.840	0.027	0.478	0.330	0.667	0.330	0.000	0.000	0.000	0.000	0.000	0.000	0.000
T32	0.000	0.000	0.943	0.000	0.000	1.000	0.000	0.637	0.833	0.637	0.000	0.000	0.000	0.000	0.000	0.000	0.000
T33	0.769	0.732	0.829	0.625	0.524	0.118	0.652	0.545	0.667	0.545	0.000	0.333	0.000	0.000	0.000	0.333	0.000
T34	0.865	0.976	0.429	0.938	0.912	0.014	0.826	0.724	0.500	0.724	0.000	0.000	0.000	0.000	0.000	0.000	0.000
T35	0.865	1.000	0.829	1.000	1.000	0.000	1.000	0.711	0.667	0.711	0.000	0.333	0.000	0.000	0.000	0.333	0.000

It is necessary to find the criteria weights to find the total utility values. Therefore, at this stage of the study, the entropy method was used, and entropy values were calculated using Equation (2.5). The entropy-based normalised decision matrix and calculated entropy values are presented in Tables 11 and 12.

Table 11. The entropy-based normalised decision matrix

Turbines & Criteria	C1	C2	C3	C4	C5	C6	C7	C8	C9	C10	C11	C12	C13	C14	C15	C16	C17
T1	0.026	0.026	0.031	0.029	0.029	0.024	0.033	0.032	0.027	0.032	0.025	0.020	0.029	0.025	0.025	0.020	0.025
T2	0.026	0.028	0.029	0.028	0.027	0.026	0.034	0.028	0.027	0.028	0.025	0.020	0.029	0.025	0.025	0.020	0.025
T3	0.026	0.027	0.025	0.029	0.029	0.024	0.026	0.029	0.027	0.029	0.025	0.020	0.029	0.025	0.025	0.020	0.025
T4	0.043	0.027	0.031	0.029	0.028	0.025	0.033	0.030	0.028	0.030	0.025	0.020	0.029	0.025	0.025	0.020	0.025
T5	0.026	0.029	0.031	0.025	0.021	0.033	0.020	0.034	0.028	0.034	0.025	0.020	0.029	0.025	0.025	0.020	0.025
T6	0.026	0.023	0.028	0.035	0.042	0.016	0.028	0.034	0.027	0.034	0.025	0.020	0.029	0.025	0.025	0.020	0.025
T7	0.026	0.025	0.025	0.032	0.036	0.020	0.021	0.031	0.028	0.031	0.025	0.020	0.029	0.025	0.025	0.020	0.025
T8	0.017	0.029	0.031	0.028	0.027	0.026	0.035	0.027	0.028	0.027	0.042	0.051	0.029	0.042	0.042	0.051	0.042
T9	0.026	0.030	0.031	0.032	0.034	0.020	0.038	0.018	0.029	0.018	0.034	0.040	0.029	0.034	0.034	0.040	0.034
T10	0.026	0.030	0.031	0.029	0.029	0.024	0.033	0.022	0.027	0.022	0.025	0.030	0.029	0.025	0.025	0.030	0.025
T11	0.026	0.023	0.025	0.033	0.036	0.019	0.033	0.037	0.027	0.037	0.034	0.030	0.029	0.034	0.034	0.030	0.034
T12	0.030	0.025	0.031	0.029	0.029	0.024	0.021	0.036	0.031	0.036	0.025	0.040	0.029	0.025	0.025	0.040	0.025
T13	0.026	0.025	0.031	0.029	0.029	0.024	0.030	0.037	0.031	0.037	0.034	0.040	0.029	0.034	0.034	0.040	0.034
T14	0.051	0.035	0.026	0.019	0.012	0.058	0.019	0.033	0.030	0.033	0.025	0.030	0.029	0.025	0.025	0.030	0.025
T15	0.051	0.036	0.031	0.019	0.013	0.054	0.019	0.028	0.030	0.028	0.025	0.040	0.029	0.025	0.025	0.040	0.025
T16	0.018	0.040	0.035	0.024	0.020	0.035	0.032	0.013	0.029	0.013	0.025	0.020	0.029	0.025	0.025	0.020	0.025
T17	0.026	0.037	0.031	0.024	0.020	0.034	0.034	0.016	0.027	0.016	0.034	0.030	0.029	0.034	0.034	0.030	0.034
T18	0.046	0.030	0.030	0.024	0.020	0.035	0.024	0.032	0.030	0.032	0.025	0.020	0.029	0.025	0.025	0.020	0.025
T19	0.030	0.035	0.025	0.019	0.013	0.054	0.022	0.031	0.028	0.031	0.025	0.020	0.029	0.025	0.025	0.020	0.025
T20	0.026	0.030	0.025	0.032	0.034	0.020	0.032	0.019	0.029	0.019	0.042	0.051	0.029	0.042	0.042	0.051	0.042
T21	0.026	0.028	0.029	0.028	0.027	0.026	0.034	0.028	0.028	0.028	0.025	0.020	0.029	0.025	0.025	0.020	0.025
T22	0.026	0.029	0.028	0.029	0.029	0.024	0.033	0.024	0.030	0.024	0.025	0.020	0.029	0.025	0.025	0.020	0.025
T23	0.026	0.029	0.028	0.029	0.029	0.024	0.033	0.024	0.028	0.024	0.034	0.030	0.029	0.034	0.034	0.030	0.034
T24	0.026	0.026	0.028	0.029	0.029	0.024	0.021	0.033	0.027	0.033	0.025	0.020	0.029	0.025	0.025	0.020	0.025
T25	0.015	0.024	0.025	0.029	0.029	0.024	0.033	0.041	0.029	0.041	0.025	0.030	0.029	0.025	0.025	0.030	0.025
T26	0.034	0.031	0.031	0.027	0.025	0.028	0.034	0.022	0.030	0.022	0.034	0.040	0.029	0.034	0.034	0.040	0.034
T27	0.026	0.026	0.013	0.029	0.029	0.024	0.026	0.032	0.028	0.032	0.034	0.030	0.029	0.034	0.034	0.030	0.034
T28	0.026	0.023	0.028	0.034	0.039	0.018	0.024	0.037	0.027	0.037	0.025	0.020	0.029	0.025	0.025	0.020	0.025
T29	0.026	0.027	0.028	0.033	0.037	0.019	0.032	0.022	0.027	0.022	0.034	0.030	0.029	0.034	0.034	0.030	0.034
T30	0.026	0.030	0.028	0.030	0.031	0.022	0.028	0.020	0.031	0.020	0.042	0.051	0.029	0.042	0.042	0.051	0.042
T31	0.026	0.026	0.028	0.035	0.042	0.017	0.024	0.023	0.028	0.023	0.025	0.020	0.029	0.025	0.025	0.020	0.025
T32	0.060	0.042	0.034	0.014	0.007	0.098	0.011	0.031	0.027	0.031	0.025	0.020	0.029	0.025	0.025	0.020	0.025
T33	0.026	0.027	0.031	0.029	0.029	0.024	0.028	0.029	0.028	0.029	0.025	0.030	0.029	0.025	0.025	0.030	0.025
T34	0.021	0.022	0.023	0.036	0.045	0.016	0.033	0.033	0.029	0.033	0.025	0.020	0.029	0.025	0.025	0.020	0.025
T35	0.021	0.022	0.031	0.038	0.048	0.014	0.038	0.033	0.028	0.033	0.025	0.030	0.029	0.025	0.025	0.030	0.025

Table 12. Entropy values

	C1	C2	C3	C4	C5	C6	C7	C8	C9	C10	C11	C12	C13	C14	C15	C16	C17
E_j	0.986	0.996	0.997	0.995	0.985	0.968	0.992	0.992	1.000	0.992	0.995	0.985	1.000	0.995	0.995	0.985	0.995

After determining the entropy values, the weight values were determined using Equations (2.6) and (2.7). Calculated weight values are shown in Table 13.

Table 13. Weight values

	C1	C2	C3	C4	C5	C6	C7	C8	C9	C10	C11	C12	C13	C14	C15	C16	C17
w_j	0.096	0.026	0.020	0.031	0.106	0.217	0.052	0.054	0.002	0.054	0.032	0.107	0.000	0.032	0.032	0.107	0.032

The total utility values obtained using the required parameters calculated above are presented in Table 14. In addition, when Table 14 is examined, it is seen that the selection of turbines with codes T8, T20 and T30 will be more appropriate. Moreover, in the consistency analysis, the consistency index and consistency ratio were determined for 17 criteria as 0.1538 and 0.0956, respectively.

Table 14. Total utility values

	C1	C2	C3	C4	C5	C6	C7	C8	C9	C10	C11	C12	C13	C14	C15	C16	C17	Total
T1	0.074	0.021	0.017	0.020	0.058	0.024	0.042	0.036	0.002	0.036	0.000	0.000	0.000	0.000	0.000	0.000	0.000	0.329
T2	0.074	0.018	0.014	0.018	0.051	0.030	0.044	0.029	0.002	0.029	0.000	0.000	0.000	0.000	0.000	0.000	0.000	0.309
T3	0.074	0.019	0.011	0.020	0.055	0.026	0.029	0.030	0.002	0.030	0.000	0.000	0.000	0.000	0.000	0.000	0.000	0.295
T4	0.037	0.019	0.017	0.019	0.053	0.028	0.043	0.031	0.001	0.031	0.000	0.000	0.000	0.000	0.000	0.000	0.000	0.279
T5	0.074	0.018	0.017	0.014	0.036	0.049	0.018	0.040	0.001	0.040	0.000	0.000	0.000	0.000	0.000	0.000	0.000	0.306
T6	0.074	0.025	0.013	0.028	0.091	0.005	0.034	0.040	0.002	0.040	0.000	0.000	0.000	0.000	0.000	0.000	0.000	0.352
T7	0.074	0.022	0.011	0.024	0.074	0.013	0.020	0.033	0.001	0.033	0.000	0.000	0.000	0.000	0.000	0.000	0.000	0.306
T8	0.092	0.018	0.017	0.018	0.050	0.031	0.047	0.026	0.001	0.026	0.032	0.107	0.000	0.032	0.032	0.107	0.032	0.668
T9	0.074	0.016	0.017	0.023	0.071	0.015	0.052	0.009	0.001	0.009	0.016	0.071	0.000	0.016	0.016	0.071	0.016	0.494
T10	0.074	0.016	0.017	0.020	0.056	0.025	0.043	0.016	0.002	0.016	0.000	0.036	0.000	0.000	0.000	0.036	0.000	0.356
T11	0.074	0.025	0.011	0.024	0.075	0.013	0.043	0.047	0.002	0.047	0.016	0.036	0.000	0.016	0.016	0.036	0.016	0.495
T12	0.065	0.022	0.017	0.020	0.055	0.026	0.020	0.044	0.000	0.044	0.000	0.071	0.000	0.000	0.000	0.071	0.000	0.454
T13	0.074	0.022	0.017	0.020	0.055	0.026	0.036	0.046	0.000	0.046	0.016	0.071	0.000	0.016	0.016	0.071	0.016	0.548
T14	0.018	0.010	0.012	0.006	0.013	0.113	0.016	0.038	0.000	0.038	0.000	0.036	0.000	0.000	0.000	0.036	0.000	0.335
T15	0.018	0.008	0.017	0.007	0.015	0.104	0.015	0.028	0.001	0.028	0.000	0.071	0.000	0.000	0.000	0.071	0.000	0.382
T16	0.091	0.003	0.020	0.013	0.033	0.054	0.040	0.000	0.001	0.000	0.000	0.000	0.000	0.000	0.000	0.000	0.000	0.255
T17	0.074	0.006	0.017	0.013	0.034	0.052	0.044	0.005	0.002	0.005	0.016	0.036	0.000	0.016	0.016	0.036	0.016	0.387
T18	0.030	0.016	0.015	0.013	0.033	0.054	0.025	0.036	0.000	0.036	0.000	0.000	0.000	0.000	0.000	0.000	0.000	0.257
T19	0.065	0.010	0.011	0.007	0.015	0.104	0.021	0.034	0.001	0.034	0.000	0.000	0.000	0.000	0.000	0.000	0.000	0.301
T20	0.074	0.016	0.011	0.023	0.070	0.016	0.040	0.011	0.001	0.011	0.032	0.107	0.000	0.032	0.032	0.107	0.032	0.614
T21	0.074	0.018	0.014	0.018	0.051	0.030	0.044	0.029	0.001	0.029	0.000	0.000	0.000	0.000	0.000	0.000	0.000	0.308
T22	0.074	0.018	0.013	0.020	0.058	0.024	0.042	0.021	0.000	0.021	0.000	0.000	0.000	0.000	0.000	0.000	0.000	0.291
T23	0.074	0.018	0.013	0.020	0.058	0.024	0.042	0.021	0.001	0.021	0.016	0.036	0.000	0.016	0.016	0.036	0.016	0.428
T24	0.074	0.021	0.013	0.020	0.057	0.025	0.020	0.039	0.002	0.039	0.000	0.000	0.000	0.000	0.000	0.000	0.000	0.309
T25	0.096	0.023	0.011	0.020	0.057	0.025	0.043	0.054	0.001	0.054	0.000	0.036	0.000	0.000	0.000	0.036	0.000	0.454
T26	0.055	0.014	0.017	0.017	0.047	0.034	0.044	0.017	0.000	0.017	0.016	0.071	0.000	0.016	0.016	0.071	0.016	0.469
T27	0.074	0.021	0.000	0.020	0.057	0.025	0.029	0.037	0.001	0.037	0.016	0.036	0.000	0.016	0.016	0.036	0.016	0.436
T28	0.074	0.025	0.013	0.026	0.082	0.009	0.025	0.046	0.002	0.046	0.000	0.000	0.000	0.000	0.000	0.000	0.000	0.348
T29	0.074	0.019	0.013	0.025	0.076	0.012	0.041	0.017	0.002	0.017	0.016	0.036	0.000	0.016	0.016	0.036	0.016	0.432
T30	0.074	0.016	0.014	0.022	0.063	0.020	0.033	0.013	0.000	0.013	0.032	0.107	0.000	0.032	0.032	0.107	0.032	0.609
T31	0.074	0.021	0.013	0.028	0.089	0.006	0.025	0.018	0.001	0.018	0.000	0.000	0.000	0.000	0.000	0.000	0.000	0.292
T32	0.000	0.000	0.019	0.000	0.000	0.217	0.000	0.034	0.002	0.034	0.000	0.000	0.000	0.000	0.000	0.000	0.000	0.306
T33	0.074	0.019	0.017	0.020	0.056	0.026	0.034	0.029	0.001	0.029	0.000	0.036	0.000	0.000	0.000	0.036	0.000	0.375
T34	0.083	0.025	0.009	0.029	0.097	0.003	0.043	0.039	0.001	0.039	0.000	0.000	0.000	0.000	0.000	0.000	0.000	0.368
T35	0.083	0.026	0.017	0.031	0.106	0.000	0.052	0.038	0.001	0.038	0.000	0.036	0.000	0.000	0.000	0.036	0.000	0.464

4. Discussion and Conclusion

Nowadays, wind energy systems are commercialised by many countries around the world to generate energy because many advantages have been proven over other renewable energy sources. Wind turbines are also the most important part of this energy conversion system. In this study, an adaptive assessment model is presented to select the best wind turbine to fill the gap in the literature studies where turbine selections are made with qualitative evaluation using limited criteria. This is the most important focus of the study. In addition, although the MAUT used in the proposed adaptive model is encountered in some of the literature studies, the studies in which it was used with the entropy method are limited. It was especially preferred in determining the weights using the entropy method's advantages.

Selection problems involve various evaluation criteria and the different stakeholders who set these criteria. For this reason, experts and stakeholders in the field of wind energy management were included in the process through interviews. The proposed model's consistency rate (0.0956) indicates that the results are also quite consistent. When the study results were evaluated, it was seen that choosing solely turbine power was not the right approach. The necessity of examining the effect of all criteria was clearly understood in the study's outcome, and a more consistent selection targeted with the proposed model was achieved. The evaluations of the analysis results are presented below:

1. 35 different turbine brands were examined using four main and 17 sub-criteria. These criteria were applied to the innovative evaluation model developed for use in turbine selection.
2. When the total benefit values obtained by the innovative evaluation model are examined, it is seen that the turbines with codes T8, T20 and T30 are more suitable, respectively.
3. The average total utility value was determined as 0.389. When an evaluation is made on this value, it is seen that 13 turbine models are above the average benefit value.
4. When the criteria are evaluated independently, the advantages of each turbine differ from the others. However, evaluating the effectiveness of all criteria leads to more consistent and realistic results. The results obtained from the consistency analysis support this.

Unlike the studies in the literature, an entropy-based approach is preferred in the method used in the proposed study. Thus, the consistency rate is increased by utilising the benefits of entropy. In addition, classical multi-criteria decision-making methods are preferred in the studies in the literature, but not as many criteria as the number of criteria used in this study. This provides the opportunity to evaluate the results in multiple ways. Although 3 MW turbines are used in this study, the developed model can be easily applied to all turbines with different powers. Evaluating with many criteria strengthens the model and adds significant value to the study. The proposed model has the property that can be applied both commercially and practically. Therefore, the results are significant and precious in engineering and economics.

Additionally, it was emphasised that this study's correct selection of wind turbines for wind energy production facilities is critical. Thus, it is possible to present different approaches for the optimal selection of wind turbines for future work. It is also planned to determine the valid features for optimal selection.

Author Contributions

They all read and approved the final version of the manuscript.
Cem Emeksiz: Analysis, Investigation, Software, Writing- Original Draft, Writing – Review, Methodology.
Abdullah Yüksel: Writing – Review & Editing, Formal Analysis, Validation, Supervision.

Conflicts of Interest

The authors declare no conflict of interest.

References

[1] E. B. Agyekum, *Energy poverty in energy rich Ghana: A SWOT analytical approach for the development of Ghana's renewable energy*, Sustainable Energy Technologies and Assessments, 40, (2020) 1–9.

[2] F. Adusah-Poku, K. Takeuchi, *Energy poverty in Ghana: any progress so far?* Renewable Sustainable Energy Reviews, 112, (2019) 853–64.

[3] C. Emeksiz, B. Demirci, *The determination of offshore wind energy potential of Turkey by using novelty hybrid site selection method*, Sustainable Energy Technologies and Assessments, 36, (2019) 1–21.

[4] Renewables Global Status Report-REN 21, https://www.ren21.net/reports/global-status-report/, 2021 (accessed 15 May 2022)

[5] M. Lydia, S. S. Kumar, A. I. Selvakumar, G. E. P. Kumar, *A comprehensive review on wind turbine power curve modeling techniques*, Renewable and Sustainable Energy Reviews, 30, (2014) 452–460.

[6] C. Carrillo, A. O. Montaño, J. Cidrás, E. Díaz-Dorado, *Review of power curve modelling for wind turbines*, Renewable and Sustainable Energy Reviews, 21, (2013) 572–581.

[7] I. Tiseo, *Global market share of wind turbine OEMs 2019*. https://www.statista.com/statistics/554377/wind-turbine-suppliers-globally-based-on-market-share/, 2021 (accessed 20 November 2021).

[8] F. A. Jowder, *Wind power analysis and site matching of wind turbine generators in Kingdom of Bahrain*, Applied Energy, 86(4), (2009) 538–545.

[9] S. E. Alimi, T. Maatallah, A. W. Dahmouni, S. B. Nasrallah, *Modeling and investigation of the wind resource in the gulf of Tunis, Tunisia*, Renewable and Sustainable Energy Reviews, 16(8), (2012) 5466–5478.

[10] L. De Araujo Lima, C. R. B. Filho, *Wind resource evaluation in são joão do cariri (sjc) – Paraiba, Brazil*, Renewable and Sustainable Energy Reviews, 16(1), (2012) 474–480.

[11] A. H. I. Lee, H. H. Chen, H. Y. Kang, *Multi-criteria decision making on strategic selection of wind farms*, Renewable Energy, 34(1), (2009)120–126.

[12] M. S. Adaramola, M. Agelin-Chaab, S. S. Paul, *Assessment of wind power generation along the coast of Ghana*, Energy Conversion and Management, 77, (2014) 61–69.

[13] M. S. Adaramola, O. M. Oyewola, O. S. Ohunakin, O. O. Akinnawonu, *Performance evaluation of wind turbines for energy generation in niger delta, Nigeria*, Sustainable Energy Technologies and Assessments, 6, (2014) 75–85.

[14] A. Kolios, M. Collu, A. Chahardehi, F. P. Brennan, M. H. Patel, A multi-criteria decision-making method to compare support structures for offshore wind turbines, in: N. Ladefoged, T. L. Destaintot, J. Mroczek, U. Nuscheler (Eds.), European Wind Energy Conference 2010, Warsaw, Poland, 2010, pp. 21–23.

[15] F. G. Montoya, F. Manzano-Agugliaro, S. Lopez-Marquez, Q. Hernandez-Escobedo, *Wind turbine selection for wind farm layout using multi-objective evolutionary algorithms*, Expert Systems with Applications, 41(15), (2014) 6585–6595.

[16] S. Nahi, S. M. H. Nabavi, *Choose suitable wind turbines for manjil wind power plant using Monte Carlo simulation*, International Journal of Computer Applications, 15(1), (2011) 26–34.

[17] S. Shokrzadeh, *Wind turbine power curve modeling using advanced parametric and nonparametric methods*, IEEE Transactions on Sustainable Energy, 5(4), (2014) 1262–1269.

[18] M. Di Somma, B. Yan, N. Bianco, G. Graditi, P. B. Luh, L. Mongibello, V. Naso, *Operation optimisation of a distributed energy system considering energy costs and exergy efficiency*, Energy Conversion and Management, 103, (2015) 739–751.

[19] B. Yan, M. Somma, N. Bianco, G. Graditi, P. B. Luh, L. Mongibello, V. Naso, *Exergy-based operation optimisation of a distributed energy system through the energy-supply chain*, Applied Thermal Engineering, 101, (2016) 741–751.

[20] R. Haaren Van, F. Vasilis, *GIS-based wind farm site selection using spatial multi-criteria analysis (SMCA): Evaluating the case for New York State*, Renewable and Sustainable Energy Reviews, 15(7), (2011) 3332–3340.

[21] S. K. Kim, O. Song, *A MAUT approach for selecting a dismantling scenario for the thermal column in KRR-1*, Annals of Nuclear Energy, 36(2), (2009) 145–150.

[22] R. Keeney, F. P. Seven, *Independence concepts and continuous multi-attribute utility functions*, Journal of Mathematical Psychology, 11(3), (1974) 294–327.

[23] E. Loken, *Use of multi-criteria decision analysis methods for energy planning problems*, Renewable and Sustainable Energy Reviews, 11(7), (2007) 1584–95.

[24] P. K. Dean Ting, C. Zhang, B. Wang, A. Deshmukh, B. Dubrosky, *Product and Process Cost Estimation with Fuzzy Multi-Attribute Utility Theory*, The Engineering Economist, 44(4), (1999) 303–331.

[25] D. Winterfeldt, W. Von Edwards, Decision analysis and behavioral research, Cambridge University Press, 1986.

[26] A. Ishızaka, P. Nemery, Multi-criteria decision analysis: Methods and software, John Wiley & Sons Ltd. Published, Chichester/UK, 2013.

[27] H. Zhang, C. L. Gu, L. W. Gu, Y. Zhang, The Evaluation of Tourism Destination Competitiveness by TOPSIS & Information Entropy–A Case in The Yangtze River Delta of China, Tourism Management, 32(2), (2011) 443–451.

[28] J. Wu, J. Sun, L. Liang, Y. Zha, *Determination of Weights for Ultimate Cross Efficiency Using Shannon Entropy*, Expert Systems with Applications, 38(5), (2011) 5162–5165.

[29] A. Karami, R. Johansson, *Utilisation of multi attribute decision making techniques to integrate automatic and manual ranking of options*, Journal of Information Science and Engineering, 30(2), (2014) 519–534.

[30] R. W. Saaty, *The analytic hierarchy process—what it is and how it is used*, Mathematical Modelling, 9(3-5), (1987) 161–76.

[31] L. Mikhailov, P. Tsventinov, *Evaluation of services using a fuzzy analytic hierarchy process*, Applied Soft Computing, 5(1), (2004) 23–33.

[32] T. L. Saaty, The analytical hierarchy process: Planning, priority setting, resource allocation, New York: McGraw-Hill, 1980.

[33] J. A. Alonso, M. T. Lamata, *Consistency in the analytic hierarchy process: A new approach.* International Journal of Uncertainty, Fuzziness and Knowledge-Based Systems, 14(4), (2006) 445−459.

[34] E. H. Forman, *Random indices for incomplete pairwise comparison matrices*, European Journal of Operational Research, 48(1), (1990) 153−155.

[35] H. Martin, G. Spano, J. F. Küster, M. Collu, A. J. Kolios, *Application and extension of the TOPSIS method for the assessment of floating offshore wind turbine support structures*, Ships and Offshore Structures, 8(5), (2013) 477−487.

[36] Wind turbine models, https://en.wind-turbine-models.com/turbines, 2022, (accessed 18 January 2022).

Journal of New Results in Science

https://dergipark.org.tr/en/pub/jnrs

Research Article

Open Access

E-ISSN: 1304-7981 https://doi.org/10.54187/jnrs.1160127

Not-ordered quasi-distance measures of generalised trapezoidal hesitant fuzzy numbers and their application to decision making problems

İrfan Deli [1], **Elif Özge Çelik** [2]

Keywords

Hesitant fuzzy set, Generalised trapezoidal hesitant fuzzy numbers, Quasi-distance measure, Multi-criteria decision-making

Abstract — As an extension of the trapezoidal fuzzy number, the generalised trapezoidal hesitant fuzzy number is an effective mathematical tool for handling uncertainty and vagueness in decision-making problems. Considering that the quasi-distance measure has a strong ability to process and analyse data, we initiated some novel quasi-distance measures to measure the strength of the relationship between generalised trapezoidal hesitant fuzzy numbers in this paper. Moreover, based on the proposed measures, a new multi-criteria decision-making approach is proposed to address uncertain real-life situations. Finally, a practical application of the proposed approach is also illustrated to demonstrate the effectiveness and applicability.

Subject Classification (2020): 03E72, 94D05.

1. Introduction

Since multiple-criteria decision-making (MCDM) problem is an inevitable part of our real life under some ambiguity and imprecision environment, fuzzy sets introduced [1] is more realistic for the decision maker to provide his uncertain linguistic term. Then, Torra [2] and Torra and Narukawa [3] developed hesitant fuzzy sets which the membership degrees of an element of universe set to a given set only by crisp numbers between 0 and 1. So far, many authors have studied on the fuzzy sets and hesitant fuzzy sets in [4–13] and especially in on real number set $\mathbb{R}$. For example, Fahmi et al [14, 15] have defined the concept of triangular cubic hesitant fuzzy number. Amin et al. [16] have propound aggregation operators for triangular cubic linguistic hesitant fuzzy set. Hussain et al. [17] have defined some new operation laws for the trapezoidal linguistic cubic fuzzy numbers including Hamming distance. They have also developed a TOPSIS method to solve the MCDM problems. Peng [18] has developed a multiple attribute decision-making (MADM) approach based on Archimedean t-norm and t-conorm in which the attribute values take the form of hesitant trapezoidal fuzzy elements. Similarly, trapezoidal fuzzy hesitant numbers have been defined and applied to several practical problems, on MADM in [19], on closeness degree and defuzzification technique of hesitant

[1] irfandeli@kilis.edu.tr (Corresponding Author); [2] celikelifozge19@gmail.com

[1,2] Kilisli Muallim Rıfat Faculty of Education, 7 Aralık University, Kilis, Turkiye

Article History: Received: 11 Aug 2022 - Accepted: 28 Aug 2022 - Published: 31 Aug 2022

trapezoidal fuzzy number in [20]. Moreover, Fahmi et al. [21] have introduced the idea of trapezoidal cubic hesitant fuzzy number and proposed a TOPSIS method. Fahmi et al. [22] then has proposed some new operation laws for trapezoidal cubic hesitant fuzzy numbers and their aggregation operators and Fahmi et al. [23] has defined some new operation laws for the trapezoidal linguistic cubic fuzzy number and Hamming distance of the numbers. Afterwards, Fahmi et al. [24] have developed an MADM method based on trapezoidal cubic fuzzy numbers.

Recently, Deli and Karaaslan [25] have defined the generalised trapezoidal hesitant fuzzy number as a generalisation of the hesitant fuzzy set and generalised fuzzy numbers and it permits the membership degrees of an subset of real numbers to a set to be represented as several possible fuzzy values and therefore it is easier to work on the generalised hesitant fuzzy numbers. Deli [26] then has proposed an advanced type of TOPSIS method to selecting an appropriate robot among the alternative robots under MADM problems by introducing some novel ordered distance measures including Hamming distance measure, Euclidean distance measure, λ-generalised distance measure, λ-generalised Hausdorff distance measure, λ-hybrid Hamming distance, hybrid Euclidean distance and λ-generalised hybrid distance measure on generalised trapezoidal hesitant fuzzy numbers.

In this paper, considering that the quasi-distance measure has a strong ability to process and analyse data and expanding the ordered distance measures given in Deli [26], we initiate some novel not-ordered quasi-distance measures to measure the strength of the relationship between generalised trapezoidal hesitant fuzzy numbers. Moreover, based on the proposed measures, a new MCDM approach is proposed to address uncertain real-life situations. Finally, a practical application of proposed approach is illustrated to demonstrate the effectiveness. This paper is derived from the second author's master's thesis [27].

2. Preliminary

In this section, some concepts and operations of fuzzy sets, hesitant fuzzy sets and generalised trapezoidal hesitant fuzzy numbers (GTHF-numbers) are briefly reviewed. More detailed explanations related to the fuzzy sets, hesitant fuzzy sets and generalised hesitant fuzzy numbers can be found in [1–3, 7, 21, 25, 26, 28].

Definition 2.1. [1] Let X be a non-empty set. A fuzzy set A on X is defined as:

$$A = \{\langle x, \mu_A(x)\rangle : x \in X\}$$

where μ_A is a membership function from X to $[0,1]$.

Definition 2.2. [2, 3] Let X be a non-empty set. A hesitant fuzzy set A on X is defined as

$$A = \{\langle x, \xi(x) = \{\xi_i : i = 1,2,...,l_A(x)\}\rangle : x \in X\}$$

where $\xi(x)$ is a set of some values in [0,1], denoting the possible membership degrees of the element $x \in X$ to the set A and $\xi = \xi(x)$ is called a hesitant fuzzy element (HFE). Here, $l_A(x)$ is the number of elements in $\xi(x)$, for $x \in X$ in hesitant fuzzy set A.

Definition 2.3. [25] Let X be a space of points (objects), $\xi_i \in [0,1]$ ($i \in I = \{1,2,...,n\}$ or $\{1,2,...,m\}$ or ...) and $a,b,c,d \in R$ such that $a \le b \le c \le d$. Then, in the set of real numbers $\mathbb{R}$, a generalised trapezoidal hesitant

fuzzy number (GTHF-number) can be represented as

$$\xi_N = \quad \langle (a,b,c,d);\{\xi_i : \xi_i \in \xi(x), \xi(x) \text{ is a set of some values in [0,1]}\}\rangle$$

whose membership functions can be described as follows:

$$\mu_A^i(x) = \begin{cases} (x-a)\xi_i/(b-a), & a \le x < b \\ \xi_i, & b \le x \le c \\ (d-x)\xi_i/(d-c), & c < x \le d \\ 0, & otherwise \end{cases}$$

In the paper, for focusing on GTHF- numbers, note that the set of all GTHF-number on $\mathbb{R}$ will be denoted by Φ.

Definition 2.4. [25] Let $\xi_N = \langle (a,b,c,d);\xi(x)\rangle$, $\xi_N^1 = \langle (a_1,b_1,c_1,d_1);\xi^1 = \xi^1(x)\rangle$, $\xi_N^2 = \langle (a_2,b_2,c_2,d_2);\xi^2 = \xi^2(x)\rangle \in \Phi$ and $\gamma \neq 0$ be any real number. Then,

i. $\xi_N^1 + \xi_N^2 = \langle (a_1+a_2, b_1+b_2, c_1+c_2, d_1+d_2); \cup_{\xi_1^1 \in \xi^1, \xi_1^2 \in \xi^2}\{\xi_1^1 + \xi_1^2 - \xi_1^1.\xi_1^2\}\rangle$

ii. $\xi_N^1 \cdot \xi_N^2 = \begin{cases} \langle (a_1a_2, b_1b_2, c_1c_2, d_1d_2); \cup_{\xi_1^1 \in \xi^1, \xi_1^2 \in \xi^2}\{\xi_1^1.\xi_1^2\}\rangle (d_1 > 0, d_2 > 0) \\ \langle (a_1d_2, b_1c_2, c_1b_2, d_1a_2); \cup_{\xi_1^1 \in \xi^1, \xi_1^2 \in \xi^2}\{\xi_1^1.\xi_1^2\}\rangle (d_1 < 0, d_2 > 0) \\ \langle (d_1d_2, c_1c_2, b_1b_2, a_1a_2); \cup_{\xi_1^1 \in \xi^1, \xi_1^2 \in \xi^2}\{\xi_1^1.\xi_1^2\}\rangle (d_1 < 0, d_2 < 0) \end{cases}$

iii. $\gamma\xi_N = \langle (\gamma a, \gamma b, \gamma c, \gamma d); \cup_{\xi \in \xi(x)}\{1-(1-\xi)^\gamma\}\rangle (\gamma \ge 0)$

iv. $(\xi_N)^\gamma = \langle (a^\gamma, b^\gamma, c^\gamma, d^\gamma); \cup_{\xi \in \xi(x)}\{\xi^\gamma\}\rangle (\gamma \ge 0)$

Definition 2.5. [26] Let $\xi_N^1, \xi_N^2 \in \Phi$, then the distance measure between ξ_N^1 and ξ_N^2 is defined as $D_{GTHF}(\xi_N^1, \xi_N^2)$ which satisfies the following properties:

i. $0 \le D_{GTHF}(\xi_N^1, \xi_N^2) \le 1$

ii. $D_{GTHF}(\xi_N^1, \xi_N^2) = 0 \Leftrightarrow \xi_N^1 = \xi_N^2$

iii. $D_{GTHF}(\xi_N^1, \xi_N^2) = D_{GTHF}((\xi_N^1, \xi_N^2))$

Note 2.6. [26] Let $\xi_N^1 = \langle (a_1,b_1,c_1,d_1);\{\xi_i^1 : \xi_i^1 \in \xi_1(x), \xi_1(x) \text{ is a set of some values in [0,1]}\}\rangle$ and $\xi^2 = \langle (a_2, b_2, c_2, d_2);\{\xi_i^2 : \xi_i^2 \in \xi_2(x), \xi_2(x)$ is a set of some values in [0,1]$\}\rangle$ be two GTHF-numbers and l^1 and l^2 be number of value ξ_i^1 in $\xi_1(x)$ and ξ_i^2 in $\xi_2(x)$, respectively. Generally, since we have $l^1 \neq l^2$ we should increase the smallest one until both of them have the same number to compare them. Therefore, thought the paper, he used to add a value to the smallest one by adding the value $\xi_k^1 = \min\{\xi_i^1 : \xi_i^1 \in \xi_1(x)\}$ to compare them.

Example 2.7. Suppose that $\xi_N^1 = \langle (1,5,6,9);\{0.1, 0.5, 0.3, 0.4\}\rangle$ and $\xi_N^2 = \langle (1,4,6,10);\{0.1, 0.5\}\rangle$ be two THF-numbers. Then, we have $l^2 = 2 < \xi_N^1 = 4$. To operate correctly, we should increase the value l_{ξ^2} until it has the same number with l^1, as $\xi_N^2 = \langle (1,4,6,10);\{0.1, 0.5, 0.1, 0.1\}\rangle$.

Definition 2.8. [26] Let $\xi_N^1 = \langle (a_1,b_1,c_1,d_1);\{\xi_i^1 : \xi_i^1 \in \xi_1(x), \xi_1(x)$ is a set of some values in [0,1]$\}\rangle$, $\xi_N^2 = \langle (a_2, b_2, c_2, d_2);\{\xi_i^2 : \xi_i^2 \in \xi_2(x), \xi_2(x)$ is a set of some values in [0,1]$\}\rangle \in \Phi$ and $l_h = \max\{l^1, l^2\}$. Then,

i. the Hamming distance measure between ξ_N^1 and ξ_N^2, denoted by $D_{GTHF}^H(\xi_N^1, \xi_N^2)$, is defined as;

$$D_{GTHF}^H(\xi_N^1, \xi_N^2) = \sum_{i=1}^{l_h} \left| \left(\frac{c_1^2 + d_1^2 - a_1^2 - b_1^2 - c_2^2 - d_2^2 + a_2^2 + b_2^2}{8.l_h} \right) . \left(\xi_{\sigma(i)}^1 - \xi_{\sigma(i)}^2 \right) \right| \tag{2.1}$$

where $\xi_{\sigma(i)}^1$ and $\xi_{\sigma(i)}^2$ are the i. largest values in $\xi_1(x)$ and $\xi_2(x)$, respectively.

ii. the Euclidean distance measure between ξ_N^1 and ξ_N^2, denoted by $D_{GTHF}^E(\xi_N^1, \xi_N^2)$, is defined as;

$$D_{GTHF}^E(\xi_N^1, \xi_N^2) = \left(\sum_{i=1}^{l_h} \left| \left(\frac{c_1^2 + d_1^2 - a_1^2 - b_1^2 - c_2^2 - d_2^2 + a_2^2 + b_2^2}{8.l_h} \right) . \left(\xi_{\sigma(i)}^1 - \xi_{\sigma(i)}^2 \right) \right|^2 \right)^{\frac{1}{2}} \tag{2.2}$$

where $\xi_{\sigma(i)}^1$ and $\xi_{\sigma(i)}^2$ are the i. largest values in $\xi_1(x)$ and $\xi_2(x)$, respectively.

iii. the λ-generalised distance measure between ξ_N^1 and ξ_N^2 for $\lambda > 0$, denoted by $D_{GTHF}^\lambda(\xi_N^1, \xi_N^2)$, is defined as;

$$D_{GTHF}^\lambda(\xi_N^1, \xi_N^2) = \left(\sum_{i=1}^{l_h} \left| \left(\frac{c_1^2 + d_1^2 - a_1^2 - b_1^2 - c_2^2 - d_2^2 + a_2^2 + b_2^2}{8.l_h} \right) . \left(\xi_{\sigma(i)}^1 - \xi_{\sigma(i)}^2 \right) \right|^\lambda \right)^{\frac{1}{\lambda}} \tag{2.3}$$

where $\xi_{\sigma(i)}^1$ and $\xi_{\sigma(i)}^2$ are the i. largest values in $\xi_1(x)$ and $\xi_2(x)$, respectively.

Remark 2.9. [26] Assume that $\xi_N^1, \xi_N^2 \in \Phi$, $l_h = \max\{l^1, l^2\}$ and $D_{GTHF}^\lambda(\xi_N^1, \xi_N^2)$ be a λ-generalised distance measure between ξ_N^1 and ξ_N^2 for $\lambda > 0$. Especially, if $\lambda = 1$, then the λ-generalised distance measure reduces to the Hamming distance measure between ξ_N^1 and ξ_N^2. If $\lambda = 2$, then the λ-generalised distance measure, reduces to the the Euclidean distance measure between ξ_N^1 and ξ_N^2 .

Example 2.10. Assume that $\xi_N^1 = \langle (0.07, 0.09, 0.12, 0.17); \{0.8, 0.5, 0.3, 0.2\} \rangle$ and $\xi_N^2 = \langle (0.2, 0.5, 0.6, 0.8); \{0.4, 0.1\} \rangle$ be two GTHF-numbers. Then, for $l_h = 4 = \max\{4, 2\}$,

i. the Hamming distance measure $D_{GTHF}^H(\xi_N^1, \xi_N^2)$ between ξ_N^1 and ξ_N^2 is calculated as;

$$\begin{aligned} D_{GTHF}^H(\xi_N^1, \xi_N^2) = & \sum_{i=1}^4 \left| \left(\tfrac{c_1^2 + d_1^2 - a_1^2 - b_1^2 - c_2^2 - d_2^2 + a_2^2 + b_2^2}{8.l_h} \right) . \left(\xi_{\sigma(i)}^1 - \xi_{\sigma(i)}^2 \right) \right| \\ = & \left| \left(\tfrac{0.12^2 + 0.17^2 - 0.07^2 - 0.09^2 - 0.6^2 - 0.8^2 + 0.2^2 + 0.5^2}{8.4} \right) . \left(0.8 - 0.4 \right) \right| + \\ & \left| \left(\tfrac{0.12^2 + 0.17^2 - 0.07^2 - 0.09^2 - 0.6^2 - 0.8^2 + 0.2^2 + 0.5^2}{8.4} \right) . \left(0.5 - 0.1 \right) \right| + \\ & \left| \left(\tfrac{0.12^2 + 0.17^2 - 0.07^2 - 0.09^2 - 0.6^2 - 0.8^2 + 0.2^2 + 0.5^2}{8.4} \right) . \left(0.3 - 0.1 \right) \right| + \\ & \left| \left(\tfrac{0.12^2 + 0.17^2 - 0.07^2 - 0.09^2 - 0.6^2 - 0.8^2 + 0.2^2 + 0.5^2}{8.4} \right) . \left(0.2 - 0.1 \right) \right| \\ = & \ 0.0234 \end{aligned}$$

ii. the Euclidean distance measure $D^E_{GTHF}(\xi^1_N,\xi^2_N)$ between ξ^1_N and ξ^2_N is calculated as;

$$\begin{aligned} D^E_{GTHF}(\xi^1_N,\xi^2_N) = & \left(\sum_{i=1}^{l_h}\left|\left(\frac{c_1^2+d_1^2-a_1^2-b_1^2-c_2^2-d_2^2+a_2^2+b_2^2}{8.l_h}\right).(\xi^1_{\sigma(i)}-\xi^2_{\sigma(i)})\right|^2\right)^{\frac{1}{2}} \\ = & \left(\left|\left(\frac{0.12^2+0.17^2-0.07^2-0.09^2-0.6^2-0.8^2+0.2^2+0.5^2}{8.4}\right).(0.8-0.4)\right|^2+\right. \\ & \left|\left(\frac{0.12^2+0.17^2-0.07^2-0.09^2-0.6^2-0.8^2+0.2^2+0.5^2}{8.4}\right).(0.5-0.1)\right|^2+ \\ & \left|\left(\frac{0.12^2+0.17^2-0.07^2-0.09^2-0.6^2-0.8^2+0.2^2+0.5^2}{8.4}\right).(0.3-0.1)\right|^2+ \\ & \left.\left|\left(\frac{0.12^2+0.17^2-0.07^2-0.09^2-0.6^2-0.8^2+0.2^2+0.5^2}{8.4}\right).(0.2-0.1)\right|^2\right)^{\frac{1}{2}} \\ = & \ 0.0079 \end{aligned}$$

iii. the λ-generalised distance measure $D^\lambda_{GTHF}(\xi^1_N,\xi^2_N)$ between ξ^1_N and ξ^2_N is calculated as; $\lambda = 0.7$,

$$\begin{aligned} D^{0.7}_{GTHF}(\xi^1_N,\xi^2_N) = & \left(\sum_{i=1}^{l_h}\left|\left(\frac{c_1^2+d_1^2-a_1^2-b_1^2-c_2^2-d_2^2+a_2^2+b_2^2}{8.l_h}\right).\left(\xi^1_{\sigma(i)}-\xi^2_{\sigma(i)}\right)\right|^{0.7}\right)^{\frac{1}{0.7}} \\ = & \left(\left|\left(\frac{0.12^2+0.17^2-0.07^2-0.09^2-0.6^2-0.8^2+0.2^2+0.5^2}{8.4}\right).(0.8-0.4)\right|^{0.7}+\right. \\ & \left|\left(\frac{0.12^2+0.17^2-0.07^2-0.09^2-0.6^2-0.8^2+0.2^2+0.5^2}{8.4}\right)(0.5-0.1)\right|^{0.7}+ \\ & \left|\left(\frac{0.12^2+0.17^2-0.07^2-0.09^2-0.6^2-0.8^2+0.2^2+0.5^2}{8.4}\right).(0.3-0.1)|^{0.7}+\right. \\ & \left.\left|\left(\frac{0.12^2+0.17^2-0.07^2-0.09^2-0.6^2-0.8^2+0.2^2+0.5^2}{8.4}\right).(0.2-0.1)\right|^{0.7}\right)^{\frac{1}{0.7}} \\ = & \ 0.0335 \end{aligned}$$

Definition 2.11. [26] Let $\xi^1_N = \langle(a_1,b_1,c_1,d_1);\{\xi^1_i : \xi^1_i \in \xi_1(x), \xi_1(x) \text{ is a set of some values in [0,1]}\}\rangle$, $\xi^2_N = \langle(a_2, b_2, c_2, d_2);\{\xi^2_i : \xi^2_i \in \xi_2(x), \xi_2(x) \text{ is a set of some values in [0,1]}\}\rangle \in \Phi$. Then, based on Hausdorff metric, the λ-generalised Hausdorff distance measure between ξ^1_N and ξ^2_N for $\lambda,\gamma > 0$, denoted by $DH_{GTHF}(\xi^1_N,\xi^2_N)$, is defined as;

$$DH_{GTHF}(\xi^1_N,\xi^2_N) = \max_i\left|\frac{1}{8}\left(c_1^2+d_1^2-a_1^2-b_1^2-c_2^2-d_2^2+a_2^2+b_2^2\right).\left(\xi^1_{\sigma(i)}-\xi^2_{\sigma(i)}\right)\right| \tag{2.4}$$

where $\xi^1_{\sigma(i)}$ and $\xi^2_{\sigma(i)}$ are the i. largest values in $\xi_1(x)$ and $\xi_2(x)$, respectively.

The hybrid distances is given as;

i. Combining the Equations 2.1 and 2.4 a γ-hybrid Hamming distance, denoted by ${}_\gamma DH^H_{GTHF}(\xi^1_N,\xi^2_N)$, is defined as;

$$\begin{aligned} {}_\gamma DH^H_{GTHF}(\xi^1_N,\xi^2_N) = & \left|\left(\frac{c_1^2+d_1^2-a_1^2-b_1^2-c_2^2-d_2^2+a_2^2+b_2^2}{16.l_h}\right)\right|. \\ & \left(\sum_{i=1}^{l_h}\gamma.\left|\left(\xi^1_{\sigma(i)}-\xi^2_{\sigma(i)}\right)\right|+(1-\gamma).\left(\max_i\left|\xi^1_{\sigma(i)}-\xi^2_{\sigma(i)}\right|\right)\right) \end{aligned} \tag{2.5}$$

where $\xi^1_{\sigma(i)}$ and $\xi^2_{\sigma(i)}$ are the i. largest values in $\xi_1(x)$ and $\xi_2(x)$, respectively.

ii. Combining the Equations 2.2 and 2.4 a hybrid Euclidean distance, denoted by ${}_{\gamma}DH^{E}_{GTHF}(\xi^1_N,\xi^2_N)$, is defined as;

$$\begin{aligned} {}_{\gamma}DH^{E}_{GTHF}(\xi^1_N,\xi^2_N) = \quad & \left(\left|\left(\tfrac{c_1^2+d_1^2-a_1^2-b_1^2-c_2^2-d_2^2+a_2^2+b_2^2}{16.l_h}\right)\right|.\left(\sum_{i=1}^{l_h}\gamma.\right.\right. \\ & \left.\left.\left|\xi^1_{\sigma(i)}-\xi^2_{\sigma(i)}\right)\right|^2+(1-\gamma).\left(\max_i\left|\xi^1_{\sigma(i)}-\xi^2_{\sigma(i)}\right|\right)^2\right)^{\frac{1}{2}} \end{aligned} \tag{2.6}$$

where $\xi^1_{\sigma(i)}$ and $\xi^2_{\sigma(i)}$ are the i. largest values in $\xi_1(x)$ and $\xi_2(x)$, respectively.

iii. Combining the Equations 2.3 and 2.4 a λ-generalised hybrid distance, denoted by ${}_{\gamma}DH^{\lambda}_{GTHF}(\xi^1_N,\xi^2_N)$, is defined as;

$$\begin{aligned} {}_{\gamma}DH^{\lambda}_{GTHF}(\xi^1_N,\xi^2_N) = \quad & \left(\left|\left(\tfrac{c_1^2+d_1^2-a_1^2-b_1^2-c_2^2-d_2^2+a_2^2+b_2^2}{16.l_h}\right)\right|.\left(\sum_{i=1}^{l_h}\gamma.\right.\right. \\ & \left.\left.\left|\xi^1_{\sigma(i)}-\xi^2_{\sigma(i)}\right)\right|^{\lambda}+\left(1-\gamma\right).\left(\max_i\left|\xi^1_{\sigma(i)}-\xi^2_{\sigma(i)}\right|\right)^{\lambda}\right)^{\frac{1}{\lambda}} \end{aligned} \tag{2.7}$$

where $\xi^1_{\sigma(i)}$ and $\xi^2_{\sigma(i)}$ are the i. largest values in $\xi_1(x)$ and $\xi_2(x)$, respectively.

Example 2.12. Assume that $\xi^1_N=\langle(0.2,0.4,0.6,0.8);\{0.7,0.6,0.5,0.3,0.2\}\rangle$ and $\xi^2_N=\langle(0.1,0.4,0.5,0.7);\{0.9,0.3,0.4\}\rangle$ be two GTHF-numbers. Then, for $l_h=5=\max\{5,3\}$,

$$\begin{aligned} DH_{GTHF}(\xi^1_N,\xi^2_N) = \quad & \max_i\left|\tfrac{1}{8}\left(c_1^2+d_1^2-a_1^2-b_1^2-c_2^2-d_2^2+a_2^2+b_2^2\right).\left(\xi^1_{\sigma(i)}-\xi^2_{\sigma(i)}\right)\right| \\ = \quad & \left|\tfrac{1}{8}\left(c_1^2+d_1^2-a_1^2-b_1^2-c_2^2-d_2^2+a_2^2+b_2^2\right)\right|\max_i\left|\xi^1_{\sigma(i)}-\xi^2_{\sigma(i)}\right| \\ = \quad & \left|\tfrac{1}{8}\left(0.6^2+0.8^2-0.2^2-0.4^2-0.5^2-0.7^2+0.1^2+0.4^2\right)\right|.\max\left\{0.2,0.3,0.1,0.1,0.2\right\} \\ = \quad & 0.0086 \end{aligned}$$

Now, we give the hybrid distance as;

i. Combining the Equations 2.1 and 2.4, 0.5-hybrid Hamming distance, denoted by ${}_{0.5}DH^{H}_{GTHF}(\xi^1_N,\xi^2_N)$, is defined as;

$$\begin{aligned} {}_{0.5}DH^{H}_{GTHF}(\xi^1_N,\xi^2_N) = \quad & \left|\left(\tfrac{c_1^2+d_1^2-a_1^2-b_1^2-c_2^2-d_2^2+a_2^2+b_2^2}{16.l_h}\right)\right|.\left(\textstyle\sum_{i=1}^{l_h}\gamma.\left|\left(\xi^1_{\sigma(i)}-\xi^2_{\sigma(i)}\right)\right|+(1-\gamma).\left(\max_i\left|\xi^1_{\sigma(i)}-\xi^2_{\sigma(i)}\right|\right)\right) \\ = \quad & 0.1504 \end{aligned}$$

ii. Combining the Equations 2.2 and 2.4 a 0.5-hybrid Euclidean distance, denoted by ${}_{0.5}DH^{E}_{GTHF}(\xi^1_N,\xi^2_N))$, is defined as;

$$\begin{aligned} {}_{0.5}DH^{E}_{GTHF}(\xi^1_N,\xi^2_N) = \quad & \left(\left|\left(\tfrac{c_1^2+d_1^2-a_1^2-b_1^2-c_2^2-d_2^2+a_2^2+b_2^2}{16.l_h}\right)\right|.\right. \\ & \left.\left(\textstyle\sum_{i=1}^{l_h}(0.5).\left|\xi^1_{\sigma(i)}-\xi^2_{\sigma(i)}\right)|^2|+(1-0.5).\left(\max_i\left|\xi^1_{\sigma(i)}-\xi^2_{\sigma(i)}\right|\right)^2\right)^{\frac{1}{2}}\right) \\ = \quad & 0.2124 \end{aligned}$$

iii. Combining the Equations 2.3 and 2.4 a 0.5-generalised hybrid distance, denoted by ${}_{0.5}DH^{0.5}_{GTHF}(\xi^1_N,\xi^2_N)$,

is defined as;

$$
\begin{aligned}
{}_{0.5}DH^{0.5}_{GTHF}(\xi^1_N,\xi^2_N) = \quad & \Big(\Big|\big(\tfrac{c_1^2+d_1^2-a_1^2-b_1^2-c_2^2-d_2^2+a_2^2+b_2^2}{16.l_h}\big)\Big|. \\
& \big(\textstyle\sum_{i=1}^{l_h}(0.5).|\xi^1_{\sigma(i)}-\xi^2_{\sigma(i)})|^{0.5}| + (1-0.5).(\max_i|\xi^1_{\sigma(i)}-\xi^2_{\sigma(i)}|)^{0.5}\big)\Big)^{\frac{1}{0.5}} \\
= \quad & 0.0754
\end{aligned}
$$

3. Not-Ordered Quasi-Distance Measures on GTHF-Numbers

In this section, we gave not-ordered quasi-distance measures on GTHF-numbers and their properties based on some definitions of hesitant fuzzy sets in [7] and GTHF-numbers in [25, 26, 28].

Definition 3.1. Let $\xi^1_N = \langle(a_1,b_1,c_1,d_1);\xi^1_1\rangle$ and $\xi^2_N = \langle(a_2,b_2,c_2,d_2);\xi^2_1\rangle$ be two GTHF-numbers. Then,

i. the Not-ordered Hamming quasi-distance measure between ξ^1_N and ξ^2_N, denoted by $d_{NoH}(\xi^1_N,\xi^2_N)$, is defined as;

$$d_{NoH}(\xi^1_N,\xi^2_N) = \frac{1}{4.k^2.l_p}\sum_{\xi^1_1\in\xi^1_N,\xi^2_1\in\xi^2_N}\Big|\big(c_1^2+d_1^2-a_1^2-b_1^2-c_2^2-d_2^2+a_2^2+b_2^2\big).\big(\xi^1_1-\xi^2_1\big)\Big| \tag{3.1}$$

where $k = \max\{|a_1|,|a_2|,|b_1|,|b_2|,|c_1|,|c_2|,|d_1|,|d_2|\}$ and l is product of number of element ξ^1_N and ξ^2_N.

ii. the Not-ordered Euclidean quasi-distance measure between ξ^1_N and ξ^2_N, denoted by $d_{NoE}(\xi^1_N,\xi^2_N)$, is defined as;

$$d_{NoE}(\xi^1_N,\xi^2_N) = \Big(\sum_{\xi^1_1\in\xi^1_N,\xi^2_1\in\xi^2_N}\Big|\frac{1}{4.k^2.l_p}\big(c_1^2+d_1^2-a_1^2-b_1^2-c_2^2-d_2^2+a_2^2+b_2^2\big).\big(\xi^1_1-\xi^2_1\big)\Big|^2\Big)^{\frac{1}{2}} \tag{3.2}$$

where $k = \max\{|a_1|,|a_2|,|b_1|,|b_2|,|c_1|,|c_2|,|d_1|,|d_2|\}$ and l is product of number of element ξ^1_N and ξ^2_N.

iii. the Not-ordered λ-generalised quasi-distance measure between ξ^1_N and ξ^2_N for $\lambda>0$, denoted by $d^\lambda_{NoG}(\xi^1_N,\xi^2_N)$, is defined as;

$$d^\lambda_{NoG}(\xi^1_N,\xi^2_N) = \Big(\sum_{\xi^1_1\in\xi^1_N,\xi^2_1\in\xi^2_N}\Big|\frac{1}{4.k^2.l_p}\big(c_1^2+d_1^2-a_1^2-b_1^2-c_2^2-d_2^2+a_2^2+b_2^2\big).\big(\xi^1_1-\xi^2_1\big)\Big|^\lambda\Big)^{\frac{1}{\lambda}} \tag{3.3}$$

where $k = \max\{|a_1|,|a_2|,|b_1|,|b_2|,|c_1|,|c_2|,|d_1|,|d_2|\}$ and l is product of number of element ξ^1_N and ξ^2_N.

iv. the Not-ordered the λ-generalised not ordered Hausdorff quasi-distance measure based on Hausdorff metric, between ξ^1_N and ξ^2_N, denoted by $d^\lambda_{NoHa}(\xi^1_N,\xi^2_N)$, is defined as;

$$d^\lambda_{NoHa}(\xi^1_N,\xi^2_N) = \max_{\xi^1_1\in\xi^1_N,\xi^2_1\in\xi^2_N}\Big|\frac{1}{4.k^2}\big(c_1^2+d_1^2-a_1^2-b_1^2-c_2^2-d_2^2+a_2^2+b_2^2\big).\big(\xi^1_1-\xi^2_1\big)\Big| \tag{3.4}$$

where $k = \max\{|a_1|,|a_2|,|b_1|,|b_2|,|c_1|,|c_2|,|d_1|,|d_2|\}$.

Theorem 3.2. Suppose that $\xi^1_N = \langle(a_1,b_1,c_1,d_1);\xi^1_1(x)\rangle$, $\xi^2_N = \langle(a_2,b_2,c_2,d_2);\xi^2_1(x)\rangle$ and $\xi^3_N = \langle(a_3,b_3,c_3,d_3);\xi^3_1=\xi^3(x)\rangle$ three GTHF-numbers and $\gamma\neq 0$ be any real number. Then, for $d\in\{d_{NoH},d_{NoE},d^\lambda_{NoG},d^\lambda_{NoHa}\}$, d satisfies the following properties:

i. $0 \le d(\xi_N^1, \xi_N^2) \le 1$

ii. $d(\xi_N^1, \xi_N^2) = d(\xi_N^2, \xi_N^1)$

iii. $\xi_N^1 = \xi_N^2 \Rightarrow d(\xi_N^1, \xi_N^2) = 0$

iv. $d(\xi_N^1, \xi_N^3) + d(\xi_N^3, \xi_N^2) \ge d(\xi_N^1, \xi_N^2)$

Proof.
Let $\xi_N^1 = \langle (a_1, b_1, c_1, d_1); \xi_1^1(x) \rangle$, $\xi_N^2 = \langle (a_2, b_2, c_2, d_2); \xi_1^2(x) \rangle$ and $\xi_N^3 = \langle (a_3, b_3, c_3, d_3); \xi_1^3 = \xi^3(x) \rangle$ three GTHF-numbers and $\gamma \neq 0$ be any real number.

i. Let $k = \max\{|a_1|, |a_2|, |b_1|, |b_2|, |c_1|, |c_2|, |d_1|, |d_2|\}$ and l_p is product of number of element ξ_N^1 and ξ_N^2.

i. Since

$$0 \le \left| \left(c_1^2 + d_1^2 - a_1^2 - b_1^2 - c_2^2 - d_2^2 + a_2^2 + b_2^2\right) \right| \le 4k^2 \quad \text{and} \quad 0 \le \left| \left(\xi_1{}^1 - \xi_1{}^2\right) \right| \le 1$$

we have

$$\begin{aligned}
0 \le \quad & \left(\left| \left(c_1^2 + d_1^2 - a_1^2 - b_1^2 - c_2^2 - d_2^2 + a_2^2 + b_2^2\right).\left(\xi_1{}^1 - \xi_1{}^2\right) \right| \right) \le 4.k^2 \\
\Rightarrow \quad & 0 \le \left(\sum_{\xi_1^1 \in \xi_N^1, \xi_1^2 \in \xi_N^2} \left| \left(c_1^2 + d_1^2 - a_1^2 - b_1^2 - c_2^2 - d_2^2 + a_2^2 + b_2^2\right).\left(\xi_1{}^1 - \xi_1{}^2\right) \right| \right) \le 4.k^2.l_p \\
\Rightarrow \quad & 0 \le \frac{1}{4.k^2.l_p} \left(\sum_{\xi_1^1 \in \xi_N^1, \xi_1^2 \in \xi_N^2} \left| \left(c_1^2 + d_1^2 - a_1^2 - b_1^2 - c_2^2 - d_2^2 + a_2^2 + b_2^2\right).\left(\xi_1{}^1 - \xi_1{}^2\right) \right| \right) \le 1 \\
\Rightarrow \quad & 0 \le d_{NoH}(\xi_N^1, \xi_N^2) \le 1
\end{aligned}$$

ii.

$$\begin{aligned}
d_{NoH}(\xi_N^1, \xi_N^2) = \quad & \frac{1}{4.k^2.l_p} \sum_{\xi_1^1 \in \xi_N^1, \xi_1^2 \in \xi_N^2} \left| \left(c_1^2 + d_1^2 - a_1^2 - b_1^2 - c_2^2 - d_2^2 + a_2^2 + b_2^2\right).\left(\xi_1{}^1 - \xi_1{}^2\right) \right| \\
= \quad & \frac{1}{4.k^2.l_p} \left(\sum_{\xi_1^1 \in \xi_N^1, \xi_1^2 \in \xi_N^2} \left| \left(c_2^2 + d_2^2 - a_2^2 - b_2^2 - c_1^2 - d_1^2 + a_1^2 + b_1^2\right).\left(\xi_1{}^2 - \xi_1{}^1\right) \right| \right) \\
= \quad & d_{NoH}(\xi_N^2, \xi_N^1)
\end{aligned}$$

iii. Since ξ_N^1 and ξ_N^2 are identical then $a = a_1 = a_2, b = b_1 = b_2, c = c_1 = c_2, d = d_1 = d_2, \xi = \xi_N^1 = \xi_N^2$. The degree of quasi-distance ξ_N^1 and ξ_N^2 are calculated as follows

$$\begin{aligned}
d_{NoH}(\xi_N^1, \xi_N^2) = \quad & \frac{1}{4.k^2.l_p} \sum_{\xi_1^1 \in \xi_N^1, \xi_1^2 \in \xi_N^2} \left| \left(c_1^2 + d_1^2 - a_1^2 - b_1^2 - c_2^2 - d_2^2 + a_2^2 + b_2^2\right).\left(\xi_1{}^1 - \xi_1{}^2\right) \right| \\
= \quad & \frac{1}{4.k^2.l_p} \sum_{\xi_1^1 \in \xi_N^1, \xi_1^2 \in \xi_N^2} \left| \left(c + d - a - b - c - d + a + b\right).\left(\xi - \xi\right) \right| \\
= \quad & 0
\end{aligned}$$

iv.

$$\begin{aligned}
d_{NoH}(\xi_N^1,\xi_N^2) &= \tfrac{1}{4.k^2.l_p}\sum_{\xi_1^1\in\xi^1,\xi_1^2\in\xi^2}\left|\left(c_1^2+d_1^2-a_1^2-b_1^2-c_2^2-d_2^2+a_2^2+b_2^2\right).\left({\xi_1}^1-{\xi_1}^2\right)\right| \\
&= \tfrac{1}{4.k^2.l_p}\sum_{\xi_1^1\in\xi_N^1,\xi_1^2,\xi_1^3\in\xi_N^2}\Big|\left(c_1^2+d_1^2-a_1^2-b_1^2+c_3^2+d_3^2-a_3^2-b_3^2\right. \\
&\quad \left.-c_2^2-d_2^2+a_2^2+b_2^2-c_3^2-d_3^2+a_3^2+b_3^2\right).\left({\xi_1}^1-{\xi_1}^2-{\xi_1}^3+{\xi_1}^3\right)\Big| \\
&\leq \sum_{\xi_1^1\in\xi_N^1,\xi_1^3\in\xi_N^3}\left|\tfrac{1}{4.k^2.l_p}\left(c_1^2+d_1^2-a_1^2-b_1^2-c_3^2-d_3^2+a_3^2+b_3^2\right).\left({\xi_1}^1-{\xi_1}^3\right)\right|+ \\
&\quad \sum_{\xi_1^3\in\xi_N^3,\xi_1^2\in\xi_N^2}\left|\tfrac{1}{4.k^2.l_p}\left(c_3^2+d_3^2-a_3^2-b_3^2-c_2^2-d_2^2+a_2^2+b_2^2\right).\left({\xi_1}^3-{\xi_1}^2\right)\right| \\
&= d_{NoH}(\xi_N^1,\xi_N^3)+d_{NoH}(\xi_N^3,\xi_N^2)
\end{aligned}$$

Similarly, for $d\in\{d_{NoE},d_{NoG}^{\lambda},d_{DNoH}\}$, proof of theorem can be made.

Remark 3.3. Assume that $d_{NoG}^{\lambda}(\xi_N^1,\xi_N^2)$ be a Not-ordered λ-generalised quasi-distance measure between ξ_N^1 and ξ_N^2 for $\lambda>0$. Especially, if $\lambda=1$, then the Not-ordered λ-generalised quasi-distance measure reduces to the Not-ordered Hamming quasi-distance measure between ξ_N^1 and ξ_N^2. If $\lambda=2$, then the Not-ordered λ-generalised quasi-distance measure, reduces to the Not-ordered Euclidean quasi-distance measure between ξ_N^1 and ξ_N^2.

Example 3.4. Assume that $\xi_N^1=\langle(10,15,20,25);\{0.7,0.8,0.5\}\rangle$ and $\xi_N^2=\langle(-13,-10,-7,-5);\{0.9,0.2\}\rangle$ be two GTHF-numbers. Then,

i. the Hamming quasi-distance measure $d_{NoH}(\xi_N^1,\xi_N^2)$ between ξ_N^1 and ξ_N^2 is calculated as;

$$\begin{aligned}
d_{NoH}(\xi_N^1,\xi_N^2) = \tfrac{1}{4.625.6} &\Big(\Big|\left(20^2+25^2-10^2-15^2-(-7)^2-(-5)^2+(-13)^2+(-10)^2\right).\left(0.7-0.9\right)\Big|+ \\
&\Big|\left(20^2+25^2-10^2-15^2-(-7)^2-(-5)^2+(-13)^2+(-10)^2\right).\left(0.7-0.2\right)\Big|+ \\
&\Big|\left(20^2+25^2-10^2-15^2-(-7)^2-(-5)^2+(-13)^2+(-10)^2\right).\left(0.8-0.9\right)\Big|+ \\
&\Big|\left(20^2+25^2-10^2-15^2-(-7)^2-(-5)^2+(-13)^2+(-10)^2\right).\left(0.8-0.2\right)\Big|+ \\
&\Big|\left(20^2+25^2-10^2-15^2-(-7)^2-(-5)^2+(-13)^2+(-10)^2\right).\left(0.5-0.9\right)\Big|+ \\
&\Big|\left(20^2+25^2-10^2-15^2-(-7)^2-(-5)^2+(-13)^2+(-10)^2\right).\left(0.5-0.2\right)\Big|\Big) \\
= \tfrac{1}{4.625.6} &\Big|\left(20^2+25^2-10^2-15^2-(-7)^2-(-5)^2+(-13)^2+(-10)^2\right)\Big| \\
&\Big|\left(0.7-0.9\right)+\left(0.7-0.2\right)+\left(0.8-0.9\right)+\left(0.8-0.2\right)+\left(0.5-0.9\right)+\left(0.5-0.2\right)\Big| \\
= 0.041
\end{aligned}$$

ii. the Euclidean quasi-distance measure $d_{NoE}(\xi_N^1, \xi_N^2)$ between ξ_N^1 and ξ_N^2 is calculated as;

$$\begin{aligned} d_{NoE}(\xi_N^1, \xi_N^2) = & \left(\left|\tfrac{1}{4.625.6}(20^2+25^2-10^2-15^2-(-7)^2-(-5)^2+(-13)^2+(-10)^2).(0.7-0.9)\right|^2+\right. \\ & \left|(20^2+25^2-10^2-15^2-(-7)^2-(-5)^2+(-13)^2+(-10)^2).(0.7-0.2)\right|^2+ \\ & \left|(20^2+25^2-10^2-15^2-(-7)^2-(-5)^2+(-13)^2+(-10)^2).(0.8-0.9)\right|^2+ \\ & \left|(20^2+25^2-10^2-15^2-(-7)^2-(-5)^2+(-13)^2+(-10)^2).(0.8-0.2)\right|^2+ \\ & \left|(20^2+25^2-10^2-15^2-(-7)^2-(-5)^2+(-13)^2+(-10)^2).(0.5-0.9)\right|^2+ \\ & \left.\left|(20^2+25^2-10^2-15^2-(-7)^2-(-5)^2+(-13)^2+(-10)^2).(0.5-0.2)\right|^2\right)^{\frac{1}{2}} \\ = & \left|\tfrac{1}{4.625.6}\left(20^2+25^2-10^2-15^2-(-7)^2-(-5)^2+(-13)^2+(-10)^2\right)^2\right| \\ & \left|\left((0.7-0.9)^2+(0.7-0.2)^2+(0.8-0.9)^2+(0.8-0.2)^2+(0.5-0.9)^2+(0.5-0.2)^2\right)\right|^{\frac{1}{2}} \\ = & \ 0.056 \end{aligned}$$

iii. the λ-generalised quasi-distance measure $d_{NoG}^{\lambda}(\xi_N^1, \xi_N^2)$ between ξ_N^1 and ξ_N^2 is calculated as; $\lambda = 0.8$,

$$\begin{aligned} d_{NoG}^{0.8}(\xi_N^1, \xi_N^2) = & \left(\left|\tfrac{1}{4.625.6}(20^2+25^2-10^2-15^2-(-7)^2-(-5)^2+(-13)^2+(-10)^2).(0.7-0.9)\right|^{0.8}+\right. \\ & \left|(20^2+25^2-10^2-15^2-(-7)^2-(-5)^2+(-13)^2+(-10)^2).(0.7-0.2)\right|^{0.8}+ \\ & \left|(20^2+25^2-10^2-15^2-(-7)^2-(-5)^2+(-13)^2+(-10)^2).(0.8-0.9)\right|^{0.8}+ \\ & \left|(20^2+25^2-10^2-15^2-(-7)^2-(-5)^2+(-13)^2+(-10)^2).(0.8-0.2)\right|^{0.8}+ \\ & \left|(20^2+25^2-10^2-15^2-(-7)^2-(-5)^2+(-13)^2+(-10)^2).(0.5-0.9)\right|^{0.8}+ \\ & \left.\left|(20^2+25^2-10^2-15^2-(-7)^2-(-5)^2+(-13)^2+(-10)^2).(0.5-0.2)\right|^{0.8}\right)^{\frac{1}{0.8}} \\ = & \left|\tfrac{1}{4.625.6}(20^2+25^2-10^2-15^2-(-7)^2-(-5)^2+(-13)^2+(-10)^2)^2\left((0.7-0.9)^{0.8}\right.\right. \\ & \left.\left.+(0.7-0.2)^{0.8}+(0.8-0.9)^{0.8}+(0.8-0.2)^{0.8}+(0.5-0.9)^{0.8}+(0.5-0.2)^{0.8}\right)\right|^{\frac{1}{0.8}} \\ = & \ 0.19 \end{aligned}$$

and $\lambda = 5$,

$$\begin{aligned} d^5_{NoG}(\xi^1_N, \xi^2_N) = & \left(\left| \tfrac{1}{4.625.6}(20^2 + 25^2 - 10^2 - 15^2 - (-7)^2 - (-5)^2 + (-13)^2 + (-10)^2).(0.7 - 0.9) \right|^5 + \right. \\ & \left| (20^2 + 25^2 - 10^2 - 15^2 - (-7)^2 - (-5)^2 + (-13)^2 + (-10)^2).(0.7 - 0.2) \right|^5 + \\ & \left| (20^2 + 25^2 - 10^2 - 15^2 - (-7)^2 - (-5)^2 + (-13)^2 + (-10)^2).(0.8 - 0.9) \right|^5 + \\ & \left| (20^2 + 25^2 - 10^2 - 15^2 - (-7)^2 - (-5)^2 + (-13)^2 + (-10)^2).(0.8 - 0.2) \right|^5 + \\ & \left| (20^2 + 25^2 - 10^2 - 15^2 - (-7)^2 - (-5)^2 + (-13)^2 + (-10)^2).(0.5 - 0.9) \right|^5 + \\ & \left. \left| (20^2 + 25^2 - 10^2 - 15^2 - (-7)^2 - (-5)^2 + (-13)^2 + (-10)^2).(0.5 - 0.2) \right|^5 \right)^{\frac{1}{5}} \\ = & \left| \tfrac{1}{4.625.6}(20^2 + 25^2 - 10^2 - 15^2 - (-7)^2 - (-5)^2 + (-13)^2 + (-10)^2)^2 \right. \\ & \left. ((0.7 - 0.9)^5 + (0.7 - 0.2)^5 + (0.8 - 0.9)^5 + (0.8 - 0.2)^5 + (0.5 - 0.9)^5 + (0.5 - 0.2)^5) \right|^{\frac{1}{5}} \\ = & \ 0.037 \end{aligned}$$

Definition 3.5. Let ξ^1_N, ξ^2_N be two GTHF-numbers. Then, for $\lambda, \gamma > 0$, the hybrid quasi-distances are given as:

i. Combining the Equations 3.1 and 3.4 a γ- not ordered hybrid Hamming quasi-distance, denoted by ${}_{\gamma}DNOH^H_{GTHF}(\xi^1_N, \xi^2_N)$, is defined as;

$$\begin{aligned} d_{{}_{\gamma}DNOH^H}(\xi^1_N, \xi^2_N) = & \ \tfrac{1}{4.k^2.l_p} \left| (c_1^2 + d_1^2 - a_1^2 - b_1^2 - c_2^2 - d_2^2 + a_2^2 + b_2^2) \right|. \\ & \left(\sum_{\xi^1_1 \in \xi^1_N, \xi^2_1 \in \xi^2_N} \gamma. \left| \xi^1_1 - \xi^2_1) \right| + (1 - \gamma).l_p.(\max_{\xi^1_1 \in \xi^1_N, \xi^2_1 \in \xi^2_N} \left| {\xi_1}^1 - {\xi_1}^2 \right|) \right) \end{aligned}$$

where $k = \max\{|a_1|, |a_2|, |b_1|, |b_2|, |c_1|, |c_2|, |d_1|, |d_2|\}$ and l_p is product of number of element ξ^1_N and ξ^2_N.

ii. Combining the Equations 3.2 and 3.4 a not-ordered hybrid Euclidean quasi-distance, denoted by $d_{{}_{\gamma}DNOH^E}(\xi^1_N, \xi^2_N)$, is defined as;

$$\begin{aligned} d_{{}_{\gamma}DNOH^E}(\xi^1_N, \xi^2_N) = & \left(\sum_{\xi^1_1 \in \xi^1_N, \xi^2_1 \in \xi^2_N} \left(\tfrac{1}{4.k^2.l_p}(c_1^2 + d_1^2 - a_1^2 - b_1^2 - c_2^2 - d_2^2 + a_2^2 + b_2^2 \right)^2 .\left(\gamma \left| {\xi_1}^1 - {\xi_1}^2 \right|^2 + \right. \right. \\ & \left. \left. (1 - \gamma). \max_{\xi^1_1 \in \xi^1_N, \xi^2_1 \in \xi^2_N} .l_p.\left({\xi_1}^1 - {\xi_1}^2 \right)^2 \right) \right)^{\frac{1}{2}} \end{aligned}$$

where $k = \max\{\left|a_1\right|, \left|a_2\right|, \left|b_1\right|, \left|b_2\right|, \left|c_1\right|, \left|c_2\right| \left|d_1\right|, \left|d_2\right|\}$ and l is product of number of element ξ^1_N and ξ^2_N.

iii. Combining the Equations 3.3 and 3.4 a λ-generalised not-ordered hybrid quasi-distance, denoted by $d_{{}_{\gamma}DNOH^{\lambda}}(\xi^1_N, \xi^2_N)$, is defined as;

$$\begin{aligned} d_{{}_{\gamma}DNOH^{\lambda}}(\xi^1_N, \xi^2_N) = & \left(\sum_{\xi^1_1 \in \xi^1_N, \xi^2_1 \in \xi^2_N} \left(\tfrac{1}{4.k^2.l_p}(c_1^2 + d_1^2 - a_1^2 - b_1^2 - c_2^2 - d_2^2 + a_2^2 + b_2^2 \right)^{\lambda} .\left(\gamma \left| {\xi_1}^1 - {\xi_1}^2 \right|^{\lambda} + \right. \right. \\ & \left. \left. (1 - \gamma). \max_{\xi^1_1 \in \xi^1_N, \xi^2_1 \in \xi^2_N} .l_p.\left({\xi_1}^1 - {\xi_1}^2 \right)^{\lambda} \right) \right)^{\frac{1}{\lambda}} \end{aligned}$$

where $k = \max\{|a_1|,|a_2|,|b_1|,|b_2|,|c_1|,|c_2|,|d_1|,|d_2|\}$ and l_p is product of number of element ξ_N^1 and ξ_N^2.

Theorem 3.6. Suppose that $\xi_N^1 = \langle((a_1,b_1,c_1,d_1);\xi_1^1(x)\rangle$, $\xi_N^2 = \langle((a_2,b_2,c_2,d_2);\xi_1^2(x)\rangle$ and $\xi_N^3 = \langle((a_3,b_3,c_3,d_3);\xi_1^3 = \xi^3(x)\rangle$ three GTHF-numbers and $\gamma \neq 0$ be any real number. Then, for $d \in \{d_{\gamma DNOH^H}, d_{\gamma DNOH^E}, d_{\gamma DNOH^\lambda}\}$, d satisfies the following properties:

i. $0 \leq d(\xi_N^1,\xi_N^2) \leq 1$

ii. $d(\xi_N^1,\xi_N^2) = d(\xi_N^2,\xi_N^1)$

iii. $\xi_N^1 = \xi_N^2 \Rightarrow d(\xi_N^1,\xi_N^2) = 0$

iv. $d(\xi_N^1,\xi_N^3) + d(\xi_N^3,\xi_N^2) \geq d(\xi_N^1,\xi_N^2)$

Proof: Proof of the theorem is clear.

Example 3.7. Assume that $\xi_N^1 = \langle(0.1,0.2,0.3,0.4);\{0.9,0.7,0.6,0.5,0.1\}\rangle$ and $\xi_N^2 = \langle(0.3,0.5,0.7,0.9);\{0.8,0.1,0.5\}\rangle$ be two GTHF-numbers. Then, for $l_p = 5.3 = 15$,

$$\begin{aligned} d_{\gamma DNOH}(\xi_N^1,\xi_N^2) = & \max\left\{\left|\tfrac{1}{4\cdot 0.9^2\cdot 15}(c_1^2+d_1^2-a_1^2-b_1^2-c_2^2-d_2^2+a_2^2+b_2^2).(\xi_1^1-\xi_1^2)\right|\right\} \\ = & \left|\tfrac{1}{48.6}(c_1^2+d_1^2-a_1^2-b_1^2-c_2^2-d_2^2+a_2^2+b_2^2)\right|.\max\left\{\left|\xi_1^1-\xi_1^2\right|\right\} \\ = & \left|\tfrac{1}{48.6}(0.3^2+0.4^2-0.1^2-0.2^2-0.7^2-0.9^2+0.3^2+0.5^2)\right| \\ & \max\{0.1,0.8,0.4,0.1,0.6,0.2,0,2,0.5,0.1,0.3,0.4,0.0,0.7,0.0,0.4\} \\ = & 0.012 \end{aligned}$$

Now, we give the hybrid quasi-distance as:

i. Combining the Equations 2.1 and 2.4 0.5-hybrid Hamming quasi-distance, denoted by ${}_{0.5}DNOH^H_{GTHF}(\xi_N^1,\xi_N^2)$, is defined as;

$$\begin{aligned} d_{0.5DNOH^H}(\xi_N^1,\xi_N^2) = & \left|\left(\tfrac{c_1^2+d_1^2-a_1^2-b_1^2-c_2^2-d_2^2+a_2^2+b_2^2}{4.k^2.l}\right)\right|. \\ & \left(\sum_{\xi_1^1\in\xi_N^1,\xi_1^2\in\xi_N^2}(0.5).\left|\left(\xi_1^1-\xi_1^2\right)\right| + (1-(0.5)).\left(\max_{\xi_1^1\in\xi_N^1,\xi_1^2\in\xi_N^2}\left|\xi_1^1-\xi_1^2\right|\right)\right) \qquad (3.5) \\ = & 0.042 \end{aligned}$$

ii. Combining the Equations 2.2 and 2.4 a 0.5not-ordered hybrid Euclidean quasi-distance, denoted by $d_{0.5DNOH^E}(\xi_N^1,\xi_N^2)$, is defined as;

$$\begin{aligned} d_{0.5DNOH^E}(\xi_N^1,\xi_N^2) = & \left(\left|\left(\tfrac{c_1^2+d_1^2-a_1^2-b_1^2-c_2^2-d_2^2+a_2^2+b_2^2}{4.k^2.l}\right)\right|.\right. \\ & \left.\left(\sum_{\xi_1^1\in\xi_N^1,\xi_1^2\in\xi_N^2}(0.5).\left|\xi_1^1-\xi_1^2\right)\right|^2\right| + (1-0.5).\left(\max_{\xi_1^1\in\xi_N^1,\xi_1^2\in\xi_N^2}\left|\xi_1^1-\xi_1^2\right|\right)^2\Big)^{\frac{1}{2}} \qquad (3.6) \\ = & 0.022 \end{aligned}$$

iii. Combining the Equations 2.3 and 2.4 a 0.5-generalised not ordered hybrid quasi-distance, denoted by ${}_{0.5}DNOH^{0.5}_{GTHF}(\xi^1_N,\xi^2_N)$, is defined as;

$$\begin{aligned} d_{{}_{0.5}DNOH^{0.5}}(\xi^1_N,\xi^2_N) = & \left(\left|\left(\frac{c_1^2+d_1^2-a_1^2-b_1^2-c_2^2-d_2^2+a_2^2+b_2^2}{4.k^2.l}\right)\right|.\right. \\ & \left.\left(\sum_{\xi^1_1\in\xi^1_N,\xi^2_1\in\xi^2_N}(0.5).\left|\xi^1_1-\xi^2_1\right|^{0.5}\right|+(1-0.5).\left(\max_{\xi^1_1\in\xi^1_N,\xi^2_1\in\xi^2_N}\left|\xi^1_1-\xi^2_1\right|\right)^{0.5}\right)^{\frac{1}{0.5}} \qquad (3.7) \\ = & \ 0.062 \end{aligned}$$

4. An Approach to MCDM Problems with GTHF-Numbers

In this section, we present an algorithm based on not-ordered quasi-distance measures of GTHF-numbers. The algorithm is given in Deli [26] for ordered quasi-distance measures.

Definition 4.1. [25] Let $A=\{a_1,a_2,...,a_m\}$ be a set of alternatives, $C=\{c_1,c_2,...,c_n\}$ be the set of criteria. If $A_{ij}=\langle(a_{ij},b_{ij},c_{ij},d_{ij});\xi_{ij}(x)\rangle\in\Phi$ $(i=1,2,...,m;\ j=1,2,...,n)$. Then

$$[A_{ij}]_{m\times n}=\begin{pmatrix} A_{11} & A_{12} & \cdots & A_{1n} \\ A_{21} & A_{22} & \cdots & A_{2n} \\ \vdots & \vdots & \vdots & \vdots \\ A_{m1} & A_{m2} & \cdots & A_{mn} \end{pmatrix}$$

is called an GTHF-MCDM matrix of the decision maker or expert. Here x_{ij} denotes evaluation of the alternative a_i with respect to the criteria c_j made by expert or decision maker.

Based on the Deli [26], we now gave an orderly algorithm for TOPSIS method of GTHF-numbers as follow:

Algorithm:

Step 1. Give the GTHF-MCDM matrix x_{ij} $(i=1,2,...,m;\ j=1,2,...,n)$ as;

$$[A_{ij}]_{m\times n}=\begin{pmatrix} A_{11} & A_{12} & \cdots & A_{1n} \\ A_{21} & A_{22} & \cdots & A_{2n} \\ \vdots & \vdots & \vdots & \vdots \\ A_{m1} & A_{m2} & \cdots & A_{mn} \end{pmatrix}$$

Step 2. Calculate the normalized GTHF-MCDM matrix n_{ij} $(i=1,2,...,m;j=1,2,...,n)$ as $n_{ij}=\langle(\frac{a_{ij}}{\eta},\frac{b_{ij}}{\eta},\frac{c_{ij}}{\eta},\frac{d_{ij}}{\eta});\xi_{ij}(x)\rangle\in\Phi$ $(i=1,2,...,m;\ j=1,2,...,n)$ where $\eta=\max_{i,j}\left\{\left|a_{ij}\right|,\left|b_{ij}\right|,\left|c_{ij}\right|,\left|d_{ij}\right|\right\}$ $(i=1,2,...,m;\ j=1,2,...,n)$

Step 3. Give the weighted vector $W=(w_1,w_2,...,w_n)$, where w_j $(j=1,2,...,n)$ is the weight of criterion c_j $(j=1,2,...,n)$ and $\sum_{j=1}^{n}w_j=1$.

Step 4. Compute the weighted normalized GTHF-MCDM matrix $n^w_{ij}=w_j\cdot n_{ij}=\langle(\widetilde{a}_{ij},\widetilde{b}_{ij},\widetilde{c}_{ij},\widetilde{d}_{ij});\widetilde{\xi}_{ij}(x)\rangle\in\Phi$ $(i=1,2,...,m;\ j=1,2,...,n)$

Step 5. Describe the GTHF-positive ideal solution A^+ and GTHF-negative ideal solution A^- for GTHF-

MCDM matrix $n_{ij}^w = w_j \cdot n_{ij} = \langle(\widetilde{a}_{ij}, \widetilde{b}_{ij}, \widetilde{c}_{ij}, \widetilde{d}_{ij}); \widetilde{\xi}_{ij}(x)\rangle \in \Phi \;\; (i = 1,2,...,m;\; j = 1,2,...,n)$ as follows;

$$A^+ = \quad \langle(\max_{i,j}\{a_{ij}\}, \langle(\max_{i,j}\{b_{ij}\}\langle(\max_{i,j}\{c_{ij}\}, \langle(\max_{i,j}\{d_{ij}\}; \{\max_{i,j}\{\xi : \xi \in \widetilde{\xi}_{ij}(x)\}\}\rangle$$

and

$$A^- = \quad \langle(\min_{i,j}\{a_{ij}\}, \langle(\min_{i,j}\{b_{ij}\}\langle(\min_{i,j}\{c_{ij}\}, \langle(\min_{i,j}\{d_{ij}\}; \{\min_{i,j}\{\xi : \xi \in \widetilde{\xi}_{ij}(x)\}\}\rangle$$

respectively.

Step 6. Compute the quasi-distance measures $r_{ij}^+ = d(n_{ij}^w, A^+),\;\; (i = 1,2,...,m;\; j = 1,2,...,n)$ and $r_{ij}^- = d(n_{ij}^w, A^-) \;\; (i = 1,2,...,m;\; j = 1,2,...,n)$ between n_{ij}^w and GTHF-positive ideal solution solution A^+ and GTHF-negative ideal solution A^-, respectively. ($d \in \{d_{NoH}, d_{NoE}, d_{NoG}^{\lambda}, d_{NoHa}^{\lambda}, d_{{}_{\gamma}DNOH^H}, d_{{}_{\gamma}DNOH^E}, d_{{}_{\gamma}DNOH^{\lambda}}\}$) or Compute the correlation measures $r_{ij}^+ = 1 - \overrightarrow{c}_k(n_{ij}^w, A^+),\;\; (i = 1,2,...,m;\; j = 1,2,...,n)$ $(k \in \{1,2,...,14\})$ and $r_{ij}^- = 1 - \overrightarrow{c}_k(n_{ij}^w, A^-) \;\; (i = 1,2,...,m;\; j = 1,2,...,n)$ between n_{ij}^w and GTHF-positive ideal solution solution A^+ and GTHF-negative ideal solution A^-, respectively.

Step 7. Calculate the total quasi-distance measures d_i^+ and $d_i^- \;\; (i = 1,2,...,m)$ of each alternative $R_i \;\; (i = 1,2,...,m)$ as;

$$d_i^+ = \sum_{j=1}^{n} r_{ij}^+ \;\; (i = 1,2,...,m;\; j = 1,2,...,n)$$

and

$$d_i^- = \sum_{j=1}^{n} r_{ij}^- \;\; (i = 1,2,...,m;\; j = 1,2,...,n)$$

Step 8. Find the score values s_i ($\overline{s}_i$) of each alternative a_i as:

$$s_i = \frac{d_i^+}{d_i^+ + d_i^-} \;\; (i = 1,2,...,m)$$

$$(or\; \overline{s}_i = \frac{d_i^-}{d_i^+ + d_i^-} \;\; (i = 1,2,...,m))$$

Step 9. Rank all alternatives $a_i \;\; (i = 1,2,...,m)$ by using the score values $s_i \;\; (i = 1,2,...,m)$ of $a_i \;\; (i = 1,2,...,m)$ and determine the best alternative.

In here, for two alternatives a_k and a_l, $a_k \prec a_l$ $(k,l \in \{1,2,...,m\})$ if $s_k > s_l$, where $\prec$ is a preference relation on A. The best alternative will be the closest to the GTHF-positive ideal solution solution and farthest from GTHF-negative ideal solution (or for two alternatives a_k and a_l $a_k \prec a_l$ $(k,l \in \{1,2,...,m\})$ if $\overline{s}_k < \overline{s}_l$, where $\prec$ is a preference relation on A).

Example 4.2. Assume that among the 5 partners (R_1 to R_5) of a limited company, it is desired to choose a chairman based on 6 criteria. Six subjective criteria are considered by decision maker as:

i. Age (c_1)

ii. Foreign language (c_2)

iii. Sociability(c_3)

iv. Technological knowledge (c_4)

v. Persuasion skill (c_5)

vi. Business environment (c_6)

The calculative procedure is summarized as follows:

Step 1. The decision makers constructed the GTHF-MCDM matrix x_{ij} ($i = 1,2,...,5$; $j = 1,2,...,6$) as follows:

$$[\tilde{x}_{ij}]_{5\times 6} = \begin{pmatrix} \langle(0,1,1,2);\{0.9,0.8,0.7\}\rangle & \langle(0,1,2,3);\{0.6,0.3,0,9\}\rangle \\ \langle(2,4,5,6);\{0.8,0.7,0.6\}\rangle & \langle(1,2,3,4);\{0.9,0.6,0.8\}\rangle \\ \langle(0,1,2,3);\{0.6,0.3,0,9\}\rangle & \langle(3,5,6,10);\{1.0,0.8\}\rangle \\ \langle(2,4,5,6);\{0.8,0.7,0.6\}\rangle & \langle(2,2,3,4);\{0.8,0.7\}\rangle \\ \langle(2,3,4,5);\{0.8,0.6,0.9\}\rangle & \langle(1,2,3,4);\{0.9,0.6,0.8\}\rangle \end{pmatrix}$$

$$\begin{pmatrix} \langle(0,1,1,2);\{0.9,0.8,0.7\}\rangle & \langle(3,4,5,7);\{0.9,0.7\}\rangle \\ \langle(2,2,3,4);\{0.8,0.7\}\rangle & \langle(3,4,5,7);\{0.9,0.7\}\rangle \\ \langle(2,3,4,5);\{0.8,0.6,0.9\}\rangle & \langle(2,2,3,4);\{0.8,0.7\}\rangle \\ \langle(2,3,4,5);\{0.8,0.6,0.9\}\rangle & \langle(0,1,1,2);\{0.9,0.8,0.7\}\rangle \\ \langle(2,2,3,4);\{0.8,0.7\}\rangle & \langle(1,2,3,4);\{0.9,0.6,0.8\}\rangle \end{pmatrix}$$

$$\begin{pmatrix} \langle(0,1,2,3);\{0.6,0.3,0,9\}\rangle & \langle(2,2,3,4);\{0.8,0.7\}\rangle \\ \langle(2,2,3,4);\{0.8,0.7\}\rangle & \langle(0,1,1,2);\{0.9,0.8,0.7\}\rangle \\ \langle(2,4,5,6);\{0.8,0.7,0.6\}\rangle & \langle(2,2,3,4);\{0.8,0.7\}\rangle \\ \langle(2,4,5,6);\{0.8,0.7,0.6\}\rangle & \langle(0,1,2,3);\{0.6,0.3,0,9\}\rangle \\ \langle(2,4,5,6);\{0.8,0.7,0.6\}\rangle & \langle(2,2,3,4);\{0.8,0.7\}\rangle \end{pmatrix}$$

Step 2. We calculated the normalized GTHF-MCDM matrix n_{ij} ($i = 1,2,...,5$; $j = 1,2,...,6$) as;
($n_{ij} = \langle(\frac{a_{ij}}{10}, \frac{b_{ij}}{10}, \frac{c_{ij}}{10}, \frac{d_{ij}}{10});\xi_{ij}(x)\rangle \in \Phi$, where $\eta = \max_{i,j}\{\left|a_{ij}\right|, \left|b_{ij}\right|, \left|c_{ij}\right|, \left|d_{ij}\right|\}$ ($i = 1,2,...,5$; $j = 1,2,...,6$))

$$[n_{ij}]_{5\times 6} = \begin{pmatrix} \langle(0.0,0.1,0.1,0.2);\{0.9,0.8,0.7\}\rangle & \langle(0.0,0.1,0.2,0.3);\{0.6,0.3,0,9\}\rangle \\ \langle(0.2,0.4,0.5,0.6);\{0.8,0.7,0.6\}\rangle & \langle(0.1,0.2,0.3,0.4);\{0.9,0.6,0.8\}\rangle \\ \langle(0.0,0.1,0.2,0.3);\{0.6,0.3,0,9\}\rangle & \langle(0.3,0.5,0.6,1.0);\{1.0,0.8\}\rangle \\ \langle(0.2,0.4,0.5,0.6);\{0.8,0.7,0.6\}\rangle & \langle(0.2,0.2,0.3,0.4);\{0.8,0.7\}\rangle \\ \langle(0.2,0.3,0.4,0.5);\{0.8,0.6,0.9\}\rangle & \langle(0.1,0.2,0.3,0.4);\{0.9,0.6,0.8\}\rangle \end{pmatrix}$$

$$\begin{pmatrix} \langle(0.0,0.1,0.1,0.2);\{0.9,0.8,0.7\}\rangle & \langle(0.3,0.4,0.5,0.7);\{0.9,0.7\}\rangle \\ \langle(0.2,0.2,0.3,0.4);\{0.8,0.7\}\rangle & \langle(0.3,0.4,0.5,0.7);\{0.9,0.7\}\rangle \\ \langle(0.2,0.3,0.4,0.5);\{0.8,0.6,0.9\}\rangle & \langle(0.2,0.2,0.3,0.4);\{0.8,0.7\}\rangle \\ \langle(0.2,0.3,0.4,0.5);\{0.8,0.6,0.9\}\rangle & \langle(0.0,0.1,0.1,0.2);\{0.9,0.8,0.7\}\rangle \\ \langle(0.2,0.2,0.3,0.4);\{0.8,0.7\}\rangle & \langle(0.1,0.2,0.3,0.4);\{0.9,0.6,0.8\}\rangle \end{pmatrix}$$

$$\begin{pmatrix} \langle(0.0,0.1,0.2,0.3);\{0.6,0.3,0,9\}\rangle & \langle(0.2,0.2,0.3,0.4);\{0.8,0.7\}\rangle \\ \langle(0.2,0.2,0.3,0.4);\{0.8,0.7\}\rangle & \langle(0.0,0.1,0.1,0.2);\{0.9,0.8,0.7\}\rangle \\ \langle(0.2,0.4,0.5,0.6);\{0.8,0.7,0.6\}\rangle & \langle(0.2,0.2,0.3,0.4);\{0.8,0.7\}\rangle \\ \langle(0.2,0.4,0.5,0.6);\{0.8,0.7,0.6\}\rangle & \langle(0.0,0.1,0.2,0.3);\{0.6,0.3,0,9\}\rangle \\ \langle(0.2,0.4,0.5,0.6);\{0.8,0.7,0.6\}\rangle & \langle(0.2,0.2,0.3,0.4);\{0.8,0.7\}\rangle \end{pmatrix}$$

Step 3. We gave the weighted vector as; $w = (w_1 = 0.20, w_2 = 0.15, w_3 = 0.25, w_4 = 0.15, w_5 = 0.20, w_6 = 0.05)$ where w_j $(j = 1,2,...,6)$ is the weight of criterion c_j $(j = 1,2,...,6)$ and $\sum_{j=1}^{n} w_j = 1$.

Step 4. We computed the weighted normalized GTHF-MCDM matrix $n_{ij}^{w} = w_j \cdot n_{ij} = \langle(\widetilde{a}_{ij}, \widetilde{b}_{ij}, \widetilde{c}_{ij}, \widetilde{d}_{ij}); \widetilde{\xi}_{ij}(x)\rangle$ $(i = 1,2,...,5;\ j = 1,2,...,6)$ as;

$$[n_{ij}^{w}]_{5\times 6} = \begin{pmatrix} \langle(0.0000, 0.0200, 0.0200, 0.0400); \{0.3690, 0.2752, 0.2140\}\rangle \\ \langle(0.0400, 0.0800, 0.1000, 0.1200); \{0.2752, 0.2140, 0.1674\}\rangle \\ \langle(0.0000, 0.0200, 0.0400, 0.0600); \{0.1674, 0.0689, 0.3690\}\rangle \\ \langle(0.0400, 0.0800, 0.1000, 0.1200); \{0.2752, 0.2140, 0.1674\}\rangle \\ \langle(0.0400, 0.0600, 0.0800, 0.1000); \{0.2752, 0.1674, 0.3690\}\rangle \end{pmatrix}$$

$$\begin{pmatrix} \langle(00.0000, 0.0150, 0.0300, 0.0450); \{0.1284, 0.0521, 0.2921\}\rangle \\ \langle(0.0150, 0.0300, 0.0450, 0.0600); \{0.2921, 0.1284, 0.2145\}\rangle \\ \langle(0.0450, 0.0750, 0.0900, 0.1500); \{0.21451.0000\}\rangle \\ \langle(0.0300, 0.0300, 0.0450, 0.0600); \{0.2145, 0.1652\}\rangle \\ \langle(0.0150, 0.0300, 0.0450, 0.0600); \{0.2921, 0.1284, 0.2145\}\rangle \end{pmatrix}$$

$$\begin{pmatrix} \langle(0.0000, 0.0250, 0.0250, 0.0500); \{0.4377, 0.3313, 0.2599\}\rangle \\ \langle(0.0500, 0.0500, 0.0750, 0.1000); \{0.3313, 0.2599\}\rangle \\ \langle(0.0500, 0.0750, 0.1000, 0.1250); \{0.3313, 0.2047, 0.4377\}\rangle \\ \langle(0.0500, 0.0750, 0.1000, 0.1250); \{0.3313, 0.2047, 0.4377\}\rangle \\ \langle(0.0500, 0.0500, 0.0750, 0.1000); \{0.3313, 0.2599\}\rangle \end{pmatrix}$$

$$\begin{pmatrix} \langle(0.0450, 0.0600, 0.0750, 0.1050); \{0.2921, 0.1652\}\rangle \\ \langle(0.0450, 0.0600, 0.0750, 0.1050); \{0.2921, 0.1652\}\rangle \\ \langle(0.0300, 0.0300, 0.0450, 0.0600); \{0.2145, 0.1652\}\rangle \\ \langle(0.0000, 0.0150, 0.0150, 0.0300); \{0.2921, 0.2145, 0.1652\}\rangle \\ \langle(0.0150, 0.0300, 0.0450, 0.0600); \{0.2921, 0.1284, 0.2145\}\rangle \end{pmatrix}$$

$$\begin{pmatrix} \langle(0.0000, 0.0200, 0.0400, 0.0600); \{0.1674, 0.0689, 0.3690\}\rangle \\ \langle(0.0400, 0.0400, 0.0600, 0.0800); \{0.2752, 0.2140\};\rangle \\ \langle(0.0400, 0.0800, 0.1000, 0.1200); \{0.2752, 0.2140, 0.1674\}\rangle \\ \langle(0.0400, 0.0800, 0.1000, 0.1200); \{0.2752, 0.2140, 0.1674\}\rangle \\ \langle(0.0400, 0.0800, 0.1000, 0.1200); \{0.2752, 0.2140, 0.1674\}\rangle \end{pmatrix}$$

$$\begin{pmatrix} \langle(0.1000, 0.1000, 0.1500, 0.2000); \{0.5528, 0.4523\}\rangle \\ \langle(0.0000, 0.0500, 0.0500, 0.1000); \{0.6838, 0.5528, 0.4523\}\rangle \\ \langle(0.1000, 0.1000, 0.1500, 0.2000); \{0.5528, 0.4523\}\rangle \\ \langle(0.0000, 0.0500, 0.1000, 0.1500); \{0.3675, 0.1633, 0.6838\}\rangle \\ \langle(0.1000, 0.1000, 0.1500, 0.2000); \{0.5528, 0.4523\}\rangle \end{pmatrix}$$

Step 5. We described the GTHF-positive ideal solution A^{+} and GTHF-negative ideal solution A^{-} for GTHF-MCDM matrix as follows:

$A^{+} = \langle(0.1000, 0.1000, 0.1500, 0.2000); \{1\}\rangle$ and $A^{-} = \langle(0.0000, 0.0150, 0.0150, 0.0300); \{0.0521\}\rangle$, respectively.

Step 6. We computed the quasi-distance measures $d_{NoH}(n_{ij}^w, A^+)$, $(i = 1,2,...,5;\ j = 1,2,...,6)$ and $d_{NoH}(n_{ij}^w, A^-)$ $(i = 1,2,...,5;\ j = 1,2,...,6)$ in Table 1 and Table 2, respectively.

Table 1. The quasi-distance measures $d_{NoH}(n_{ij}^w, A^+)$, $(i = 1,2,...,5;\ j = 1,2,...,6)$

$d_{NoH}(n_{ij}^w, A^+)$	c_1	c_2	c_3	c_4	c_5	c_6
R_1	0.1825	0.2096	0.1643	0.1517	0.1881	0.0000
R_2	0.1274	0.1872	0.1403	0.1517	0.1685	0.0888
R_3	0.1881	0.0480	0.1055	0.1958	0.1274	0.0000
R_4	0.1274	0.1958	0.1055	0.2018	0.1274	0.0465
R_5	0.1427	0.1872	0.1403	0.1872	0.1274	0.0000

Table 2. The quasi-distance measures $d_{NoH}(n_{ij}^w, A^-)$ $(i = 1,2,...,5;\ j = 1,2,...,6)$

$d_{NoH}(n_{ij}^w, A^-)$	c_1	c_2	c_3	c_4	c_5	c_6
R_1	0.0010	0.0012	0.0029	0.0112	0.0036	0.1171
R_2	0.0162	0.0036	0.0148	0.0112	0.0071	0.0291
R_3	0.0036	0.0765	0.0283	0.0035	0.0162	0.1171
R_4	0.0162	0.0025	0.0283	0.0000	0.0162	0.0642
R_5	0.0141	0.0036	0.0148	0.0036	0.0162	0.1171

Step 7. We calculated the total quasi-distance measures d_i^+ and d_i^- $(i = 1,2,...,5)$ of each alternative R_i $(i = 1,2,...,5)$ in Table 3 based on Table 1 and Table 2, respectively;

Table 3. The total quasi-distance measures d_i^+ and d_i^- $(i = 1,2,...,5)$

i	1	2	3	4	5
d_i^+	0.8961	0.8640	0.6649	0.8045	0.7849
d_i^-	0.1371	0.0819	0.2442	0.1273	0.1693

Step 8. We found the score values s_i $(i = 1,2,...,5)$ of each alternative a_i $(i = 1,2,...,5)$ in Table 4.

Table 4. The score values s_i $(i = 1,2,...,5)$ of each alternative a_i $(i = 1,2,...,5)$

i	1	2	3	4	5
s_i	0.8674	**0.9134**	**0.7314**	0.8634	0.8226

Step 9. We ranked all alternatives according to the score values s_i, in decreasing order by the rule $s_2 > s_1 > s_4 > s_5 > s_3$ and we obtained $R_2 \prec R_1 \prec R_4 \prec R_5 \prec R_3$. Therefore, the best chairman is R_3. Moreover, we ranked all alternatives according to other quasi-distance measures in Table 5 and we obtained the same results for the best chairman.

Table 5. A ranking for all alternatives (alt) according to other introduced quasi-distance measures (DM)

DM	i	1	2	3	4	5	The worst alt.	The best alt.
d_{NoE}	s_i	0.8334	**0.8461**	**0.6980**	0.8258	0.7909	R_2	R_3
$d^{0.5}_{NoG}$	s_i	0.8726	**0.9722**	**0.7499**	0.9074	0.8302	R_2	R_3
d^{4}_{NoG}	s_i	0.7815	0.7928	**0.6656**	**0.7953**	0.7562	R_4	R_3
d^{20}_{NoG}	s_i	0.7061	0.7305	**0.6342**	**0.7560**	0.7126	R_4	R_3

5. Conclusion

In this paper, we proposed some novel not-ordered quasi-distance measuresunder GTHF-numbers. Then, we applied the quasi-distance measures to TOPSIS method of GTHF-numbers in Deli [26]. Also, we gave a numerical example, to show the efficiency and the applicability of the proposed method. In future, we may study some different quasi-distance and similarity measures and aggregation operators on GTHF-numbers. Researchers can also define similarity measures based on cendroid point of the GTHF-numbers.

Author Contributions

All the authors contributed equally to this work. They all read and approved the last version of the manuscript.

Conflicts of Interest

The authors declare no conflict of interest.

References

[1] L. A. Zadeh, *Fuzzy sets*, Information and Control, 8(3), (1965) 338–353.

[2] V. Torra, *Hesitant fuzzy sets*, International Journal of Intelligent Systems, 25(6), (2009) 529–539.

[3] V. Torra, Y. Narukawa, *On hesitant fuzzy sets and decision*, IEEE International Conference on Fuzzy Systems 2009, Jeju Island, Korea, 2009, pp. 1378–1382.

[4] S. K. Tyagi, *Multiple attribute decision making using hesitant triangular fuzzy sets*, International Conference on Electrical, Electronics, and Optimization Techniques (ICEEOT) 2016, Chennai, India, 2016, pp. 1502–1510.

[5] J. J. Chen, X. J. Huang, *Hesitant triangular intuitionistic fuzzy information and its application to multi-attribute decision making problem*, Journal of Nonlinear Science and Application 10, (2017) 1012–1029.

[6] M. Erdoğan, I. Kaya, *Selection of the best outsourcing firm for WEEE under hesitant fuzzy environment*, Journal of Intelligent and Fuzzy Systems, 35(3), (2018) 3295–3306.

[7] Z. S. Xu, M. M. Xia, *On distance and correlation measures of hesitant fuzzy information*, International Journal of Intelligent Systems, 26(5), (2013) 410–425.

[8] A. Fahmi, S. Abdullah, A. Ali, R. Ahmad, F. Ghani, *Triangular cubic linguistic hesitant fuzzy aggregation operators and their application in group decision making*, Journal of Intelligent and Fuzzy Systems, 34(4), (2018) 2401–2416.

[9] F. J. Estrella, S. C. Onar, R. M. RodrÃguez, B. Oztaysi, L. Martinez, C. Kahraman, *Selecting firms in uni-*

versity technoparks: A hesitant linguistic fuzzy TOPSIS model for heterogeneous contexts, Journal of Intelligent and Fuzzy Systems, 33(2), (2017) 1155–1172.

[10] C. Kahraman, S. C. Onar, B. Öztayşi, *Present worth analysis using hesitant fuzzy sets*, in: J. M. Alonso, H. Bustince, M. Reformat (Eds.) Conference of the International Fuzzy Systems Association and the European Society for Fuzzy Logic and Technology 2015, Gijon, Asturias (Spain), 2015, pp. 255–259.

[11] G. Qian, H. Wang, X. Feng, *Generalized of hesitant fuzzy sets and their application in decision support system*, Knowledge-Based Systems, 37, (2013) 357–365.

[12] T. Rashid, S. M. Husnine, *Multicriteria group decision making by using trapezoidal valued hesitant fuzzy sets*, The Scientific World Journal, 2014, (2014) Article ID: 304834, 1–8.

[13] S. Memiş, S. Enginoğlu, U. Erkan, *Numerical data classification via distance-based similarity measures of fuzzy parameterized fuzzy soft matrices*, IEEE Access, 9, (2021) 88583–88601.

[14] A. Fahmi, M. Aslam, S. Abdullah, *Analysis of migraine in mutlicellular organism based on trapezoidal neutrosophic cubic hesitant fuzzy TOPSIS method*, International Journal of Biomathematics, 12(8), (2019). https://doi.org/10.1142/S1793524519500840

[15] A. Fahmi, M. Aslam, F. A. A. Almahdi, F. Amin, *New type of cancer patients based on triangular cubic hesitant fuzzy TOPSIS method*, International Journal of Biomathematics, 13(1), (2019) 1–24. doi:10.1142/s1793524520500023.

[16] A. Fahmi, M. Aslam, S. Abdullah, F. Amin, A. Asada, W. A. Khan, *Some geometric operators with triangular cubic linguistic hesitant fuzzy number and their application in group decision making*, Journal of Intelligent and Fuzzy Systems, 35(2), (2018) 2485–2499.

[17] S., Hussain, M. Aslam, F. Amin, S. Abdullah, A. Fahmi, *Trapezoidal linguistic cubic fuzzy TOPSIS method and application in a group decision making problem*, Journal of Intelligent Systems, 29(1), (2019) 1283–1300.

[18] X. Peng *Hesitant trapezoidal fuzzy aggregation operators based on Archimedean t-norm and t-conorm and their application in MADM with completely unknown weight information*, International Journal for Uncertainty Quantification, 7(6), (2017) 475–510.

[19] X. Zhang, Z. Xu, M. Liu, *Hesitant trapezoidal fuzzy QUALIFLEX method and its application in the evaluation of green supply chain initiatives*, Sustainability, 8(9), (2016) 1–17.

[20] X. Zhang, T. Yang, W. Liang, M. Xiong, *Closeness degree-based hesitant trapezoidal fuzzy multicriteria decision making method for evaluating green suppliers with qualitative information*, Discrete Dynamics in Nature and Society, 2018, (2018) Article ID: 3178039, 1–13.

[21] F. Amin, A . Fahmi, S. Abdullah, *Dealer using a new trapezoidal cubic hesitant fuzzy TOPSIS method and application to group decision-making program*, Soft Computing, 23(14), (2019) :5353–5366.

[22] A. Fahmi, S. Abdullah, F. Amin, A. Ali, R. Ahmed, M. Shakeel, *Trapezoidal cubic hesitant fuzzy aggregation operators and their application in group decision-making*, Journal of Intelligent and Fuzzy Systems, 36(4), (2019) 3619–3635.

[23] A. Fahmi, S. Abdullah, F. Amin, M. Aslam, S. Hussain, *Trapezoidal linguistic cubic fuzzy TOPSIS method*

and application in a group decision making program, Journal of Intelligent Systems 29(1), (2020) 1283–1300.

[24] A. Fahmi., F. Amin, S. Abdullah, M. Shakeel, *Power average operators of trapezoidal cubic fuzzy numbers and application to multi-attribute group Decision making*, Journal of Intelligent Systems, 29(1), (2020) 1643–1661.

[25] İ. Deli, F. Karaaslan, *Generalized trapezoidal hesitant fuzzy numbers and their applications to multiple criteria decision making problems*, Soft Computing, 25(2), (2021) 1017–1032.

[26] İ. Deli, *A TOPSIS method by using generalized trapezoidal hesitant fuzzy numbers and application to a robot selection problem*, Journal of Intelligent and Fuzzy Systems, 38(1), (2020) 779–793.

[27] E. Ö. Çelik, *Some distance and correlation coefficient measures of generalized trapezoidal hesitant fuzzy numbers and their application to decision making problems*, Master's Thesis, Kilis 7 Aralık University (2022), Kilis, Turkiye (in Turkish).

[28] İ. Deli, *Bonferroni mean operators of generalized trapezoidal hesitant fuzzy numbers and their application to decision-making problems*, Soft Computing, 25(6), (2021) 4925–4949.